The impact of adipose tissue on COVID-19 disease severity.

A dissertation

for the doctoral degree of

DOCTOR RERUM NATURALIUM

submitted to the

Faculty of Mathematics, Informatics and Natural Sciences

Department of Biology

at the University of Hamburg

by

Martin Zickler

from Berlin, Germany

Hamburg

2023

Date of Oral Defense: 17.11.2023

First reviewer:

Prof. Dr. Gülşah Gabriel

Research Department Viral Zoonoses-One Health, Leibniz Institute of Virology (LIV),

Hamburg, Germany; University of Veterinary Medicine, Hannover, Germany.

Second reviewer:

Prof. Dr. Thomas Dobner

Research Department Viral Transformation, Leibniz Institute of Virology (LIV),

Hamburg, Germany; Department of Biology, University of Hamburg, Hamburg, Germany

Table of Contents

Table of Abbreviations

3CLpro	3C-like proteinase
5-Adiol	Androstenediol
A4	Androstenedone
ACACA	Acetyl-CoA Carboxylase 1
ACE2	Angotensin-converting enzyme 2
ACLY	ATP citrate lyase
Ang II	Angiotensin II
AR	Androgen receptor
ARDS	Acute respiratory distress syndrome
AT	Adipose tissue
ATGL	Adipose triglyceride lipase
ATP	Adenosine triphosphate
BAT	Brown adipose tissue
BMI	Body mass index
C75	3-carboxy-4-octyl-2-methylenebutyrolactone
CD	Cluster of differentiation
CHD	Coronary heart disease
COVID-19	Coronavirus disease 2019
CVD	Cardiovascular disease
CYP	Cytochrome P450
CYP19A1	Cytochrome P450 19A1 „Aromatase"
DC	Dendritic cell
DDT	Dichlorodiphenyltrichloroethane
DHT	Dihydrotestosterone
DMV	Double membrane vesicle
DNA	Deoxyribonucleic acid
dsRNA	double stranded RNA
E1	Estrone
E2	Estradiol
EBV	Epstein-Barr virus
ECMO	Extracorporal membrane oxygenation
EMA	European Medicines Agency
ER	Estrogen receptor
ERE	Estrogen response element
ERGIC	Endoplasmic-reticulum-Golgi-intermediate compartment

FA	Fatty acid
FABP4	Fatty acid binding protein 4
FASN	Fatty acid synthase
FDA	(american) Food and Drug Administration
FFA	Free fatty acid
FL	Fusion loop
GBD	Global Burden of Disease Study
GnRH	Gonadotropin releasing hormone
gRNA	genomic RNA
HAV	Hepatitis A virus
HBV	Hepatitis B virus
HCV	Hepatitis C virus
Hel	Helicase
HIF	Hypoxia-inducible factor
HIV	Human immunodeficiency virus
HMG-CoA	β-Hydroxy β-methylglutaryl coenzyme A
hMSC-TERT	Human mesenchymal stem cell (immortalized by) telomerase reverse transcriptase
HPA	Human protein atlas
HPG	Hypothalamic-pituitary-gonadal axis
HR	Heptad repeat
HRE	Hormone response element
HSD	Hydroxysteroid dehydrogenoase
HSL	Hormone-sensitive lipase
HSV	Herpes simplex virus
IAV	Influenza A virus
ICU	Intensive care unit
IDL	intermediate-density lipoprotein
IFN	Interferon
Ig	Immunoglobulin
IHME	Institute for Health Metrics and Evaluation
IL	Interleukin
IL-RA	Interleukin receptor antagonist
IRF	Interferon regulatory factor
ISG	interferon-stimulated gene
kb	Kilobases
LCMV	Lymphocytic choriomeningitis virus

LDL	Low-density lipoprotein
LDLR	Low-density-lipoprotein receptor
LH	Luteinizing hormone
LPL	Lipoprotein lipase
MCP-1	Monocyte chemoattractant protein 1
MDA5	melanoma differentiation-associated protein 5
MERS-CoV	Middle East respiratory syndrome-related coronavirus
MGL	Monoacylglycerol lipase
MIP	Macrophage inflammatory protein
MOSH	Male obesity secondary hypogonadism
mRNA	messenger RNA
MUFA	Mono-unsaturated fatty acid
MV	Measles virus
NAFLD	Non-alcoholic fatty liver disease
NF-κB	Nuclear factor kappa-light-chain-enhancer of activated B cells
NHC	N^4-hydroxycitidine
NIH	National Institutes of Health
NK cell	Natural killer cells
NS	non-structural protein (influenza virus)
NSP	non-structural protein (coronaviurs)
NTD	N-terminal domain
ORF	Open reading frame
PBMC	Peripheral blood mononuclear cell
PCK1	Phosphoenolpyruvate Carboxykinase 1
PLpro	Papain-like protease
polyI:C	Polyinosinic:polycytidylic acid
pp	Polyprotein
PRR	Pattern recognition receptor
PUFA	Poly-unsaturated fatty acid
RAAS	Renin-angiotensin-aldosteron system
RBD	Receptor binding domain
RdRp	RNA-dependent RNA polymerase
RIG-I	Retinoic acid-inducible gene I
RLR	RIG-I-like receptor
RNA	Ribonucleic acid
RO	Replication organelles
ROS	Reactive oxygen species

RTC	Replication and transcription complex
SARS-CoV	Severe acute respiratory syndrome coronavirus type 2
SAT	Subcuataneous adipose tissue
SD	Subdomain
SFA	Saturated fatty acid
SHBG	Sex hormone-binding protein
SOFA	Sequential organ failure assessment
SREBP	Sterol regulatory element-binding protein
SVF	Stromal vascular fraction
TG	Triglyceride
TGF	Transforming growth factor
THL	Tetrahydrolipstatin
TLR	Toll-like receptor
TM	Transmembrane domain
TMPRSS2	Transmembrane protease, serine 2
TNF	Tumor necrosis factor
Treg cell	Regulatory T cell
USP18	Ubiquitin specific peptidase
VAT	Visceral adipose tissue
VLDL	very low-density lipoprotein
VOC	Variants of concern
WAT	White adipose tissue
WHO	World Health Organization

Table 1: Abbreviations

List of Tables

List of Figures

Publications related to this Dissertation

Publication #1: **Zickler M.**, Stanelle-Bertam S., Ehret S., Heinrich F., Lange P., Schaumburg B., Mounogou Kouassi N., Beck S., Jaeckstein M Y., Mann O., Krasemann S., Schroeder M., Jarczak D., Nierhaus A., Kluge S., Peschka M., Schlüter H., Renné T., Pueschel K., Kloetgen A., Scheja L., Ondruschka B., Heeren J., Gabriel G., Replication of SARS-CoV-2 in adipose tissue determines organ and systemic lipid metabolism in hamsters and humans. *Cell Metab.* (2022) DOI: 10.1016/j.cmet.2021.12.002

Publication #2: Schroeder M., Schaumburg B., Mueller Z., Parplys A., Jarczak D., Roedl K., Nierhaus A., de Heer G., Grensemann J., Schneider B., Stoll F., Bai T., Jacobsen J., **Zickler M.**, Stanelle-Bertram S., Klaetschke K., Renné T., Meinhardt A., Aberle J., Hiller J., Peine S., Kreienbrock L., Klingel K., Kluge S., Gabriel G., High estradiol and low testosterone levels are associated with critical illness in male but not in female COVID-19 patients: a retrospective cohort study. *Emerg Microbes Infect.* (2021) DOI: 10.1080/22221751.2021.1969869

Abstract

Since the first outbreak of SARS-CoV-2 at the end of 2019, the virus spread very rapidly around the world and was declared a pandemic in March of 2020 by the World Health Organizaition (WHO). Upon infection, it can cause the Coronavirus disease 2019 (COVID-19) with mild to severe progression and death. Early in the pandemic, it was found that male patients and individuals suffering from obesity or obesity-related diseases have a higher risk for adverse disease outcome. However, the underlying mechanisms for the increased risk are not yet fully understood.

To gain insight into the role of obesity during SARS-CoV-2 infection, the replication in adipose tissue upon infection and its consequences on metabolism were investigated. The results showed that SARS-CoV-2 productively infects mature adipocytes and actively disseminates from the lungs to the fat, causing an antiviral response within the adipose tissue. Inhibition of lipid synthesis and breakdown within the adipocytes reduced virus replication significantly, demonstrating a viral dependency on lipid metabolism. This effect was further enhanced by additional inhibition of cholesterol synthesis, causing a downregulation of the SARS-CoV-2 receptor. Metabolomic analysis revealed a profound organ-specific and systemic dysregulation of the lipid metabolism in a hamster model and human plasma samples. Further, SARS-CoV-2 RNA was found in adipose tissue from autopsy samples of patients, who succumbed to COVID-19. In male but not female patients, virus-positive samples correlated with excess weight (BMI>25 kg/m^2), linking metabolic disease with sex differences.

In this thesis, results showed that adipose tissue serves as a reservoir for SARS-CoV-2 replication, leading to alterations of the organ-specific and systemic lipid metabolism. Furthermore, virus-positive adipose tissue samples from deceased patients were associated with excess weight in men. This shows that large amounts of adipose tissue directly contribute to severe disease and that pharmacological treatment of obesity may improve the outcome of infection.

Zusammenfassung

Seit dem ersten Ausbruch von SARS-CoV-2 Ende 2019 hat sich das Virus sehr schnell weltweit verbreitet und wurde im März 2020 von der Weltgesundheitsorganisation (WHO) zur Pandemie erklärt. Bei einer Infektion kann es die COVID-19-Erkrankung, mit leichtem bis schwerem Verlauf und Tod, verursachen. Zu Beginn der Pandemie wurde festgestellt, dass männliche Patienten und Personen, die an Fettleibigkeit oder mit Fettleibigkeit verbundenen Krankheiten leiden, ein höheres Risiko für einen schweren Krankheitsverlauf haben. Die zugrundeliegenden Mechanismen für das erhöhte Risiko sind jedoch noch nicht vollständig geklärt.

Um die Rolle der Fettleibigkeit während der SARS-CoV-2-Infektion zu erforschen, wurde die Replikation im Fettgewebe nach Infektion und ihre Auswirkungen auf den Stoffwechsel untersucht. Die Ergebnisse zeigten, dass SARS-CoV-2 reife Fettzellen produktiv infiziert und sich aktiv von der Lunge in das Fettgewebe ausbreitet, was zu einer antiviralen Reaktion im Fettgewebe führt. Die Hemmung der Lipidsynthese und des Lipidabbaus in den Adipozyten reduzierte die virale Replikation signifikant, was eine Abhängigkeit des Virus vom Lipidstoffwechsel nahelegt. Dieser Effekt wurde durch eine zusätzliche Hemmung der Cholesterinsynthese, was zu einer Herunterregulierung des SARS-CoV-2-Rezeptors führte, noch verstärkt. Metabolom-Analysen zeigten eine tiefgreifende organspezifische und systemische Dysregulation des Lipidstoffwechsels im Hamstermodell und in menschlichen Plasmaproben. Außerdem wurde SARS-CoV-2-RNA im Fettgewebe von Autopsieproben von Patienten gefunden, die an COVID-19 erkrankt und verstorben waren. Bei männlichen, aber nicht bei weiblichen Patienten korrelierten die viruspositiven Proben mit Übergewicht (BMI>25 kg/m2), was einen Zusammenhang zwischen Stoffwechselerkrankungen und Geschlechtsunterschieden herstellt.

Die Ergebniss dieser Arbeit zeigten, dass Fettgewebe als Reservoir für die Replikation von SARS-CoV-2 dient, was zu Veränderungen des organspezifischen und systemischen Fettstoffwechsels führt. Darüber hinaus wurden virus-positive Fettgewebeproben von verstorbenen Patienten mit Übergewicht bei Männern in Verbindung gebracht. Dies zeigt, dass große Mengen an Fettgewebe möglicherweise direkt zu einer schweren Erkrankung beitragen und dass eine pharmakologische Behandlung von Fettleibigkeit den Ausgang der Infektion verbessern könnte.

1 Introduction

1.1 Severe Acute Respiratory Syndrome Coronavirus type 2 (SARS-CoV-2)

Severe acute respiratory syndrome coronavirus 2 (SARS-CoV-2) is one of the latest viruses in a long line of zoonotic pathogens to cross the species barrier and infect humans. Zoonotic infections are not a new phenomenon. In this century alone, there have already been multiple zoonotic outbreaks of smaller and larger scale, including two pandemics: the H1N1 influenza virus (swine flu) pandemic in 2009 and the ongoing SARS-CoV-2 pandemic that started in early 2020. Spillover infections are thought to occur regularly, because at least two thirds of all human viruses are of zoonotic origin (Woolhouse *et al.*, 2012). Anthropogenic factors such as changes in climate and land use will increase the opportunities for zoonotic events in the future by altering the habitats of previously isolated species (Carlson *et al.*, 2022).

1.1.1 Taxonomy

SARS-CoV-2 is categorized as a severe acute respiratory syndrome-related coronavirus in the Sarbecovirus subgenus of *Betacoronavirus*. Betacoronaviruses belong to the subfamily of *Orthocoronavirinae* within the family of *Coronaviridae* of the order *Nidovirales* (*Taxon Details | ICTV*, 2021, accessed: 18 May 2023).

1.1.2 Virion structure and genome organization

SARS-CoV-2 is an enveloped particle of spherical shape has a diameter of 60-120 nm. Inside, it carries the single stranded RNA genome of positive orientation complexed by the nucleocapsid protein (N), forming the nucleocapsid. The matrix protein (M) and the envelope protein (E), mainly involved in assembly and viral morphogenesis, are located within the envelope. The spike (S) protein, arranged in trimers and located on the surface of the particle, facilitates receptor binding and cell entry (Zhang *et al.*, 2021; Safiabadi Tali *et al.*, 2021, Fig. 1 A). The SARS-CoV-2 genome consists of approximately 29.9 kb and shares ~79 % and ~50 % sequence identity with SARS-CoV-1 and MERS-CoV, respectively (Yadav *et al.*, 2021). The open reading frames 1a and 1b (ORF1a, ORF1b) are located downstream of the 5' terminus and span two thirds of the whole genome. They encode two polyproteins, pp1a and pp1ab. The polyprotein pp1ab is produced by a programmed -1 ribosomal frameshift at the overlap of the two open reading frames (V'kovski *et al.*, 2021). The 3' end encodes the structural as well as accessory proteins (Chen *et al.*, 2021, Fig.1 B).
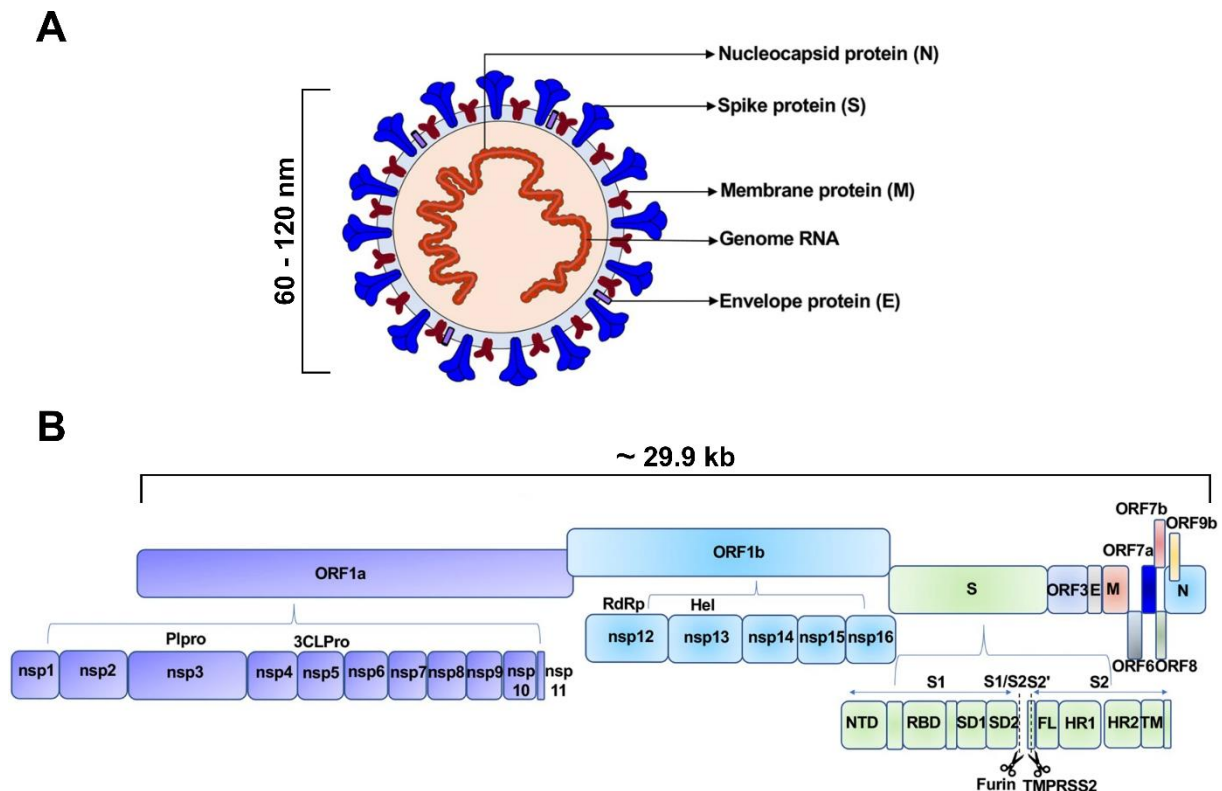
Figure 1: SARS-CoV-2 particle and genome organization with corresponding proteins. A) Depiction of viral particle: Enveloped SARS-CoV-2 particle with genomic RNA complexed with the nucleocapsid protein (N) on the inside, and the envelope protein (E), matrix protein (M) embedded in the envelope and the spike protein (S) on the surface. **B) Schematic of viral genome with corresponding proteins:** Genome organization from 5' to 3' ORF1a, ORF1b, S, ORF3, E, M, ORF6, ORF7 (a, b), ORF8, ORF9, N. ORF1a and ORF1b encode 16 non-structural proteins (NSP1-11, 12-16). Plpro, papain-like protease; 3CLPro, 3C-like proteinase; RdRp, RNA-dependent RNA polymerase; Hel, Helicase; NTD, N-terminal domain; RBD, receptor binding domain; SD1, subdomain 1; SD2, subdomain 2; FL, fusion loop; HR1, heptad repeat 1; HR2, heptad repeat 2; TM, transmembrane domain; TMPRSS2, transmembrane serine protease 2. Scissors indicated S1/S2 and S2 cleavage sites (modified from Zhang *et al.*, 2021).

1.1.3 Replication cycle

The SARS-CoV-2 replication cycle starts with binding of the spike protein to the main surface receptor angiotensin-converting enzyme 2 (ACE2). Cellular proteases such as the transmembrane serine protease 2 (TMPRSS2) or furin cleave the S protein into S1 and S2 subunits. This cleavage is a prerequisite for the fusion of viral and host cell membranes and subsequent release of the viral genome into the cytoplasm. Due to the positive genome orientation, the 5'-cap and 3'-polyadenylation, the viral genomic RNA (gRNA) is immediately translated by host ribosomes into the polyproteins pp1a and pp1ab. These proteins are subsequently cleaved by viral proteases papain-like protease (Plpro) and 3C-like proteinase (3CLpro) into the 16 non-structural proteins (NSP). The NSPs assemble into replication and transcription complexes (RTCs). Infection leads to a profound reorganization of cellular compartments and *de novo* synthesis of ER (endoplasmic reticulum)-derived organelles to

produce double membrane vesicles (DMVs, Cortese *et al.*, 2020). The DMVs are part of the replication organelles (RO), where newly synthesized RNA is shielded from enzymatic degradation and recognition by innate immune pattern recognition receptors (PRR). The RTCs produce subgenomic mRNAs that are translated into structural and accessory proteins. New positive-strand gRNAs are complexed with N proteins, forming nucleocapsids. These structures are enveloped in the ER-Golgi intermediate compartment (ERGIC), thereby generating new virions with M and E proteins in the lipid bilayer and S proteins on the surface. Assembled viral particles are transported via the secretory pathway and leave the cell by exocytosis (Malone *et al.*, 2022, Fig. 2).
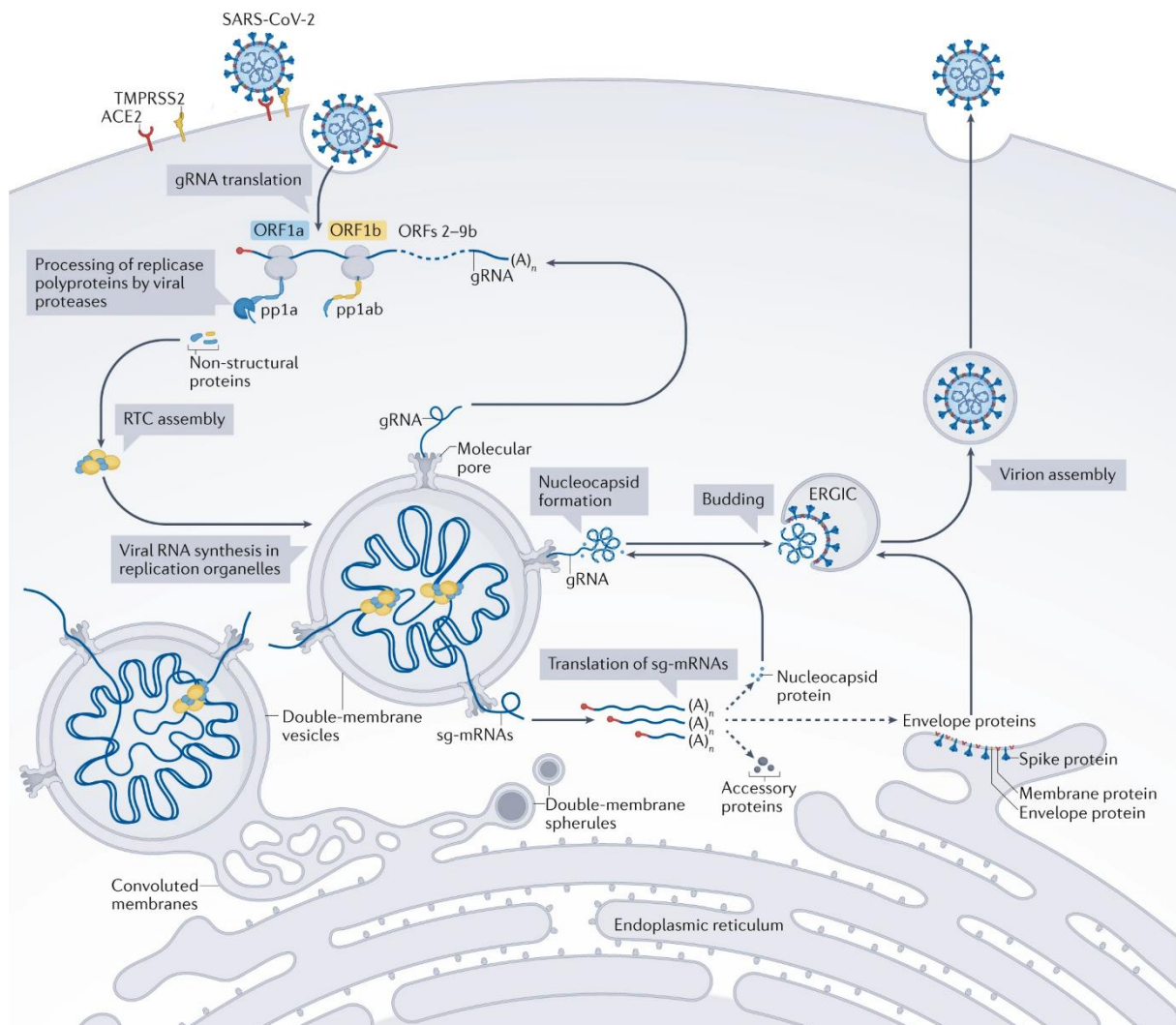
Figure 2: SARS-CoV-2 replication cycle. SARS-CoV-2 binds to the surface receptor ACE2 via the S protein. Genomic RNA (gRNA) is released into the cytoplasm after membrane fusion and immediately translated into the polyproteins. These proteins are cleaved into the 16 nsps by Plpro and 3CLpro. The nsps assemble into RTCs and viral RNA synthesis takes place in ROs consisting of DMVs. Subgenomic RNAs are synthesized for the translation of structural and accessory proteins. Newly formed gRNAs are complexed by N proteins and enveloped in the ERGIC thereby generating new viral particles with M and E proteins in the lipid bilayer and S proteins on the surface. Assembled virions are then transported to the cell membrane via the secretory pathway and leave the cell by exocytosis (adapted from Malone *et al.*, 2022).

1.1.4 SARS-CoV-2 pandemic

First cases of SARS-CoV-2 infections were reported in late December 2019 in Wuhan, Hubei Province, China as pneumonia of unknown etiology (*Pneumonia of unknown cause – China*, WHO Disease outbreak news - 05 January 2020 accessed: 18 May 2023), later termed COVID-19 (Coronavirus disease 2019). The origin of SARS-CoV-2 remains unclear, but the epicenter of the outbreak was most probably the Huanan market in Wuhan (Worobey *et al.*, 2022). On March 11th 2020, the WHO declared the SARS-CoV-2 outbreak a pandemic (*WHO Director-General's opening remarks at the media briefing on COVID-19 - 11 March 2020 accessed: 18 May 2023*). At the time of writing, more than 766 million SARS-CoV-2 infections and approximately 6.93 million COVID-19 deaths had been reported worldwide (*WHO Coronavirus (COVID-19) Dashboard | WHO Coronavirus (COVID-19) Dashboard With Vaccination Data*, accessed: 18 May 2023).

SARS-CoV-2 infection can cause a wide spectrum of symptoms, from asymptomatic to life-threatening disease. Clinical manifestations range from mild upper respiratory infection to pneumonia, respiratory failure and death (F. Zhou *et al.*, 2020). Throughout the course of the pandemic, a number of different variants emerged. The average incubation time of the ancestral strain is 5 to 7 days, but up to 14 days is possible (McAloon *et al.*, 2020). Later variants exhibit shorter incubation periods, serial intervals, heightened transmission efficiency, with possibly lower morbidity and mortality (Du *et al.*, 2022; Peacock *et al.*, 2022). Most human-to-human transmissions occur shortly before or at symptom onset at the peak of contagiousness (He *et al.*, 2020). SARS-CoV-2 is transmitted mainly by inhalation of virus-containing aerosols (Wang *et al.*, 2021). Most patients suffer from mild symptoms such as headache, fever, cough, tiredness, loss of taste and smell as well as sore throat. Nevertheless, a smaller percentage develops symptoms warranting the immediate need for medical attention like difficulty breathing, loss of speech or mobility, confusion or chest pain (*Coronavirus* - WHO fact sheet, accessed 18 May 2023). To date, approximately 0.9 % of infected people have died from the disease worldwide (*WHO Coronavirus (COVID-19) Dashboard | WHO Coronavirus (COVID-19) Dashboard With Vaccination Data*, accessed: May 18 2023).

The probability of severe disease progression or fatal outcome is not evenly distributed throughout the population. Multiple risk factors increase the likelihood for an adverse outcome of infection. These include old age, male gender, comorbidities like obesity, type 2 diabetes, hypertension, coronary heart disease (CHD), cancer and immunosuppression (Takahashi *et al.*, 2020; Treskova-Schwarzbach *et al.*, 2021; Sawadogo *et al.*, 2022). Interestingly, COVID-19 manifestations are not limited to the respiratory tract. Other organs affected by the infection are the brain, gastro-intestinal tract, cardiovascular system, gonads and kidneys (Long *et al.*, 2020; Mao *et al.*, 2020; Stanelle-Bertram *et al.*, 2020; X. Yang *et al.*, 2020; Song *et al.*, 2021).

Moreover, medical conditions can persist long after the acute phase of infection ended. This phenomenon is termed Long-COVID or Post-COVID syndrome (Nalbandian *et al.*, 2021).

1.1.5 Mitigation strategies against SARS-CoV-2

1.1.5.1 Antivirals

Over the course of the pandemic several different therapy options have been developed. Therapeutic approaches include targeted antiviral treatment, general immunosuppression and symptomatic treatment. Antivirals available to date are a range of monoclonal antibodies, directed against the S protein, inhibitors of the viral polymerase (RdRp) and a viral protease inhibitor. The monoclonal antibodies bind to the S protein of SARS-CoV-2, inhibit binding to its cellular receptor and thereby the entry into the cell. The two RdRp inhibitors currently approved are Remdesivir and Molnupiravir (only conditional approval in the UK). Remdesivir (Gilead Sciences) was originally developed for the treatment of Ebola and Marburg virus infections. It is administered as a prodrug and metabolized into its active form Remdesivir-triphosphate. The active metabolite serves as an analogue for Adenosine triphosphate (ATP) and is efficiently incorporated into the RNA by the RdRp, which leads to a delayed chain termination (Gordon *et al.*, 2020). This termination results in decreased production of viral RNA. Molnupiravir (MSD, Ridgeback Biotherapeutics) is also administered as a prodrug and metabolized into its active form β-D-N^4-hydroxycytidine (NHC) triphosphate. The mode of action involves a two-step process. The compound has tautomeric characteristics and can swap between two forms, which mimic either cytidine (C) or uridine (U). During RNA replication, the active metabolite is incorporated by the RdRp and escapes proofreading. In subsequent replications of RNA containing Molnupiravir, the compound is interpreted either as C or U, leading to mutations in the newly synthesized RNA. These products cannot support correct assembly of new virions (Kabinger *et al.*, 2021). The only protease inhibitor authorized is Nirmatrelvir (Pfizer), an inhibitor of the 3C-like proteinase of SARS-CoV-2. It is co-administered with Ritonavir as a combination drug called Paxlovid. Nirmatrelvir acts by binding to the active center and forming tight conjugates with 3CLpro. Ritonavir, originally a HIV-1 protease inhibitor, is used in this combination as a booster for Nirmatrelvir. The compound inhibits CYP3A4, the main enzyme metabolizing Nirmatrelvir, thereby slowing the reduction of its serum concentrations (*Ritonavir-Boosted Nirmatrelvir (Paxlovid) | COVID-19 Treatment Guidelines* - NIH, accessed: 18 May 2023).

1.1.5.2 General immune modulation

General immune modulation with medication originally used for rheumatoid arthritis such as Tocilizumab (RoActemra, Roche) and Anakinra (Kineret, Swedish Orphan Biovitrum) are also authorized for COVID-19 treatment. Tocilizumab is a monoclonal antibody directed against the IL-6 receptor. Anakinra is a copy of the human interleukin (IL)-1 receptor antagonist (IL-1RA). It binds to the IL-1 receptor without causing a cellular response, thereby making it unavailable for IL-1 (Seckinger *et al.*, 1987). Both compounds diminish the pro-inflammatory response of the immune system (*RoActemra | European Medicines Agency*, *Kineret | European Medicines Agency*, accessed: 18 May 2023).

1.1.5.3 Vaccines

Research on a potential SARS-CoV-2 vaccine began immediately with the onset of the pandemic. So far, 4 different classes of vaccines, mRNA-based, vector-based, protein-based and inactivated virus, are available in Europe and the United States. The mRNA-based vaccines (Comirnaty, BioNTech/Pfizer and Spikevax, Moderna) were the first to be approved in Europe in late 2020/early 2021. *In vitro* transcribed mRNA of the S protein is shuttled into muscle cells, where the S protein is expressed. The immune system recognizes the protein as foreign and reacts with synthesis of antibodies and activation of T cells.

The second kind of approved vaccine are the vector-based vaccines (Vaxzevria, Astra-Zeneca and Jcovden, Janssen-Cilag International) in the spring of 2021. The adenoviral vector carries the gene encoding the SARS-CoV-2 spike (S) protein. Like with mRNA vaccines, this protein is expressed, recognized by the immune system and antibody and T cell response is initiated. In late 2021, a protein-based vaccine (Nuvaxovid, Novavax) was approved where a recombinant S protein is given in combination with an adjuvant. The immune system detects the foreign protein and initiates the immune response. Similar to Nuvaxovid, 2 further protein based vaccines were authorized. VidPrevtyn Beta (Sanofi Pasteur), a vaccine containing a recombinant S protein of the SARS-CoV-2 Beta variant was authorized in November 2022. In late March of 2023 Bimervax (HIPRA Human Health S.L.U.) was given marketing authorization, containing a recombinant S protein consisting of a part of each, the SARS-CoV-2 Alpha and Beta variant. Both vaccines contain an adjuvant to boost the immunogenicity of the SARS-CoV-2 S protein. VidPrevtyn Beta and Bimervax are intended as a booster (third dose) only.

The fourth type of vaccine authorized to date contains the original SARS-CoV-2 strain, which is inactivated. The inactivated virus is recognized as foreign by the immune system and an antibody response as well as specific T-cells are elicited. It contains two adjuvants to boost the immunogenicity. The vaccine was authorized in June 2022 under the name COVID-19 Vaccine

(inactivated, adjuvanted) Valneva (Valneva Austria GmbH) (*COVID-19 vaccines: authorised | European Medicines Agency*, accessed: 18 May 2023). All compounds require two injections for full immunization, but the second dose (4-6 weeks after first dose) does not necessarily have to be the same vaccine or vaccine type as the first one. A booster was introduced in autumn of 2021 in order to counteract the decline in vaccine protection observed after 6 months. A meta-regression showed a decline in effectiveness against infection and symptomatic disease of 20-30 % and against severe disease of approximately 10 % after 6 months for the mRNA and vector-based vaccines, warranting further analyses of immune response at a later time point (Feikin *et al.*, 2022).

1.2 Obesity as a high-risk factor for severe COVID-19 outcome

1.2.1 Adipose tissue – energy storage and secretory organ

Adipose tissue (fat tissue) is the primary site of storage for excess energy in the form of triglycerides (TGs) but is also recognized as a metabolically active organ. It consists of adipocytes and the stromal vascular fraction (SVF), which includes adipocyte precursor, endothelial and immune cells.

Fat tissue is formed by a process called adipogenesis, the differentiation of pre-adipocytes into mature fat cells by a shift in gene expression patterns and subsequent morphological and functional changes. This development varies according to sex and age (Fonseca-Alaniz *et al.*, 2007). Adipose tissue has the ability to expand in two different ways, by hyperplasia and by hypertrophy. Hyperplastic expansion is achieved by differentiation of pre-adipocytes into mature fat cells within the adipose tissue, while hypertrophic growth enlarges the size of mature adipocytes to accommodate increased storage needs in times of overnutrition (Gray and Vidal-Puig, 2008).

There are two different types of adipose tissues with distinctly different functions in humans, brown and white adipose tissue (BAT, WAT respectively). BAT is found at birth, but the amount declines with age. Its main function is heat production. WAT does not contribute to thermogenesis, but has a wide variety of physiological functions. It offers mechanical protection of internal organs, helps maintain body temperature by means of insulation and stores energy in the form of TGs (Saely, Geiger and Drexel, 2011). Furthermore, it synthesizes and secretes substances called adipokines, which influence energy homeostasis and inflammation (Kershaw and Flier, 2004).

Leptin was the first adipokine to be described functioning as a hormone, increasing energy expenditure and promoting satiety by binding to its receptor in the central nervous system

(Coelho, Oliveira and Fernandes, 2013). It also functions as a classical adipokine, acting on immune cells, directly enhancing the production of pro-inflammatory cytokines and chemokines. Furthermore, leptin promotes the interaction of leukocytes and endothelial cells by increasing the expression of adhesion molecules on vascular endothelial cells (Mancuso, 2016).

A second pro-inflammatory adipokine is resistin, which is produced primarily by monocytes and macrophages. Adipocytes are also capable of synthesis and secretion, although in lower quantities. Resistin levels increase with the amount of WAT and lead to insulin resistance within adipose tissue (Coelho, Oliveira and Fernandes, 2013).

Adipose tissue also produces anti-inflammatory adipokines such as adiponectin. It is mainly produced in bone marrow adipose tissue and increases during calorie restriction, aging, estrogen deficiency and type 1 diabetes. Conversely, obesity, type 2 diabetes, oxidative stress and cigarette-smoke exposure lead to a decrease in adiponection plasma levels. It acts in an anti-inflammatory manner by inhibiting NF-κB signaling and influences energy expenditure through inhibition of fatty acid (FA), cholesterol and TG synthesis and enhancement of FA uptake and β-oxidation (Mancuso, 2016).

1.2.2 Lipid synthesis, transport and metabolism

Lipids are vital to the human body and play a role in a variety of processes, from energy storage to membrane synthesis and homeostasis. There are four different kinds of lipids. First, are fats and oils, consisting of glycerol as a backbone and three FA tails with various degrees of saturation. These TGs are used for insulation, energy storage and absorption of fat-soluble vitamins. Second, the phospholipids, an essential cell membrane component. Lipids are composed of a glycerol backbone, two FA tails and a phosphate group. The third group are waxes, esters of long-chained alcohol and one FA. Fourth are the steroids, for example cholesterol. They are produced in the liver and function as source material for hormones like estrogen, testosterone or cortisol. Cholesterol is also a part of cell membranes, influencing their fluidity (Ahmed and Ahmed, 2019).

Lipids are sourced in two ways, exogenously by diet or endogenously by biosynthesis mainly in the liver and adipose tissue, in a process termed *de novo* lipogenesis (DNL, Feingold and Grunfeld, 2000; Ameer *et al.*, 2014). The transport mechanisms differ between the two pathways. In short, the exogenous pathway starts with the breakdown of dietary TGs and cholesterol and subsequent uptake into the enterocytes. There they are re-esterified to TGs and packaged into cellular lipid droplets for temporary storage or lipoproteins, called chylomicrons. These leave the cells and enter the circulation via the lymphatic system and the thoracic duct (D'Aquila *et al.*, 2016). At their target tissues (muscle cells and adipocytes), the

membrane-associated lipoprotein lipase (LPL) is activated and breaks down TGs to facilitate their uptake into the target cells. The absorbed free fatty acids (FFAs) are subsequently used for energy production or storage in lipid droplets. The remnants left after unloading of TGs are transported to the liver, where the cholesterol is used in the production of very low-density lipoprotein (VLDL) for the endogenous pathway (Feingold and Grunfeld, 2000).

The endogenous pathway starts with the production of TGs from surplus carbohydrates by DNL. Carbohydrates, in the form of glucose enter glycolysis and generate pyruvate. This in turn is transformed to acetyl-CoA, which enters the tricarboxylic acid (TCA) cycle. The resulting citrate is then converted back to acetyl-CoA by the ATP citrate lyase (ACLY). Subsequently, the acetyl-CoA is converted to malonyl-CoA by the acetyl-CoA carboxylase 1 (ACC1), which in turn is used as a substrate for the fatty acid synthase (FASN) to generate fatty acids. These fatty acids are then esterified to TGs (Ameer *et al.*, 2014). The TGs and cholesterol are loaded into the VLDL particles and transported to the peripheral target tissues, where unloading takes place in a similar fashion to the exogenous pathway (Dallinga-Thie *et al.*, 2010; Tiwari and Siddiqi, 2012). The unloading results in the formation of intermediate-density lipoproteins, which are either cleared by the liver or whose cargo is hydrolyzed by the hepatic lipase. This leaves low-density lipoprotein (LDL) particles, distributing cholesterol to the liver and extrahepatic tissues like gonads, adrenal glands or the skeletal muscle as building blocks for different molecules. In summary, the exogenous and endogenous pathways deliver lipids and cholesterol to the peripheral tissues for energy production, storage or synthesis of molecules dependent on cholesterol (Feingold and Grunfeld, 2000).

When the body is in need of energy, stored fat in lipid droplets can be broken down. The hormone glucagon and catecholamines like epinephrine activate the adipose triglyceride lipase (ATGL), the hormone sensitive lipase (HSL) and monoglyceride lipase (MGL) for FA liberation. In adipocytes, the FFAs are released into the bloodstream and transported to target cells by lipoproteins or taken up by other cells. In non-adipose tissues, the FAs are used for energy production in β-oxidation and citric acid cycle (Feingold and Grunfeld, 2000; Ahmed and Ahmed, 2019).

1.2.3 Overweight and obesity

Obesity has become a disease of pandemic proportions within the last decades, tripling since 1975. Globally, 39 % of adults were overweight and 13 % obese in 2016. Statistics show a similar trend for children (5-19 years old) with a rise in overweight from 4 % to 19 % and obesity from 1 % to 8 %, for girls and boys (*Obesity and overweight* - WHO fact sheet, accessed: 18 May 2023). In 2019, obesity was ranked 5th in risk factor assessment for premature death. Interestingly, ranked 1st was high blood pressure and 4th high blood sugar, both being common

consequences of obesity (*Obesity - Our World in Data,* accessed: 18 May 2023). It is estimated that obesity is linked to more deaths worldwide than underweight, with more people being overweight than underweight, except in parts of sub-Saharan Africa and Asia (*Obesity and overweight* - WHO fact sheet, accessed: 18 May 2023).

Overweight and obesity are commonly defined by the Body-Mass-Index (BMI) of a person. The BMI is a simple weight for height measure in kg/m^2. The different categories range from underweight (BMI < 18.5), via normal weight (BMI 18.5 - 24.9) and overweight (BMI 25 - 29.9) to obesity (BMI ≥ 30, *Obesity and overweight* - WHO fact sheet, accessed: 18 May 2023).

Obesity is caused by a chronically disturbed balance of energy intake vs. energy expenditure. There are several different factors driving the development of obesity such as lack of physical activity, unhealthy eating behavior including high consumption of energy-dense and micronutrient-poor foods as well as a diet high in saturated fats and sugars. Furthermore, lack of sleep, high amounts of stress, genetic predisposition and some medications like antidepressants, antipsychotics, beta-blockers, birth control, glucocorticoids and insulin can contribute to obesity (*Overweight and Obesity - Causes and Risk Factors | NHLBI, NIH*, accessed: 18 May 2023).

1.2.4 Obesity and infectious diseases

It has been shown that obese individuals are prone to a more severe outcome of infectious diseases. For example, during the 2009 influenza A (IAV) pandemic, severely obese patients were twice as likely to be admitted to the intensive care unit (ICU) than lean patients. Additionally, obesity was associated with prolonged IAV-related hospitalization, mechanical ventilation and time in intensive care (Painter, Ovsyannikova and Poland, 2015). Similar results were found for obese COVID-19 patients (Lighter *et al.*, 2020; Moriconi *et al.*, 2020). In addition to a higher probability of adverse outcome in respiratory infections, obese individuals have a higher risk of worse disease progression in other infections, for example hepatitis B virus (HBV). The obesity-related pre-existing burden on liver function could contribute to serious complications from virus-mediated hepatitis (Painter, Ovsyannikova and Poland, 2015).

Furthermore, it has been shown that people suffering from obesity mount less effective vaccine responses to different pathogens such as IAV, hepatitis A virus (HAV), HBV, rabies virus and tetanus (Painter, Ovsyannikova and Poland, 2015). Metabolic disorders rooted in obesity seem to also have an impact on vaccine-breakthrough infections in the ongoing SARS-CoV-2 pandemic (Stefan, 2022).

The rapid expansion of adipose tissue, especially in a hypertrophic way, leads to a change in the composition of the SVF. In lean adipose tissue anti-inflammatory cytokines like IL-4, IL-13, IL-10 and transforming growth factor-β (TGF-β) maintain an M2 macrophage phenotype (anti-

inflammatory, involved in tissue repair and remodeling). In the obese state, the hypertrophy leads to rarefaction and subsequent adipocyte apoptosis. M1 macrophages surround the apoptotic adipocytes, forming crown-like structures. Additionally, mast cells was well as CD4^{+} and CD8^{+} T cells infiltrate the hypertrophic adipose tissue. Pro-inflammatory cytokines such as IL-6, IL-12, IL-18, IL-17, interferon (IFN)-γ, tumor necrosis factor (TNF)-α and monocyte chemoattractant protein (MCP)-1 are produced and released into the circulation. At the same time, the concentration of pro-inflammatory adipokines increases while that of anti-inflammatory adipokines decreases, leading to chronic low-grade inflammation, favoring metabolic diseases associated with obesity (Mancuso, 2016, Fig. 3).

This chronic low-grade inflammation not only promotes metabolic consequences, but also increases the chance of severe disease progression following infections by altering the systemic immune response. Obesity directly influences the innate immune response causing altered neutrophil function, an increase in M1 macrophages, abnormal natural killer (NK) cell phenotypes, increased inflammatory dendritic cells (DCs) and aberrant T cells response. The adaptive immune response is also altered under excess weight conditions resulting in increased CD4^{+} T cell phenotypes, decreased number of regulatory T cells and impaired B cell function (Pugliese *et al.*, 2022).

Other factors, related to excess weight, also affect the susceptibility to infections such as ineffective respiratory function, dysregulation of processes in skin and soft tissues as well as classic obesity-related disorders (Pugliese *et al.*, 2022).
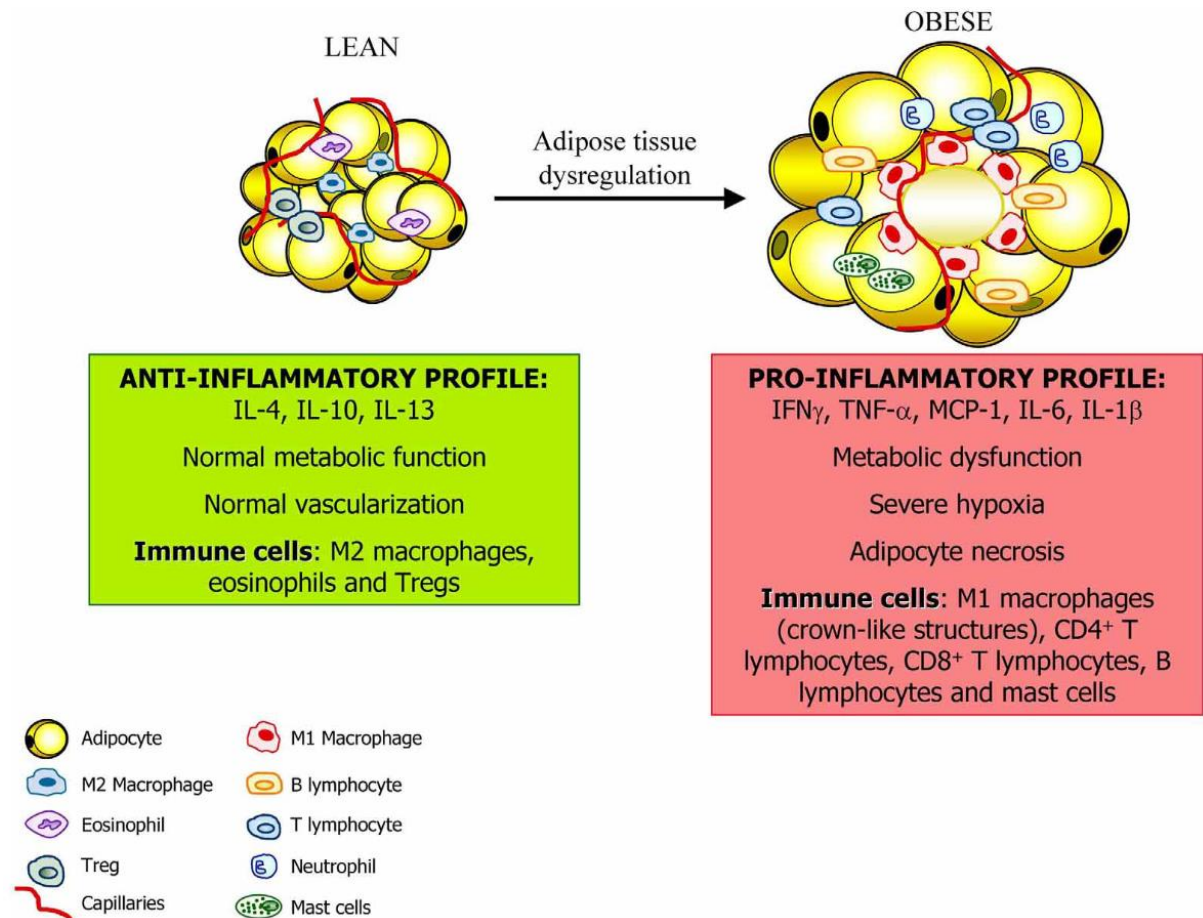
Figure 3: Adipose tissue dysregulation. In obese, hypertrophied adipose tissue the cytokine profile changes from anti-inflammatory to pro-inflammatory. The composition of the SVF changes from M2 macrophages, eosinophils and regulatory T cells (Tregs) to M1 macrophages, T cells, B cells and mast cells, favoring the progression of metabolic diseases and systemic low-grade inflammation (adapted from Catalán *et al.*, 2013).

1.2.5 Treatment of obesity

Adiposity is generally characterized by a severe expansion of white adipose tissue throughout the body in different fat depots. The increase in adiposity has multiple consequences such as heightened adipokine synthesis, increased lipid production, higher activity of the sympathetic nervous system and renin-angiotensin-aldosterone system. These consequences can ultimately lead to a plethora of diseases such as type 2 diabetes, non-alcoholic fatty liver disease (NAFLD), steatohepatitis, cirrhosis, coronary heart disease, congestive heart failure, stroke and chronic kidney disease (Heymsfield and Wadden, 2017). Furthermore, mechanical stress on organs increases, which promotes conditions like obstructive sleep apnea, osteoarthritis and gastroesophageal reflux disease. On top of the metabolic and physiological effects, the prevalence of psychological problems like mood, anxiety and psychiatric disorders increase, especially in patients with severe obesity. Treatment of obesity is generally carried

out by lifestyle intervention, pharmacotherapy or bariatric surgery, depending on the severity of obesity (Heymsfield and Wadden, 2017).

1.2.5.1 Lifestyle intervention

The preferred strategy to reduce weight is a change of lifestyle, especially in diet and exercise. The main goal of dietary therapy is the reduction of energy intake. This can be achieved by change in macronutrient composition (fat, carbohydrates, proteins), direct calorie restriction through low calorie (800-1600) kcal/day or very low calorie (≤ 800 kcal/day) diets or meal replacements (Ruban *et al.*, 2019). Additionally, physical exercise is recommended to increase energy expenditure. Adults are advised to be physically active in a moderately intense manner for 150 min/week (*Obesity causes & treatments - Illnesses & conditions | NHS inform*, accessed 18 May 2023). Other factors contributing to weight loss and healthy weight management include the reduction of stress or the implementation of appropriate coping mechanisms as well as sufficient, good quality sleep (*Overweight and Obesity - Prevention | NHLBI, NIH*, accessed 18 May 2023).

1.2.5.2 Pharmacological and surgical treatment options

In people suffering from obesity there are multiple different medications used to achieve weight loss. A direct-acting substance is Tetrahydrolipstatin (brand name Orlistat), which inhibits the gastric and pancreatic lipases. This leads to the decreased breakdown of dietary fats and TGs are excreted unchanged, thereby limiting the FFA uptake into to mucosal cells of the small intestine (Guerciolini, 1997). Tetrahydrolipstatin was also found to inhibit the fatty acid Synthase (FASN), thereby decreasing the *de novo* lipogenesis in cells (Kridel *et al.*, 2004). Liraglutide and Semaglutide are glucagon-like peptide-1 (GLP-1) receptor agonists. GLP-1 is naturally released from the gastro-intestinal (GI) tract after sugar and fat intake. It slows the GI transit and suppresses the appetite. By mimicking the GLP-1 action, Liraglutide and Semaglutide lead to a reduction in energy intake and subsequently to weight loss (Ruban *et al.*, 2019). Other substances, that act on the central nervous system to suppress appetite and increase energy expenditure include Lorcaserin, a serotonin agonist, and a combination of Phentermine (appetite suppressant) and Topiramate (antiepileptic) (Ruban *et al.*, 2019). In recent years, inhibitors of the DNL-related enzymes have been studied for their potential to treat obesity. One of these is the FAS inhibitor C75. This inhibitor increases peripheral energy expenditure in diet-induced obese mice (Thupari *et al.*, 2002). Further, C75 acts centrally in the hypothalamus of mice. It blocks the fasting-induced upregulation of the orexigenic neuropeptide Y and the agouti-related protein in lean and obese mice. The latter show normalization of hyperglycemia and hyperinsulinemia, caused by obesity (Shimokawa, Kumar

and Lane, 2002). In patients where lifestyle changes and pharmacological interventions have failed, surgical treatment is possible. There are different bariatric surgery techniques (*e.g.* adjustable gastric banding, Roux-en-Y gastric bypass, sleeve gastrectomy, bilio-pancreatic diversion with a duodenal switch), all focused on the reduction of calorie intake (Ruban *et al.*, 2019). These surgical interventions show superior effects to non-surgical interventions in regard to weight loss and associated comorbidities (Colquitt *et al.*, 2014).

Obese individuals are prone to develop comorbidities belonging to the spectrum of metabolic syndrome, including dyslipidemia, hypertension and impaired fasting glucose or impaired glucose tolerance (Wilson *et al.*, 2005; Ritchie and Connell, 2007). Patients suffering from diseases of the metabolic syndrome show an increased risk of diabetes mellitus type 2 and cardiovascular disease (Wilson *et al.*, 2005). The underlying diseases can be treated with pharmacological interventions. The treatment of dyslipidemia focuses on lowering of the lipid content of the blood, since VLDL, IDL and LDL act atherogenic. One class of substances used are statins. These agents inhibit the rate-limiting enzyme in the cholesterol synthesis, HMG-CoA reductase (Endo, 1992). Less cholesterol directly decreases the amount of VLDL particles produced by the liver and in turn LDL particles in the circulation. At the same time, cells sense low cholesterol concentration in cells and react by upregulating the LDLR on the cell surface. This leads to increased LDL uptake from the blood. By removing cholesterol from the circulation, statins exert a positive effect on coronary events (Goldstein and Brown, 2015). Hypertension is treatable with different medications such as thiazides, beta-blockers or ACE inhibitors (Wright, Musini and Gill, 2018). These substances lower blood pressure through different modes of action and patients often need to receive more than one drug to control high blood pressure (Go *et al.*, 2014). Impaired glucose tolerance is treated with acarbose, an anti-diabetic drug. Acarbose reversibly inhibits the α-glucosidase, thereby blocking the breakdown of complex carbohydrates into absorbable monosaccharides. This leads to a reduction of postprandial hyperglycemia (Martin and Montgomery, 1996). Of note, the treatment of the above mentioned conditions can be positively influenced by lifestyle changes regarding diet and exercise (*Manage High Blood Pressure | cdc.gov*, accessed: 18 May 2023; Santaguida *et al.*, 2005; Tonkin and Byrnes, 2014).

2 Objective

In recent years, obesity has been recognized to be a major contributor to morbidity and mortality globally and ranked 5th in risk factor assessment for premature death in 2019. Obese individuals are prone to suffering from metabolic diseases, due to a chronic low-grade inflammation caused by the massively increased adipose tissue mass. This chronic low-grade inflammation also alters the systemic immune response, leading to an increased probability of developing severe disease upon infection. For example, during the 2009 H1N1 influenza A pandemic an increased risk of adverse outcome of infection was observed in obese individuals. Further, vaccine protection seems to be diminished in patients suffering from diet-induced obesity. Similar observations were made early in the SARS-CoV-2 pandemic. Obesity was recognized as an independent risk factor for hospitalization, prolonged need of mechanical ventilation and adverse outcome early on. The causes for worse outcomes of infections in obese patients are not yet fully understood. Therefore, the objective of this work was to investigate the role of adipose tissue in SARS-CoV-2 infection.

This study focused on the potential of adipose tissue to serve as a reservoir for SARS-CoV-2 replication and the metabolic consequences of an infection. For this, adipocytes from different origins were subjected to SARS-CoV-2 infection and human autopsy samples were tested for SARS-CoV-2 RNA. Additionally, the Syrian golden hamster model was utilized to investigate the dissemination of SARS-CoV-2 from the lung to the adipose tissue and to examine the subsequent tissue-specific immune activation.
Further, the dysregulation of the lipid metabolism following SARS-CoV-2 infection was characterized in golden hamsters as well as in human patients.

The results of this work provide a basis for further investigation into the relevance of adipose tissue in SARS-CoV-2 infection.

3 Materials and Methods

3.1 Materials

3.1.1 Chemicals

Chemical	Manufacturer
4',6-diamidino-2-phylindole (DAPI)	Thermo Scientific
Atorvastatin	biomol
Avicel RC-591 MCC/Carboxymethylcellulose	DUPONT
Bovine serum albumin (BSA)	Sigma-Aldrich/Merck
Crystal violet	Merck
Ethanol	Sigma-Aldrich/Merck
Ethanol (denatured, for disinfection)	Sigma-Aldrich/Merck
Hydrochloric acid (HCl, 37 %)	Merck
Paraformaldehyde	AppliChem
Paraformaldehyde solution (EM-grade, 20%)	Electron Microscopy Sciences
Polyinosinic-polycytidylic acid sodium salt	Sigma-Aldrich/Merck
Potassium chloride (KCl)	Merck
Potassium dihydrogen phosphate (KH_2PO_4)	Merck
Pursept A-Express, for disinfection	Schülke & Mayr AG
Saponin	Sigma-Aldrich/Merck
Sodium Chloride (NaCl)	Chemsolute
Sodium dihydrogen phosphate (NaH_2PO_4)	Merck
Tetrahydrolipstatin	biomol
Triton X-100	Merck
TRIzol™	Life Technologies
Tween 20 (pure)	Serva
Virkon S	MedicAnimal

Table 2: Chemicals

3.1.2 Buffers and solutions

Buffers/Solutions	Content/manufacturer

Avicel solution (2.5 %)	25 g of Avicel in 1 l ddH$_2$O (autoclaved)
SuperBlock™ T20 (TBS) Blocking-Puffer	Thermo Scientific
Crystal violet solution	1 g of Crystal violet in 1 l Paraformaldehyde solution (4 %)
Fluoromount G	Thermo Scientific
Immunofluorescence permeabilization/staining buffer	D-PBS
	3 % BSA
	0.2 % Saponin
Paraformaldehyde solution (4 %, for general fixation)	40 g of Paraformaldehyde in 1 l PBS
Paraformaldehyde solution (4 %, for immunofluorescence)	100 ml of D-PBS
	20 ml of 20 % EM-grade PFA solution
Phosphate buffered saline (PBS) (1x)	diluted from 10 x PBS
PBS (10x)	1.37 M NaCl
	26.8 mM KCl
	51.3 mM NaH$_2$PO$_4$·2H$_2$O
	17.6 mM KH$_2$PO$_4$
	pH 7.2-7.4
	autoclaved
Ribolock RNase inhibitor (40 U/µl)	Thermo Scientific
RNAprotect Tissue Reagent	Qiagen
RNAse free H$_2$O	Gibco/Life Technologies
SYBR Green PCR Mastermix	Thermo Fisher
Washing buffer (IAV-NP staining)	1 x PBS
	0.05 % Tween 20

Table 3: Buffers of solutions

3.1.3 Commercial kits

Kit	Manufacturer
High Capacity cDNA RT kit	Invitrogen
innuPREP RNA mini Kit 2.0	Analytik Jena
MxP Quant 500 Kit	Biocrates Life Sciences
NucleoSpin RNA/Protein kit	Macherey & Nagel
QIAamp Viral RNA Mini Kit	Qiagen

quanty COVID-19v2 kit	Clonit
RealStar SARS-CoV-2-RT-PCR Kit 1.0	Altona Diagnostics
Venor®GeM Classic Mycoplasma PCR Detection Kit	Minerva Biolabs GmbH

Table 4: Commercial kits

3.1.4 Antibodies

Antibodies	Species/dilution/manufacturer
anti-influenza A NP antibody primary	mouse, 1:1000, abcam ab43821
anti-mouse IgG-HRP	rabbit, 1:1000, Southern Biotech SBA-6170-05
anti-SARS-CoV-2 NP antibody clone 4A8 (primary)	mouse, 1:1000, Histosure, Synaptic Systems HS-452011
anti-mouse Alexa Fluor 488 (secondary)	donkey, 1:1000, Invitrogen A-21202

Table 5: Antibodies

3.1.5 Animals

Species	Sex	Age	Provider
Hamster-RjHan:AURA	male	8-12 weeks	Janvier-Labs
Hamster-RjHan:AURA	female	8-12 weeks	Janvier-Labs

Table 6: Animals

3.1.6 DNA Oligonucleotides

Oligonucleotides	Sequence/manufacturer
Acaca forward	5'-GTGGCATTGAAGGAGCTGTC-3'
Acaca reverse	5'-ACATGGTGTCAGGACGTTCT-3'
Ace2 forward	5'-CAGAGGGAGCAGATGGCTAC-3'
Ace2 reverse	5'-CCCACATGTCACCAAGCAAA-3'
Acly forward	5'-GACTACGTCCTGTTCCACCA-3'
Acly reverse	5'-AACAGGCCAGAGATGAAGCT-3'
Ccl2 forward	5'-AGCCAGACTCCGTTAACTCC-3'
Ccl2 reverse	5'-GGGTCAGCACAGATCTCTCT-3'
Ccl5 forward	5'-GCTGTCCTCACTGTCATCCT-3'
Ccl5 reverse	5'-CACACTTGACGGGTTCCTTCG-3'

Fabp4 forward	5'-CCATCCGAACAGAGAGCACA-3'
Fabp4 reverse	5'-ACCCTCACGCTTCCTCTTTA-3'
Fasn forward	5'-GCTCACGCTTCGGAAACTAG-3'
Fasn reverse	5'-TCTGCACTGAGTTGAGTCGT-3'
Il6 forward	5'-TCACCTCTGGTCTTCTGGACT-3'
Il6 reverse	5'-TCTGGACCCTTTACCTCTTGTT-3'
Isg15 forward	5'-TGAGAGAGAGCAGCCAGAAG-3'
Isg15 reverse	5'-CTTTCATGGACCAGGCGTTG-3'
Lpl forward	5'-AGAGCGACTCCTACTTCAGC-3'
Lpl reverse	5'-AAACACTGCGGGGTCTTTTC-3'
TaqMan assay for human ACE2	Thermo Fisher assay ID: Hs01085333_m1
Tbp forward	5'-CGGTTTGCTGCTGTCATCAT-3'
Tbp reverse	5'-AGCCCAACTTTTGCACAACT-3'
Tnfa forward	5'-GCATTGCTGTGTCCTACGAG-3'
Tnfa reverse	5'-AGTCGGTCACCTTTCTCCA-3'

Table 7: DNA oligonucleotides

3.1.7 Narcotics and Supplements

Substance	Manufacturer
Ketamine (100 mg/ml)	WDT
Narcoren (pentobarbital)	Boehringer Ingelheim Vetmedica
Sodium chloride solution 0.9 %	B. Braun Melsungen AG
Xylazine (20 mg/ml)	WDT

Table 8: Narcotics and supplements

3.1.8 Eukaryotic cell lines

Cell line	Origin/manufacturer
hMSC-TERT20	Telomerase immortalized cell line, Kassen lab, Odense
Madin-Darby Canine Kidney (MDCKII)	immortalized canine kidney cell line, ATCC CRL-2936
Vero E6	African green monkey kidney cell line, ATCC (CCL-81), CVCL_0059

Table 9: Eukaryotic cell lines

3.1.9 Media and supplements for eukaryotic cell culture

Medium/supplement	Content/Manufacturer
Albumin solution from bovine serum, 35 % (BSA)	Sigma-Aldrich/Merck
Basal Medium (hMSC-TERT20)	DMEM Glutamax high glucose
	5 % FBS
	1 % P/S
Cryoconservation medium	FBS, 10 % DMSO
Dexamethasone (Glucocorticoid)	Sigma-Aldrich/Merck
Differentiation medium (hMSC-TERT20 to adipocytes)	Basal medium
	0.1 µM Dexamethasone
	450 µM IBMX
	2 µM Insulin
	1 µM Rosiglitazone
	1 µM U0126
DMSO (Dimethylsulfoxid)	Sigma-Aldrich/Merck
Dulbecco's Modified Eagle Medium (DMEM)	Sigma-Aldrich/Merck
Dulbecco's Modified Eagle Medium (DMEM) Glutamax high glucose	Gibco
Dulbecco's Modified Eaglem Medium (DMEM) Glutamax low glucose	Gibco
Dulbecco's Phosphate Buffered Saline (D-PBS)	Sigma-Aldrich/Merck
Fetal Bovine Serum (FBS) Superior	Biochrom GmbH
Growth Medium (hMSC-TERT20)	DMEM Glutamax high glucose
	10 % FBS
	1 % P/S
Growth Medium (MDCKII)	MEM
	10 % FBS
	1 % L-Glutamine
	1 % P/S
Growth medium (Vero E6)	DMEM
	10 % FBS
	1 % L-Glutamine
	1 % P/S
	1 % P/S
IBMX (3-isobutyl-1-methylxanthine)	Sigma-Aldrich/Merck

Infection medium (coronavirus hMSC-TERT20)	Basal medium
Infection medium (influenza virus hMSC-TERT20)	Basal medium without FBS
	0.2 % BSA
	1 µg/ml TPCK-treated trypsin
Infection medium (coronavirus Vero E6)	DMEM
	5 % FBS
	1 % L-Glutamine
	1 % P/S
Infection medium (influenza virus MDCKII)	MEM
	0.2 % BSA
	1 % L-Glutamine
	1 % P/S
	1 µg/ml TPCK-treated trypsin
Insulin	Sigma-Aldrich/Merck
L-Glutamine (200 mM)	Sigma-Aldrich/Merck
L-(tosylamido-2-phenyl) ethyl chloromethyl ketone (TPCK)-treated trypsin	Sigma-Aldrich/Merck
Minimal Essential Medium (MEM)	Sigma-Aldrich/Merck
Modified Eagle Medium 2x (2x MEM) without Phenol red	Gibco
Overlay medium for plaque test	1:1 mixture of 2x MEM (+0.4 % BSA, 2 % L-Glutamine, 2 % P/S) and 2.5 % Avicel in H_2O
Penicillin/Streptomycin (P/S), 10,000 Units penicillin, 10 mg streptomycin	Sigma-Aldrich/Merck
Rosiglitazone (antidiabetic drug)	Cayman chemical
Trypsin-EDTA	Sigma-Aldrich/Merck
U0126 (MEK inhibitor)	Calbiochem

Table 10: Media and supplements for eukaryotic cell culture

3.1.10 Virus strains

Virus strain	Origin
A/Hamburg/NY1580/09 (H1N1)	Sigrid Baumgarte, Institut für Hygiene und Umwelt, Hamburg, Germany

A/Anhui/1/13 (H7N9)	John McCauly (National Institute of Medical Research, London, UK)
SARS-CoV-2/Germany/ Hamburg/01/2020 ENA study PRJEB41216 and sample ERS5312751	Leibniz Institute of Virology, Hamburg, Germany

Table 11: Virus strains

3.1.11 Consumables

Article	Manufacturer
12-well tissue culture plate	Sarstedt
24-well tissue culture plate	Falcon/BD Biosciences
6-well tissue culture plate	Sarstedt
96-well tissue culture plate	Sarstedt
Cannula BD Microlance™ 3 (26G x 3/8 ", 0.45 mm x 10 mm)	BD Microlance
Capillaries (EDTA tubes for blood collection)	Kabe Labortechnik GmbH
Cryo vials (2.0 ml)	Sarstedt
Metal beads (Ø 2.0 mm)	Retsch (#22.455.0010)
Microscopy Coverslips round (Ø 13 mm)	VWR
Microscopy slides	Carl Roth GmbH & Co. KG
Millex-HA filter (0.45 µM)	Merck
Parafilm (Laboratory film)	VWR
PCR tubes	Sarstedt
Pipette filter tips (10, 100, 200, 1000 µl)	Sarstedt
Reaction tubes (1.5, 2.0 ml)	Sarstedt
Safe seal reaction tubes (2.0 ml)	Sarstedt
Screw cap tubes (2.0 ml)	Sarstedt
S-Monovette® Serum-Gel	Sarstedt
S-Monovette® Lithium-Heparin-Gel	Sarstedt
Syringe TERUMO®, without needle, U-100 Insulin (1 ml, 6 % Luer)	TERUMO Cooperation
Syringe Omnifix® (3 ml / Luer Lock Solo)	B. Braun Melsungen AG
T25 cell culture flask	Sarstedt
T75 cell culture flask	Sarstedt
Transfer pipettes (5, 10, 25 ml)	Sarstedt

Table 12: Consumables

3.1.12 Safety equipment

Article	Manufacturer
Duct tape Extra Universal	TESA
Particulate respirator mask Aura^{TM} type 9332 FFP3	3M
Gloves Biogel	Mölnlycke Health Care GmbH
Gloves Latex	Kimberly-Clark
Gloves purple nitrile	Kimberly-Clark
Lab coat	Leiber
Lab shoes	Suecos
OP mask	Mölnlycke Health Care GmbH
OP nurse cap	Mölnlycke Health Care GmbH
OP pants	Sattelmacher
safety goggles	UVEX
shoe covers	Ansell Health Care
TYVEK® 500 boot covers	DUPONT
TYVEK® overalls classic/Xpert 500	DUPONT

Table 13: Safety equipment

3.1.13 Laboratory equipment

Article	Manufacturer
Animal scale	Kern
AQUITY UPLC I-Class (UPLC system)	Waters
Biological Safety cabinet HeraSafe KS12	Thermo Scientific
Biological Safety cabinet HeraSafe KS18	Thermo Scientific
Centrifuge 5417R	Eppendorf
Centrifuge 5810R	Eppendorf
Centrifuge Varifuge 3.0R	Thermo Scientific
Confocal laser scanning microscope C2 plus	Nikon
Cryoconservation container	Nalgene
Heraeus temperature-controlled CO_2 incubator B6120	Thermo Scientific
Heraeus temperature-controlled CO_2 incubator BBD 6220	Thermo Scientific

Heraeus temperature-controlled CO_2 incubator Heracell 150	Thermo Scientific
LightCycler® 96	Roche
Magnetic stirrer MR3001	Heidolph
Microliter pipettes Eppendorf Research 2 (1-10, 10-100, 20-200, 100-1000 µl)	Eppendorf
Mixer mill MM 400	Retsch
Multichannel pipettes (12 channel, 5-50, 20-200 µl)	Brand
Nikon Ts2 inverse light microscope	Nikon
Nanodrop 1000 (ND-1000) spectrophotometer	peqlab
Nanophotometer	Implen
pH meter pHenomenal®	VWR
Pipetus	Hirschmann
Precision scale Extend ED224S	Sartorius
Pressure manifold	Waters
Quantstudio 5 Real time PCR system	Thermo Scientific
reversed phase chromatography column C18	Biocrates
Shaker WT17	Biometra
Shaking waterbath SW22	Julabo
Surgical forceps	F.S.T.
Surgical scissors	F.S.T.
Thermostat Precitherm PFV	Labora Mannheim
Vortex-Mixer 7-2020	neoLab
Xevo TQ-S (mass sprectrometer)	Waters

Table 14: Laboratory equipment

3.1.14   Software

Software	Provider
Graphpad Prism (Version 9.2)	Graphpad
ImageJ/Fiji	NIH
LightCycler® 96 software, V 1.1.0.1320	Nikon
Microsoft Office	Microsoft
NIS-Elements	Nikon
R package MetabAnalystR	GitHub

Table 15: Software

3.2 Methods

3.2.1 Ethics statement

The Ethics Committee of the Hamburg Chamber of Physicians reviewed and approved the sampling from laboratory-confirmed COVID-19 and non-COVID-19 patients (PV7311, 2020-10353-BO-ff, WF-051/20, WF-053/20).

All animal experiments were carried out in strict accordance to the guidelines of the German animal protection law and were reviewed and approved by the Behörde für Gesundheit und Verbraucherschutz, State of Hamburg, Germany (N032/2020).

3.2.2 Collection of human samples

Tissue samples, including lung, liver, subcutaneous and mesenteric white adipose tissue were collected during the clinical autopsies of 30 deceased, laboratory-confirmed COVID-19, patients (18 male, 12 female). The autopsies were performed at the Institute of Legal Medicine of the University Medical Center Hamburg-Eppendorf, Hamburg, Germany. The median post-mortem interval was 5 days. The tissue samples were stored at -80° C until further processing.

Plasma samples from 38 male COVID-19 patients (median age 63 ± 19.7 years) were collected at the Intensive Care Unit of the University Medical Center Hamburg-Eppendorf on the day of admission (Schroeder *et al.*, 2021). As controls, plasma samples from 8 healthy male donors of approximately the same age were collected at the Blood Donation Center of the University Medical Center Hamburg-Eppendorf.

3.2.3 *In vivo* experiments in Syrian golden hamsters

In this study we used Syrian golden hamsters for *in vivo* studies, since early in the pandemic the Syrian golden hamster was shown to be suitable animal model for the investigation of SARS-CoV-2 pathogenesis (Sia *et al.*, 2020). The animals used here were purchased from Janvier. The 8-12 week-old male and female hamsters were housed under standard conditions (21 ± 2° C, 40-50 % humidity, food and water *ad libitum*) and a 12:12 h light-dark cycle in individually ventilated cages (IVC) at the Leibniz Institute of Virology. The hamsters showed normal behavior and were in good health prior to infection. The infections with SARS-CoV-2 were performed under BSL-3 conditions.

3.2.3.1 Narcosis of Syrian golden hamsters

The animals were anesthetized with 150 mg/kg ketamine and 10 mg/kg Xylazine, prepared in sterile 0.9 % sodium chloride solution, by intraperitoneal (i.p.) injection. The dosage was calculated according to the animal weight and applied with a 1 ml syringe and a 26G cannula.

3.2.3.2 Intranasal infection of Syrian golden hamsters

After the animals were anesthetized (described in 3.2.3.1), the hamsters were infected by intranasal inoculation with 10^5 plaque forming units (p.f.u.) SARS-CoV-2. As controls 1 mg/kg poly(I:C) or D-PBS was used. For inoculation, 80 µl of the respective inoculum was applied into the nostrils of the animals using a microliter pipette. After that, the breathing was observed and the hamsters were placed in their home cage. Over the course of infection (up to 6 days), the animals were monitored and weighed on a daily basis.

3.2.3.3 Collection of blood and organs of the hamsters

Blood and organs of the animals were harvested 1, 3 or 6 days post infection. The animals were euthanized by with an overdose of pentobarbital (800mg/kg) applied intraperitoneally (i.p.). Afterwards, blood was collected into EDTA tubes by cardiac puncture. For plasma collection from whole blood, the EDTA tubes were centrifuged at 2,500 x g for 10 min. The plasma was aliquoted and stored at -80° C until further processing. The weight of subcutaneous adipose tissue was recorded and the samples were homogenized in 1 ml of sterile D-PBS with 5 stainless steel beads at 30 Hz for 10 min using the Mixer mill MM 400 and stored at -80° C until further processing. For gene expression analysis, adipose tissue was cut and incubated for at least 24 h in RNAprotect Tissue Reagent at 4° C and subsequently stored at -80° C.

3.2.4 Cell culture techniques

3.2.4.1 Cultivation of eukaryotic cells

Vero E6 cells were cultured in DMEM, supplemented with 10 % FBS, 1 % L-Glutamine and 1 % P/S. MDCKII cells were maintained in MEM, supplemented with 10 % FBS, 1 % L-Glutamine and 1 % P/S. hMSC-TERT20 cells were cultured in growth medium (DMEM Glutamax high glucose, supplemented with 10 % FBS and 1 % P/S). All cells were grown in a

temperature-controlled incubator at 37° C, 5 % CO_2 and 95 % relative humidity. All eukaryotic cell lines used in this study were regularly tested for *Mycoplasma sp.* contamination using the Venor®GeM Classic Mycoplasma PCR Detection Kit according to the manufacturer's instructions.

3.2.4.2 Freezing and thawing of eukaryotic cells

Eukaryotic cells were kept in liquid nitrogen for long term storage. Cells from a confluent T75 cell culture flask were trypsinized and centrifuged at 1000 x g for 5 min at room temperature. The cell pellets were re-suspended in cryoconservation medium, aliquoted into cryo vials and transferred to the cryoconservation container. The samples were then frozen at -80° C for at least 24 h before transfer to the liquid nitrogen storage.

For re-cultivation, frozen cells from the liquid nitrogen storage were transported on dry ice to the cell culture and thawed in the water bath at 37° C. To remove DMSO, the cells were washed once in their respective growth medium, centrifuged at 300 x g for 5 min. The pellets were then re-suspended in 5 ml of warm growth medium, seeded into T25 cell culture flasks and grown at 37° C, 5 % CO_2 and 95 % relative humidity.

3.2.4.3 Differentiation of hMSC-TERT20 cells into adipocytes

For adipogenic differentiation, hMSC-TERT20 cells were seeded in 12-well plates and grown in growth medium to confluence (day 0). After washing the cells once with D-PBS, the medium was switched to differentiation medium (Basal medium, supplemented with 0.1 μM dexamethasone, 450 μM IBMX, 2 μM insulin, 1 μM rosiglitazone and 1 μM U0126). The differentiation medium was renewed three times per week for 2 weeks. Prior to infection experiments, all additives were washed out by replacing the differentiation medium with basal medium for 48 h.

3.2.5 Virological techniques

3.2.5.1 Propagation of SARS-CoV-2 in Vero E6 cells

The SARS-CoV-2 stock (SARS-CoV-2/Germany/Hamburg/01/2020) was propagated on Vero E6 cells. The cells were grown in T75 cell culture flasks until they reached approximately 90 % confluency. The growth medium was replaced by 10 ml infection medium (DMEM, 5 % FBS, 1

% L-Glutamine, 1 % P/S) and inoculated with 10 µl of virus stock. The cells were incubated at 37° C, 5 % CO_2 and 95 % relative humidity for 72 h. Afterwards, the cytopathic effect (CPE) was observed and the supernatants of two to three flasks were united. The supernatants were centrifuged at 2000 x g and 4° C for 10 min. To remove remaining cell debris, the supernatant was filtered through a 0.45 µm syringe filter and aliquoted in cryo vials á 100 µl. All aliquots were stored at -80° C and the virus titer was determined by plaque assay (described in 3.2.5.7) after one freeze-thaw cycle. Propagation as well as titration were carried out under BSL-3 conditions.

3.2.5.2 Propagation of influenza A virus in MDCKII cells

The 2009 pandemic H1N1 (pH1N1) influenza A virus(A/Hamburg/NY1580/09) and the H7N9 influenza A virus (A/Anhui/1/13) were propagated in MDCKII cells. The cells were grown in T75 flask until they reached approximately 90 % confluency. Growth medium was replaced by infection medium (MEM, supplemented with 0.2 % BSA, 1 % L-Glutamine, 1 % P/S, 1 µg/ml TPCK-treated trypsin) and inoculated with 10 µl of the respective virus stock. The cells were incubated at 37° C, 5 % CO_2 and 95 % relative humidity for 16 to 48 h depending on the observed CPE. After appropriate incubation time the supernatants of two to three T75 flasks were united, centrifuged at 2000 x g, 4° C for 10 min and filtered through a 0.45 µm syringe filter before being aliquoted á 100 µl. All aliquots were stored at -80° C and the virus titer was determined by plaque assay (described in 3.2.5.7) after one freeze-thaw cycle. Propagation as well as titration was carried out under BSL-2 conditions for H1N1 and BSL-3 conditions for H7N9.

3.2.5.3 Replication kinetics of SARS-CoV-2 and influenza A virus in hMSC-TERT20-derived adipocytes

To determine the growth of SARS-CoV-2, 2009 pH1N1 and H7N9 in hMSC-TERT20-derived adipocytes, cells were differentiated in 12-well tissue culture plates (described in 3.2.4.3). The cells per well were counted and the virus stock volume for a multiplicity of infection (MOI) of 0.35 was calculated. The inoculum was set up in basal medium (without FBS). The basal medium was removed and cells were washed once with D-PBS. Cells were then inoculated with 150 µl virus solution per well of either SARS-CoV-2/Germany/Hamburg/01/2020, A/Hamburg/NY1580/09 or A/Anhui/1/13 and incubated for 45 min at 37° C, 5 % CO_2 and 95 % relative humidity. After the incubation, the inoculum was removed and cells were washed three

times with D-PBS and 1 ml of appropriate infection medium was added. 200 µl of supernatants were collected at 0, 24, 48 and 72 h post infection and stored at -80° C until titration. Infection and titration were carried out under BSL-2 conditions for H1N1 and BSL-3 conditions for SARS-CoV-2 and H7N9.

3.2.5.4 Replication kinetics of SARS-CoV-2 in of hMSC-TERT20-derived adipocytes of different maturity status

To investigate the influence of the differentiation status of hMSC-TERT20-derived adipocytes on SARS-CoV-2 replication, cells were infected at different stages of the differentiation. Infection with SARS-CoV-2 was carried out as described in 3.2.5.3 at days 0, 5, 7 and 14 of differentiation. Infection and titration (described in 3.2.5.3 and 3.2.5.7) were performed under BSL-3 conditions.

3.2.5.5 Replication kinetics of SARS-CoV-2 in primary adipocytes

To assess the growth of SARS-CoV-2 in primary hamster adipocytes, 8-12 week old male and female Syrian golden hamsters were euthanized with an overdose of pentobarbital (800 mg/kg). Subcutaneous, visceral and brown adipose tissue was collected and cells were grown on 24-well tissue culture plates. Before infection, cells per well were counted and the virus stock volume for an MOI of 0.35 was calculated. The inoculum was set up in infection medium (DMEM, 2 % FBS, 0.5 % L-Glutamine, 0.5 % P/S). The growth medium was removed, cells were washed once with D-PBS and 100 µl of inoculum per well was added. The cells were incubated for 45 min at 37° C, 5 % CO_2 and 95 %. After incubation, the cells were washed three times with D-PBS and 1 ml of infection medium was added to each well. 200 µl of supernatants were collected at 0, 24, 48 and 72 h post infection and stored at -80° C until titration. Infection and titration were carried out under BSL-3 conditions.

For assessment of replication in human primary adipocytes, patient adipose tissue was provided by the Department of General, Visceral and Thoracic Surgery at the University Medical Center Hamburg-Eppendorf, Hamburg, Germany. Cells were grown on 24-well tissue culture plates and counted before infection to calculate the virus stock volume needed for an MOI of 0.35. The inoculation was set up in infection medium (DMEM, 2 % FBS, 0.5 % L-Glutamine, 0.5 % P/S). The growth medium was removed, cells were washed once with D-PBS and 100 µl of inoculum was added per well. The cells were incubated for 45 min at 37° C, 5 % CO_2 and 95 %, subsequently washed three times with D-PBS and 1 ml of infection medium

was added to each well. Supernatants were collected at 0, 24, 48 and 72 h post infection and stored at -80° C until further processing. Virus titers were determined by plaque assay. Infection and titration were carried out under BSL-3 conditions.

3.2.5.6 Replication kinetics of SARS-CoV-2 in adipocytes treated with Atorvastatin and Tetrahydrolipstatin

In order to determine the effect of the manipulation of the lipid metabolism on SARS-CoV-2 growth in hMSC-TERT20-derived and primary Syrian golden hamster adipocytes, the cells were treated with two clinically approved substances, Atorvastatin (Atorva) and Tetrahydrolipstatin (THL). For hMSC-TERT20-derived adipocytes, the basal medium was changed to basal medium containing either 10 µM Atorvastatin, 50 µg/ml THL or the combination of both substances 4 h prior to infection. The cells, grown on 12-well tissue culture plates, were infected with SARS-CoV-2 as described in 3.2.5.3, but in the presence of the substances. For primary Syrian golden hamster adipocytes, the cells were collected and grown on 24-well plates (described in 3.2.5.5). At 4 h prior to infection the growth medium was changed to infection medium supplemented with either 10 µM Atorva, 50 µg/ml THL or the combination of the two compounds. Infection with SARS-CoV-2 was performed as described in 3.2.5.5. After incubation, the cells were washed three time with D-PBS and 1 ml infection medium, containing either Atorva, THL or the combination was added to each well. 200 µl of supernatants was collected after 0, 24 and 48 h and stored at -80° C until titration. Infection and titration (described in 3.2.5.3 and 3.2.5.7) were performed under BSL-3 conditions.

3.2.5.7 Determination of viral titers by plaque assay

To determine viral titers in infectious samples from cell culture supernatants or organ homogenates, a plaque assay using a semi-viscose overlay medium was performed according to a modified protocol following Matrosovich *et al.*, 2006. For titration of SARS-CoV-2 Vero E6 cells are used, whereas influenza A viruses were titrated on MDCKII cells.
For the plaque assay, the samples were diluted in D-PBS in a 10-fold dilution series. The cells were seeded on 12-well tissue culture plates for the titration of supernatants from virus-infected cells. The growth medium was removed, the cells were washed once with D-PBS, inoculated with 150 µl per well of the virus dilutions and incubated for 30 min at 37° C, 5 % CO_2 and 95 % relative humidity. The plates were swiveled every 5-10 min to avoid dehydration. Afterwards, 1.5 ml of overlay medium with 1 µg/ml TPCK-treated trypsin was added to each well. The cells

were then incubated at 37° C, 5 % CO_2 and 95 % relative humidity for 72 h. After the incubation, the overlay medium was removed, the cells washed once with D-PBS and 1 ml of 4 % PFA was added to each well. The cells were kept at 4° C for at least 30 min.

Virus stocks and organ homogenates were titrated following the same protocol, but using 6-well plates, 333 µl of virus dilutions, 3 ml of overlay medium per well and 2 ml of 4 % PFA for fixation.

SARS-CoV-2 and H7N9 viral titers could be detected by counterstaining with crystal violet solution due to the formation of large visible plaques in the cell layer.

The titers of 2009 pH1N1 IAV were determined by influenza A nucleoprotein-specific antibody staining. After the removal of the 4 % PFA solution, cells were permeabilized with PBS containing 0.3 % Triton X-100 for 30 min. Afterwards, the cells were incubated with 200 µl (12-well) or 400 µl (6-well) of the primary anti-IAV-NP antibody for 1 h at room temperature. Cells were then washed three times with washing buffer (PBS, 0.05 % Tween 20) and then incubated with 200 µl (12-well) or 400 µl (6-well) of the secondary HRP-coupled anti-mouse antibody for 1 h at room temperature. Both antibodies were diluted 1:1,000 in Superblock buffer. After the second antibody incubation, cells were washed twice. For detection, the HRP substrate containing True-Blue dye was applied to the cells.

Plaques were then counted in each well and the plaque forming units per milliliter (p.f.u./ml) or per gram tissue (p.f.u./g) were calculated.

3.2.6 Nucleic acid techniques

3.2.6.1 Isolation of total RNA from hMSC-TERT20-derived adipocytes

Total RNA from hMSC-TERT20-derived adipocytes was isolated using TRIzol™ and the innuPREP RNA mini kit 2.0. Medium was removed and cells were washed once with D-PBS. 1 ml of TRIzol™ reagent was added to each well and incubated for 5 min at room temperature to achieve complete lysis of the cells. The lysed cell solution was then transferred to a 2 ml reaction tube and stored at -80° C until further processing. To isolate RNA, the samples were thawed and 250 µl of chloroform were added, followed by 30 seconds of vigorous shaking to ensure the thorough mix of chloroform and lysed cell solution. Following a centrifugation at 12,000 x g, 4° C for 15 min, the aqueous phase was transferred to the spin filter D from the innuPREP RNA mini kit 2.0 and centrifuged at 11,000 x g, 4° C for 2 min. Ethanol was added to each flow-through in 1:1 (v:v) ratio. Isolation continued using the NucleoSpin RNA Mini kit according to the manufacturer's instructions. The RNA content and quality was measured using the Implen Nanophotometer. Samples were directly processed further or stored at -80° C until processing.

3.2.6.2 Isolation of viral RNA from human autopsy samples

Human tissue samples, including lung, liver and adipose tissue, collected from autopsies (described in 3.2.2) were thawed and homogenized in 1 ml sterile D-PBS and 5 stainless steel beads at 30 Hz for 10 min with the Mixer mill MM 400. Viral RNA was isolated using the QIAamp Viral RNA Mini Kit following the manufacturer's instructions.

3.2.6.3 Isolation of total RNA from hamster adipose tissue

In order to isolate total RNA from adipose tissue of hamsters, the samples, conserved in RNAprotect, were homogenized in 1 ml TRIzol^{TM} and 5 stainless steel beads at 30 Hz for 10 min in the mixer mill MM 400. Afterwards, 350 µl of chloroform was added to each sample followed by vigorous shaking for 30 seconds to ensure complete mix of chloroform and the lysed tissue solution. Subsequently, all samples were centrifuged at 13,000 rpm, 4° C for 15 min. The aqueous phase was carefully transferred to spin filter D from the innuPREP RNA mini kit 2.0 and centrifuged at 10,000 x g, room temperature for 2 min. The flow-through was collected and mixed with ethanol in a ratio of 1:1 (v:v). Further isolation was performed according to the manufacturer's instructions including an on column DNase digestion. RNA samples were mixed with Ribolock RNase inhibitor (0.75 µl/30 µl) and stored at -80° C until further use.

3.2.6.4 Detection of SARS-CoV-2 in human autopsy samples

Following isolation of viral RNA from human autopsy samples (described in 3.2.6.2) SARS-CoV-2 RNA was detected by qRT-PCR using the RealStar SARS-CoV-2 RT-PCR Kit 1.0 and the quanty COVID-19v2 Kit following manufacturer's instructions. SARS-CoV-2 RNA-positve tissue samples were examined in a plaque assay in order to determine the amount of viable virus particles (described in 3.2.5.7).

3.2.6.5 Analysis of gene expression in hamster adipose tissue

After total RNA isolation from hamster adipose tissue (described in 3.2.6.3) cDNA was prepared from the RNA (400 ng input) with the High-Capacity cDNA Archive Kit following manufacturer's instructions. SYBR green primers, which were premixed with SYBR green PCR master mix were used to analyze the gene expression in the adipose tissue. The analysis was

performed with the Quantstudio 5 Real Time PCR system and primers listed under 3.1.6. The relative mRNA levels were calculated using the $\Delta\Delta CT$ method and data were normalized to housekeeping genes.

3.2.6.6 ACE2 expression analysis in hMSC-TERT20-derived adipocytes

Total RNA from hMSC-TERT20-derived adipocytes was defrosted and cDNA was prepared using the High-Capacity cDNA Archive Kit according to the manufacturer's instructions (400 ng RNA input). Gene expression of ACE2 was analyzed using TaqMan Assays for human ACE2 (listed under 3.1.6) following the manufacturer's instructions.

3.2.7 Microscopy techniques

3.2.7.1 Preparation of hMSC-TERT20-derived adipocytes for immunofluorescence analysis

For immunofluorescence analysis of SARS-CoV-2 infected hMSC-TERT20-derived adipocytes, cells were grown on microscopy coverslips in 12-well tissue culture plates. Following SARS-CoV-2 infection (described in 3.2.5.3) with an MOI of 5, cells were fixed in 4 % EM-grade PFA 48 h post infection. Samples were kept at 4° C until further processing.

3.2.7.2 Immunofluorescence staining of SARS-CoV-2 infected hMSC-TERT20-derived adipocytes

For the immunofluorescence staining, the 4 % EM-grade PFA was removed from the cells and samples were washed once with 1 ml of D-PBS. Subsequently, the adipocytes were incubated with immunofluorescence permeabilization buffer for 10 min at room temperature. The primary antibody (mouse-anti-SARS-CoV-2-NP) was diluted 1:1,000 in immunofluorescence permeabilization buffer and a 50 µl drop was applied to a sheet of parafilm in a wet chamber. Coverslips with the samples were then placed upside down on the antibody solution and incubated over night at 4° C. The next day, samples were washed 3 times with 1 ml D-PBS for 2 min each and then incubated in a mix of secondary antibody (donkey-anti-mouse Alexa Fluor 488) diluted 1:1000 and DAPI (diluted 1:1,000) in immunofluorescence permeabilization buffer. Following a 1 h incubation period in the dark, samples were washed 3 times with 1 ml

D-PBS for 2 min each in the dark. Subsequently, each sample was washed once in double distilled H_2O to wash off all remaining salts and then mounted on a microscopy slide using the mounting medium Fluoromount G. Microscopy slides were incubated at room temperature in the dark over night for the mounting medium to dry. Samples were then either stored in the dark at room temperature or directly imaged using with the confocal laser scanning microscope C2 plus. Analysis of the images was performed using ImageJ/Fiji software.

3.2.8 Metabolomic analysis of human and hamster plasma samples

For targeted metabolomic analysis, plasma samples from laboratory-confirmed COVID-19 patients and healthy controls (described in 3.2.2) as well as from Syrian golden hamsters (described in 3.2.3.3) were collected. They were inactivated with ethanol at a sample-solvent ratio of 1:2 (v:v). The samples were processed using the MxP Quant 500 kit following the manufacturer's instructions and the acquired data was processed with the R package MetaboAnalystR (described in detail in Zickler *et al.*, 2022).

3.2.9 Statistical Analyses

The data presented in this work are expressed as mean ± standard error of the mean (SEM). When two groups were compared, student's t test was used. Comparison of more than two groups was performed with analysis of variance (ANOVA) followed by Sidak's or Tukey's correction for multiple comparison. Because gene expression data were not normally distributed, log transformation was performed prior to statistical analysis.

Since the work was exploratory and the availability of tissue samples was limited, the experimental sample sizes were not predetermined. All samples were processed, and data was acquired without regard to the specificity of the sample.

No criteria for exclusion or inclusion of samples were used for data analysis. Statistical calculations and graphical representation of the data were performed with Microsoft Excel and Graphpad prism 9.2. Statistical significance was defined as $p < 0.05$ (*$p < 0.05$, **$p < 0.01$, ***$p < 0.001$).

3.2.10 Collaborations

All experiments conducted in this study were performed by internal or external collaborators. The collaborations are listed below. Experimental design, data evaluation and interpretation are not included.

3.2.10.1 Provision of patient materials

Plasma samples from COVID-19 patients were provided by study nurses of the intensive care unit of the University Medical Center Hamburg-Eppendorf, Hamburg, Germany.

Contact: Dr. Maria Schröder, Dr. Dominik Jarczak, Dr. Axel Nierhaus, Prof. Dr. Stefan Kluge Intensive Care Unit, University Medical Center Hamburg-Eppendorf, Hamburg, Germany

Plasma samples from healthy individuals were provided by the blood bank at the University Medical Center Hamburg-Eppendorf, Hamburg, Germany.

Contact: Dr. Jens Hiller, Dr. Sven Peine, Institute for Transfusion Medicine, University Medical Center Hamburg-Eppendorf, Hamburg, Germany

Human adipose tissue samples were provided by the Department of General, Visceral and Thoracic Surgery at the University Medical Center Hamburg-Eppendorf, Hamburg, Germany.

Contact: Dr. Oliver Mann, Department of General, Visceral and Thoracic Surgery, University Medical Center Hamburg-Eppendorf, Hamburg, Germany

Tissue samples from deceased COVID-19 patients were provided by the Institute of Legal Medicine at the University Medical Center Hamburg-Eppendorf, Hamburg, Germany.

Contact: Fabian Heinrich, Prof. Dr. Klaus Püschel, Prof. Dr. Benjamin Ondruschka, Institute of Legal Medicine, University Medical Center Hamburg-Eppendorf, Hamburg, Germany

3.2.10.2 Measurement of gene expression

Measurement of gene expression in hMSC-TERT20-derived adipocytes and hamster subcutaneous adipose tissue was performed at the Department of Biochemistry and Molecular Cell Biology at the University Medical Center Hamburg-Eppendorf, Hamburg, Germany.

Contact: Dr. Ludger Scheja, Prof. Dr. Jörg Heeren, Department of Biochemistry and Molecular Cell Biology, University Medical Center Hamburg-Eppendorf, Hamburg, Germany

3.2.10.3 Measurement of human plasma triglycerides

Measurement of COVID-19 patient and healthy control plasma triglyceride levels was performed at the Institute for Clinical Chemistry and Laboratory Medicine at the University Medical Center Hamburg-Eppendorf, Hamburg, Germany.

Contact: Prof. Dr. Thomas Renné, Institute for Clinical Chemistry and Laboratory Medicine, University Medical Center Hamburg-Eppendorf, Hamburg, Germany

3.2.10.4   Metabolomic measurements

Metabolomic measurements of COVID-19, healthy control and hamster plasma was conducted at the Institute for Clinical Chemistry and Laboratory Medicine at the University Medical Center Hamburg-Eppendorf, Hamburg, Germany.

Contact: Prof. Hartmut Schlüter, Institute for Clinical Chemistry and Laboratory Medicine, University Medical Center Hamburg-Eppendorf, Hamburg, Germany.

3.2.10.5   Processing and analysis of metabolomic data

The processing and analysis of metabolomic measurement data was performed at the Department of Computational Biology for Infection Research at the Helmholtz Center for Infection Research, Braunschweig, Germany.

Contact: Dr. Andreas Kloetgen, Department of Computational Biology for Infection Research, Helmholtz Center for Infection Research, Braunschweig, Germany

4 Results

4.1 Replication of SARS-CoV-2 in adipocytes

4.1.1 SARS-CoV-2 replicates in adipocytes *in vitro.*

Early in the SARS-CoV-2 pandemic, obesity was identified as a risk factor for hospital admission and severe disease in patients (Lighter *et al.*, 2020).

Initially, it was investigated if human adipocytes are permissible for SARS-CoV-2 infection. For this, stem cell-derived adipocytes (hMSC-TERT20) were infected with SARS-CoV-2, and with the seasonal 2009 pH1N1 and the highly pathogenic avian H7N9 Influenza strains as controls.

In hMSC-TERT20-derived adipocytes, efficient replication of SARS-CoV-2 (Fig. 4 A, black bars) was observed starting from 24 h post infection (p.i.), reaching its peak at 48 h p.i. and the virus titer remained unchanged at 72 h after infection. Interestingly, the highly pathogenic avian H7N9 Influenza A virus subtype showed replication comparable to SARS-CoV-2 in these adipocytes (Fig. 4 A, grey bars). In contrast, the seasonal 2009 pH1N1 Influenza A virus subtype did not grow in hMSC-TERT20-derived adipocytes, as indicated by the highly significant difference in virus titers when compared to SARS-CoV-2 and H7N9 (Fig. 4 A, white bars).

To verify SARS-CoV-2 infection of hMSC-TERT20-derived adipocytes, cells were mock infected or infected at an MOI of 5.0 and then processed for immunofluorescence analysis at 48 h post infection. As expected, no SARS-CoV-2 viral proteins was detected by antibody staining against SARS-CoV-2 NP in the uninfected control (Fig. 4 B, left panel, Mock). Conversely, SARS-CoV-2 protein was clearly visible in the cytoplasm of infected cells (Fig. 4 B, right panel, SARS-CoV-2). Plaque assay titration, performed in parallel with the same samples, corroborated the findings of the immunofluorescence analyses: SARS-CoV-2 replicated efficiently in the hMSC-TERT20-derived adipocytes, shown in Fig. 4 C.
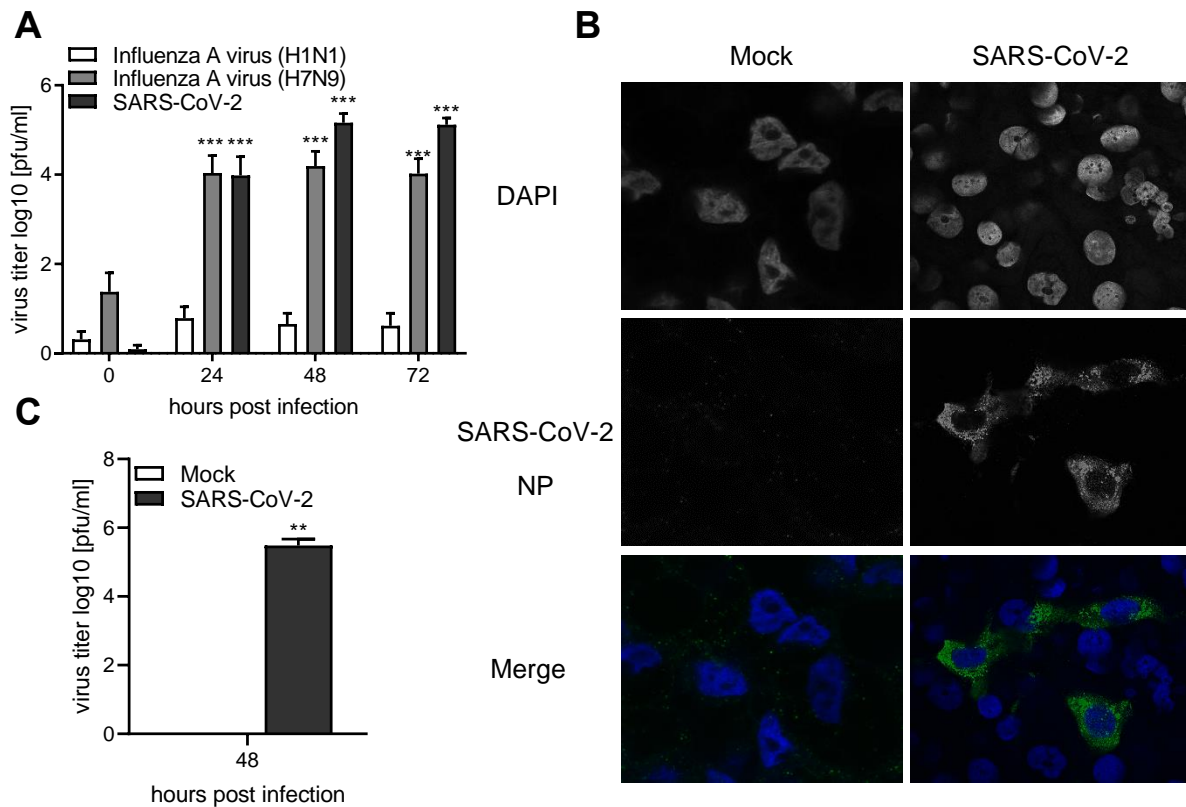
Figure 4: Infection of stem cell-derived adipocytes with SARS-CoV-2, seasonal 2009 pH1N1 and highly pathogenic H7N9 influenza A virus. hMSC-TERT20-derived adipocytes were infected with SARS-CoV-2 (SARS-CoV-2/Germany/Hamburg/01/2020), seasonal 2009 pH1N1 (A/Hamburg/NY1580/09) or highly pathogenic avian H7N9 (A/Anhui/1/13) influenza A virus. **A)** Immortalized human mesenchymal stem cells were differentiated to mature adipocytes and infected with SARS-CoV-2 (black bars), pH1N1 (white bars) or H7N9 influenza A virus (grey bars) at an MOI of 0.35. Supernatants were taken at indicated timepoints and virus titers were determined by plaque assay. **B)** hMSC-TERT20-derived adipocytes were infected with SARS-CoV-2 at an MOI of 5.0. After 48 h of infection, supernatants were collected, and samples were processed for immunofluorescence analysis. Nuclei were stained with DAPI (upper panel), viral protein was stained using an anti-SARS-CoV-2 NP primary and an Alexa Fluor 488 donkey anti-mouse secondary antibody (middle panel). In the merged image (lower panel) nuclei are visualized in blue, SARS-CoV-2 NP in green. Confocal microscopy was performed using the Nikon confocal laser scanning microscope C2 plus and the accompanying software. **C)** Supernatants from the immunofluorescence samples (uninfected control (white bar) and SARS-CoV-2 infected (black bar)) were analyzed for virus replication. Virus titers were determined by plaque assay. Statistical significance of titer differences between infected and uninfected samples was determined by multiple t-tests with Welsh correction and defined as $p < 0.05$ (*$p < 0.05$, **$p < 0.01$, ***$p < 0.001$).

In the following, it was investigated if adipose tissue could pose as a reservoir for SARS-CoV-2 replication. For this, we utilized the Syrian golden hamster model, a suitable animal model for the investigation of SARS-CoV-2 pathogenesis (Sia *et al.*, 2020). Different adipose tissue depots (brown, subcutaneous and visceral) from three male and female Syrian golden hamsters each were collected. The isolated adipocytes were grown *ex vivo* in cell culture and infected with SARS-CoV-2. Efficient viral replication in all adipocytes from different depots from male and female Syrian golden hamsters was observed (Fig. 5 A, B). Although virus titers

differed between adipocyte types, the data showed that in both male and female hamsters, the replication was highest in visceral adipocytes throughout the course of infection (0-72 h post infection, male, blue bars; female, red bars). To analyze if SARS-CoV-2 is also able to replicate in human fat tissue, subcutaneous and visceral adipose tissue samples from one donor were provided by collaborators at the University Medical Center Hamburg-Eppendorf. Following *ex vivo* cell culture, these cells were also infected with SARS-CoV-2. In primary human adipocytes, SARS-CoV-2-replication in both subcutaneous and visceral adipose tissue was also observed (Fig. 5 C). In contrast to the Syrian golden hamster adipocytes, no marked difference in virus titers between the two adipose tissue depots was noticed, but rather a similar replication until 72 h post infection, at which timepoint the virus titer in visceral adipocytes declined. Because the number of human samples analyzed was very limited compared to the samples of Syrian golden hamsters due to availability, these analyses would have to be repeated in order to draw a reliable conclusion.
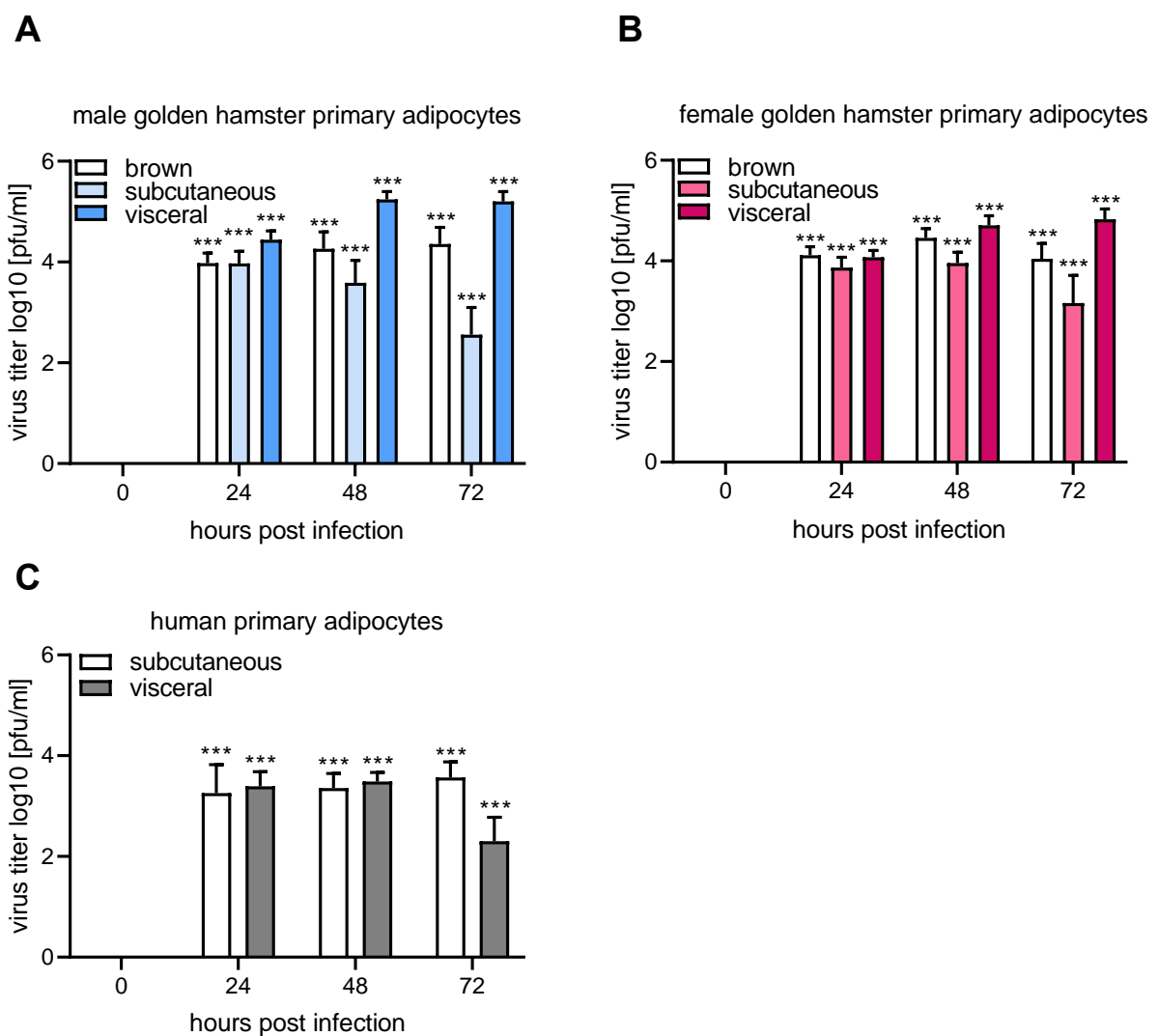
A

male golden hamster primary adipocytes

B

female golden hamster primary adipocytes

C

human primary adipocytes

Figure 5: SARS-CoV-2 infection of primary hamster and human adipocytes. Primary adipocytes from different adipose tissue depots of three male and female Syrian golden hamsters each, as well as primary human adipocytes from one donor were collected, cultured *ex vivo*, and infected with SARS-CoV-2 at an MOI of 0.35. Supernatants were taken at indicated timepoints and virus titers were determined by plaque assay. **A)** Infection of male golden hamster primary brown (white bars), subcutaneous (light blue bars) and visceral (blue bars) adipocytes. **B)** Infection of female golden hamster primary brown (white bars), subcutaneous (light red bars) and visceral (red bars) adipocytes. **C)** Infection of primary human subcutaneous (white bars) and visceral (grey bars) adipocytes. Statistical significance of titer differences between infected and uninfected samples determined by two-way ANOVA and defined as $p < 0.05$ (*$p < 0.05$, **$p < 0.01$, ***$p < 0.001$).

4.1.2 Replication of SARS-CoV-2 in adipocytes depends on their maturity.

The experiments for the previously shown results were carried out in mature, fully differentiated hMSC-TERT20-derived and primary adipocytes. In the following, the permissibility of undifferentiated mesenchymal stem cells (hMSC-TERT20) and preadipocytes to SARS-CoV-2 infection was analyzed, to assess the relevance of adipocyte maturity for SARS-CoV-2 infection.

For this, hMSC-TERT20-derived adipocytes were infected with SARS-CoV-2 at different stages of differentiation on day 0, 5, 7 and 14 (full differentiation). SARS-CoV-2 replicated neither in undifferentiated hMSC-TERT20 cells (Fig. 6 A, white bars) nor in cells differentiated for 5 days (Fig. 6 A, light grey bars) over the course of infection. On day 7 of differentiation, moderate replication of SARS-CoV-2 was visible, starting at 24 h p.i.. Virus titers started to decline at 72 h p.i.. Compared to 0 and 5 days of differentiation, the virus titer at day 7 of differentiation was significantly increased (Fig. 6 A, grey bars). The most efficient replication of SARS-CoV-2 was observed in fully differentiated adipocytes after 14 days of differentiation, starting at 24 h p.i. with the peak at 48 h and a slight decline in virus titer at 72 h after infection. Throughout the course of infection, the SARS-CoV-2 titer in fully differentiated cells was significantly higher, when compared to all other differentiation stages, indicating that full maturity is a prerequisite for efficient replication of SARS-CoV-2 (Fig. 6 A, dark grey bars).

To elucidate one possible reason for the observed differences in SARS-CoV-2 growth at the different stages of maturity, the gene expression levels of the main entry receptor for SARS-CoV-2, ACE2, were examined in undifferentiated as well as fully mature hMSC-TERT20-derived adipocytes. The data showed that ACE2 was not expressed at all in undifferentiated hMSC-TERT20 cells on day 0 (Fig. 6 B, day 0). In contrast, the ACE2 expression was found to be massively increased by the timepoint of full differentiation (day 14), illustrated by the highly significant rise in *ACE2* gene copy numbers on day 14, when compared to day 0 (Fig. 6

B, day 14). This result showed that one reason for the lack of SARS-CoV-2 replication in undifferentiated hMSC-TERT20 cells and adipocytes in early stages of differentiation (day 5) is the absence of the entry receptor ACE2. This corroborates the finding that full adipocyte maturity is a requirement for efficient replication of SARS-CoV-2.
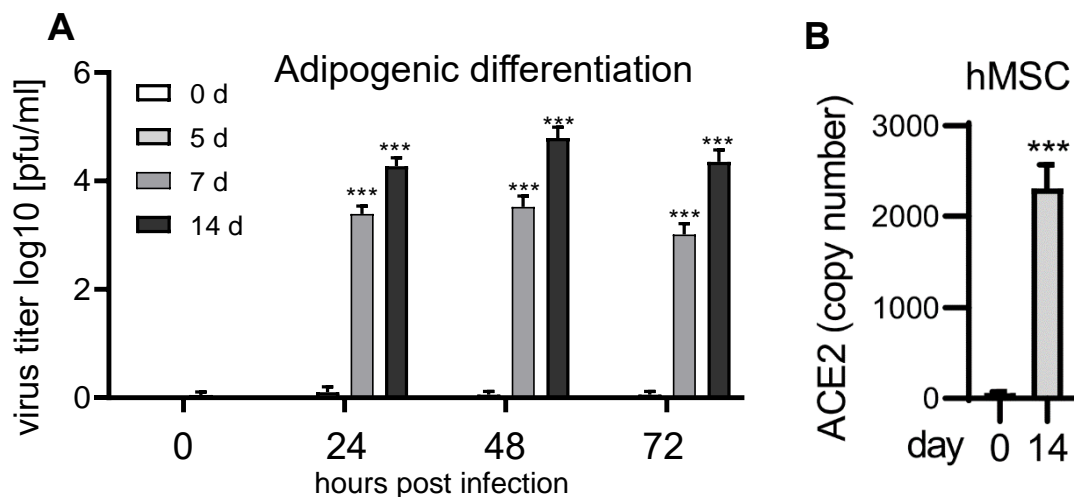
Figure 6: SARS-CoV-2 infection of hMSC-TERT20-derived adipocytes of different maturity and entry receptor gene expression analysis. hMSC-TERT20-derived adipocytes were infected at different stages of differentiation and the expression of the SARS-CoV-2 entry receptor ACE2 was assessed. **A)** Stem cell-derived adipocytes were infected with SARS-CoV-2 at day 0 (white bars), 5 (light grey bars), 7 (grey bars) and 14 (dark grey bars) of differentiation at an MOI of 0.35. Supernatants were taken at indicated timepoints. Virus titers were determined by plaque assay. **B)** hMSC-TERT20 cells were either differentiated to mature adipocytes for 14 days (grey bar) or left undifferentiated (day 0, white bar). RNA was isolated and ACE2 gene expression was assessed by qPCR. Statistical significance of titer (**A**) or expression (**B**) difference between the different timepoints was determined by two-way ANOVA and multiple t-tests with Welsh correction and defined as $p < 0.05$ (*$p < 0.05$, **$p < 0.01$, ***$p < 0.001$).

4.1.3 Manipulation of the lipid metabolism reduces the replication of SARS-CoV-2 in mature adipocytes *in vitro*.

Overweight and obesity can be treated, among other strategies, by pharmacological manipulation of the lipid metabolism within adipocytes and adipose tissue (described in 1.2.5.2). Since virus replication depends on cell metabolism (Mayer *et al.*, 2019), the question whether the alteration of the lipid metabolism had an effect on SARS-CoV-2 replication was addressed. To this end the effect of two clinically approved substances used for the treatment of obesity and high levels of blood lipids was examined. Firstly, Atorvastatin (Atorva), a lipid-lowering drug, and secondly, Tetrahydrolipstatin (THL), an anti-obesity drug. The mechanism of action of both substances is described in 1.2.5.2.

Fully mature hMSC-TERT20-derived adipocytes were treated 4 h prior to infection with one of the compounds or a combination of both. Upon infection with SARS-CoV-2, the viral replication was monitored over the course of 48 h. The Atorva treatment alone (Fig. 7 A, light orange bars) did not have a significant effect on viral growth at 24 h post infection. However, 48 h after infection we observed a significant decrease in SARS-CoV-2 replication of approximately one log in virus titer, when compared to the untreated control (Fig. 7 A, white bars). In contrast, treatment with THL (Fig. 7 A, orange bars) led to a highly significant reduction in virus growth of nearly two log at 24 h as well as 48 h post infection compared to untreated control (Fig. 7 A, white bars). The strongest decrease in SARS-CoV-2 replication, however, was achieved by treatment with a combination of Atorva and THL (Fig. 7 A, red bars). The virus titer decreased highly significantly by approximately three log or 99.9 %, when compared to the untreated control (Fig. 7 A, white bars).

To test the effect of these substances in primary adipocytes, adipose tissue from Syrian golden hamsters was collected and cells were grown *ex vivo*. The infection with SARS-CoV-2 in presence of Atorva, THL, or their combination showed similar results to the infection of hMSC-TERT20-derived adipocytes. Here, treatment with Atorva (Fig. 7 B, light orange bars) alone had no effect on the virus titer after 24 h and only a slight, non-significant reduction in SARS-CoV-2 replication occurred at 48 h post infection compared to the untreated control (Fig. 7 B, white bars). In contrast, THL treatment (Fig. 7 B, orange bars) showed a significant reduction of SARS-CoV-2 replication at 24 as well as 48 h post infection compared to the untreated control (Fig. 7 B, white bars), although the restriction was not as substantial as observed in the hMSC-TERT20-derived adipocytes. The combination of the two substances (Fig. 7 B, red bars) showed a very similar result when compared to the stem cell-derived adipocytes with a highly significant reduction in viral replication compared to the untreated control (Fig. 7 B, white bars) at both 24 and 48 h post infection.

These results showed that manipulation of cholesterol and lipid synthesis, as well as lipid breakdown within adipocytes had a negative effect on SARS-CoV-2 replication.

Next, one possible reason for this treatment-mediated reduction of SARS-CoV-2 replication was investigated. It has been shown recently that statin treatment can downregulate the SARS-CoV-2 receptor expression on the cell surface (Teixeira *et al.*, 2022). Therefore, the possible effect of the drug treatment on ACE2 expression was investigated. To account for possible effects of SARS-CoV-2 infection on receptor expression itself, the experiments were performed without infection as well as in the infection context at the 48 h timepoint post infection.

For this, mature hMSC-TERT20-derived adipocytes were either left untreated (Fig. 7 C, white bars), treated with Atorva or THL only (Fig. 7 C, light orange bars, orange bars, respectively) or with the combination of the two compounds (Fig. 7 C, red bars). The relative gene expression levels of ACE2 were measured by qPCR. The treatment with Atorva showed a highly significant reduction of ACE2 gene expression in the adipocytes compared to the untreated control. The SARS-CoV-2 infection had no effect on the Atorva-mediated consequence. In contrast, THL treatment alone did not show any significant change in receptor gene expression compared to control treated cells, regardless of infection status. The combination treatment with Atorva and THL led to a similar result as the treatment with Atorva alone, reducing the ACE2 gene expression highly significantly, when compared with the untreated control. This was the case in both uninfected and infected cells. This indicated that the strong reduction of receptor expression is mainly caused by Atorva rather than THL treatment.

These results showed that the treatment with these clinically approved drugs has an impact on the gene expression levels of the SARS-CoV-2 entry receptor. Although treatment with THL led to a slight, non-significant, decrease of ACE2 gene expression, Atorva seems to be primarily responsible for the strong reduction of receptor expression when combined with THL. Interestingly, treatment with THL alone showed a stronger reduction in SARS-CoV-2 replication compared to the single treatment with Atorva. This indicated that THL employs a different mechanism to restrict SARS-CoV-2 growth in adipocytes. The highly significant decrease in virus titer after the combination treatment with seemed to be a synergistic effect of the two mechanisms of action.
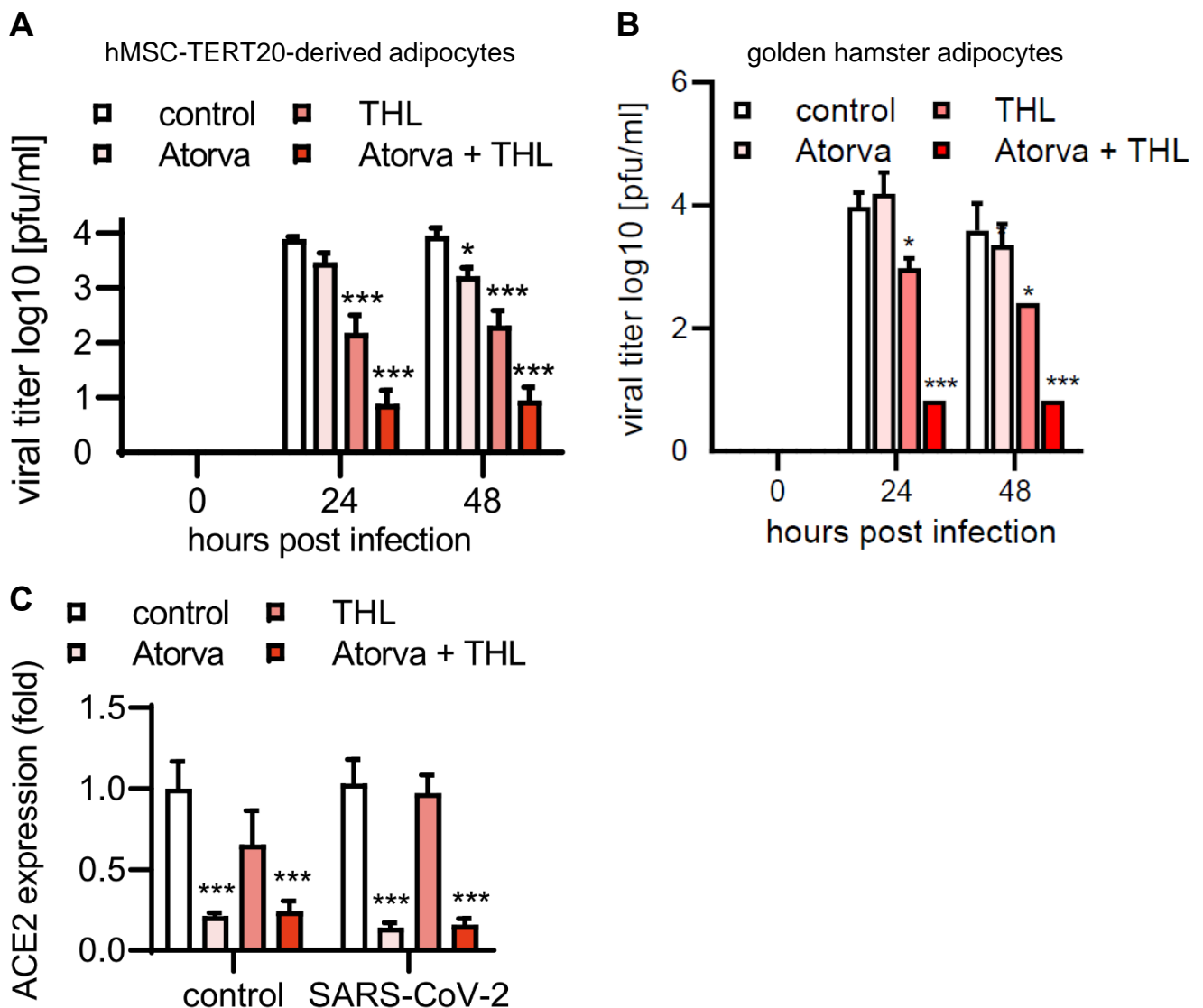
Figure 7: The effect of lipid metabolism manipulation on SARS-CoV-2 replication and ACE2 expression in adipocytes. Mature hMSC-TERT20-derived and primary Syrian golden hamster adipocytes were either left untreated (white bars), treated with Atorva (light orange bars), THL (orange bars) or a combination of Atorva and THL (red bars). The cells were infected with SARS-CoV-2 at an MOI of 0.35 and virus replication was determined. Supernatants were taken at indicated timepoints and virus titers were determined by plaque assay. hMSC-TERT20-derived adipocytes were additionally subjected to ACE2 expression analysis **A)** Mature stem cell-derived adipocytes. **B)** Syrian golden hamster adipocytes **C)** ACE2 gene expression analysis in h-MSC-TERT20-derived adipocytes. The relative ACE2 expression levels were measured by qPCR at 48 h post infection. Statistical significance of titer (**A**, **B**) or expression (**C**) differences between the treatments was determined by multiple t-tests with Welsh correction as $p < 0.05$ (*$p < 0.05$, **$p < 0.01$, ***$p < 0.001$).

4.2 SARS-CoV-2 infection of adipose tissue *in vivo*

4.2.1 SARS-CoV-2 disseminates to the adipose tissue of the Syrian golden hamster and triggers an antiviral immune response.

The previously shown results illustrated that SARS-CoV-2 readily replicates in mature hMSC-TERT20-derived adipocytes, as well as primary adipocytes from Syrian golden hamsters and humans. In the following, the potential of SARS-CoV-2 to infect the adipose tissue of Syrian golden hamsters *in vivo* was analyzed.

To this end, male and female Syrian golden hamsters were infected intranasally with SARS-CoV-2. As uninfected controls, one group of animals was treated with PBS and another group received immune stimulant treatment with poly(I:C) to account for virus-independent immune activation. Subcutaneous adipose tissue of infected was collected on day 1, 3 and 6 post infection for SARS-CoV-2 titration and gene expression analysis of a selection of immune markers including CCL2, CCL5, TNF-α, IL-6, IFN-γ and ISG15.

Intranasal infection of male as well as female Syrian golden hamsters resulted in relatively high titers of SARS-CoV-2 in subcutaneous adipose tissue 1 day post infection (Fig. 8 A, B blue dots). As expected, no virus replication was observed in the uninfected PBS group (Fig. 8 A, B white dots) or the poly(I:C) treated group (Fig. 8 A, B red dots). Over the course of infection, SARS-CoV-2 titers declined, starting on day 3 post infection, and no replication-competent virus particles were found on day 6 after infection in both male and female animals. This result showed that SARS-CoV-2 was cleared within 6 days from the start of infection, indicating an appropriate immune response in adipose tissue of the animals.
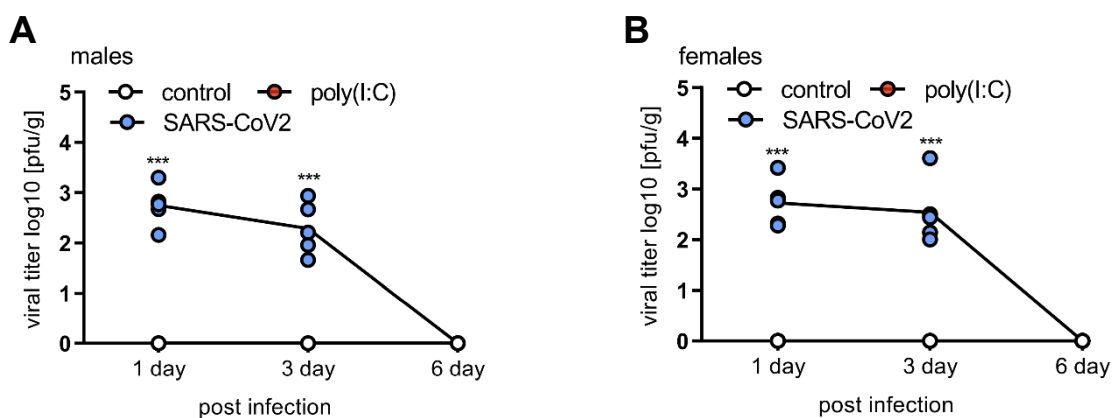
Figure 8: Replication of SARS-CoV-2 in subcutaneous adipose tissue of the Syrian golden hamster *in vivo.* Syrian golden hamsters were either treated with PBS (white dots), poly(I:C) (red dots) or infected with 10^5 pfu SARS-CoV-2 (blue dots). Subcutaneous adipose tissue was collected at indicated timepoints and SARS-CoV-2 titers were determined by plaque assay. **A)** Male Syrian golden hamsters **B)** Female Syrian golden hamsters. Statistical

significance of titer differences between the treatment groups was determined by two-way ANOVA as $p < 0.05$ (*$p < 0.05$, **$p < 0.01$, ***$p < 0.001$).

To examine the induction of a pro-inflammatory immune response in adipose tissue following SARS-CoV-2 infection, mRNA expression of a selection of immune markers was analyzed at the same timepoints as SARS-CoV-2 titers.

In male Syrian golden hamsters, the CCL2 mRNA expression level did not change significantly in any of the treatment groups on day 1 after infection (Fig. 9 A, Ccl2). In contrast, on day 3 and 6 post infection the expression level was significantly downregulated in infected animals compared to uninfected controls (Fig. 9 C, E, Ccl2, blue bars). The CCL5 mRNA expression showed an increasing, but non-significant, trend in infected animals, but not uninfected controls at 1 and 3 days post infection (Fig. 9 A, C, Ccl5, blue bars). At 6 days after infection, the expression was significantly upregulated in the infected versus uninfected animals (Fig. 9 E, Ccl5, blue bars). TNF-α mRNA expression was upregulated in infected animals compared to uninfected controls at 1 day post infection (Fig. 9 A, Tnfa, blue bar), but reverted to basal levels in infected animals on day 3 p.i. and remained comparable to uninfected controls at day 6 after infection Fig. 9 C, E, Tnfa).

For IL-6, a significant upregulation of mRNA expression in the poly(I:C)-treated group was observed on day 1 post infection (Fig. 9 A, Il6, red bar). This significant increase in expression disappeared on day 3 post infection and no significant differences in mRNA expression level between the groups were found on day 3 and 6 after infection (Fig. 9 C, E, Il6). The levels of IFN-γ mRNA expression did not change significantly throughout the course of infection, although a non-significant trend towards elevated expression was noticed in infected animals compared to uninfected controls (Fig. 9 A, C, E, Ifng, blue bars).

The most pronounced changes were found for ISG15. The mRNA expression was upregulated highly significantly in infected, as well as poly(I:C)-treated animals on day 1 post infection (Fig. 9 A, Isg15, blue and red bars respectively). On day 3 after infection the mRNA level in infected animals remained highly significantly elevated, while the poly(I:C)-induced increase in expression was lost at this timepoint (Fig. 9 C, Isg15, blue and red bars respectively). The mRNA expression levels in infected animals reverted to basal levels, comparable to uninfected controls on day 6 post infection (Fig. 9 E, Isg15 blue bar).

In female animals, the mRNA expression of CCL2 did not show any change throughout the course of infection, regardless of the treatment (Fig. 9 B, D, F, Ccl2). CCL5 mRNA was not differentially regulated on day 1 post infection in any treatment group (Fig. 9 B, Ccl5). In contrast, infected animals showed a significant increase in CCL5 mRNA expression on day 3 and 6 post infection compared to uninfected controls (Fig. 9 D, F, Ccl5, blue bars). The levels

of TNF-α and IL-6 mRNA expression remained unchanged in all treatment groups throughout the course of infection (Fig. 9 B, D, F, Tnfa, Il6).

For, IFN-γ a significant increase of mRNA expression in infected animals versus uninfected controls was observed at all sampled timepoints of infection (Fig. 9 B, D, F, Ifng, blue bars). As seen in the male animals, the most pronounced change in mRNA expression was detected for ISG15. On day 1 post infection, the mRNA expression was significantly upregulated in infected and poly(I:C)-treated animals compared to the PBS-treated controls (Fig. 9 B, Isg15, blue and red bars respectively). The poly(I:C)-induced mRNA expression level declined but was still significantly elevated compared to the PBS-treated animals on day 3 post infection (Fig. 9 D, Isg15 red bar). In contrast, the expression level in infected animals remained highly significantly increased compared to the uninfected controls (Fig. 9 D, Isg15, blue bar). On day 6 after infection, the ISG15 mRNA expression level in infected animals reverted to basal levels, comparable to the uninfected controls (Fig. 9 F, Isg15)

In summary, the results in male an female Syrian golden hamsters were similar and showed that i) SARS-CoV-2 successfully disseminated from the lungs to the adipose tissue in male and female Syrian golden hamsters and ii) SARS-CoV-2 infection of the adipose tissue elicited a controlled pro-inflammatory immune response in both sexes.
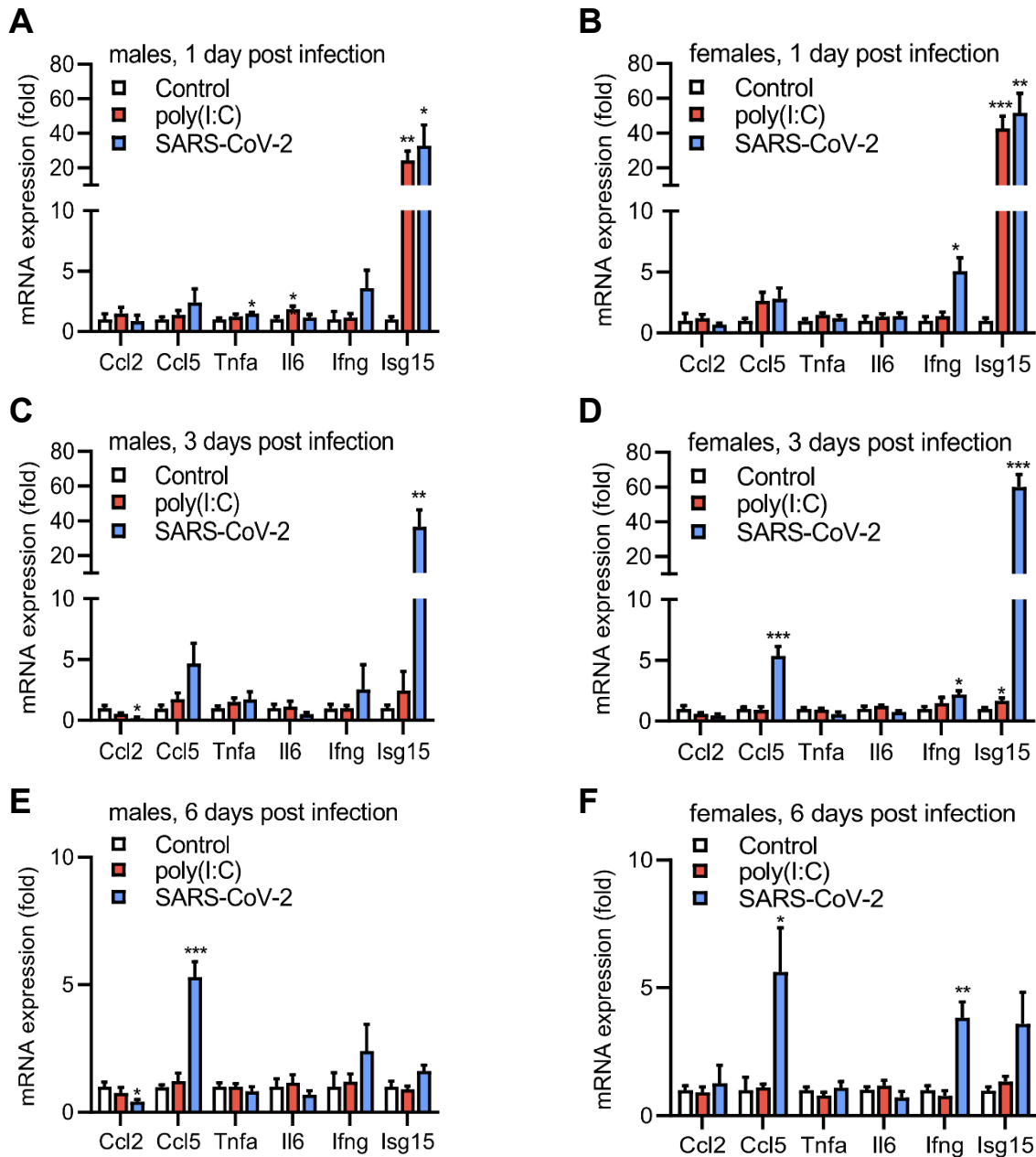
Figure 9: Gene expression analysis of immune markers in subcutaneous adipose tissue of Syrian golden hamsters. Male and female animals were either treated with PBS (control, white bars), treated with poly(I:C) (red bars) or infected intranasally with SARS-CoV-2 (blue bars) and the gene expression of immune markers was analyzed in subcutaneous adipose tissue. **A, C, E)** Expression analysis of immune markers in male Syrian golden hamsters 1, 3 and 6 days post infection. **B, D, F)** Expression analysis of immune markers in female Syrian golden hamsters 1, 3 and 6 days post infection. The gene expression levels of immune markers were determined by qPCR. Statistical significance of expression differences between treatments was determined by two-way ANOVA and defined as $p < 0.05$ (*$p < 0.05$, **$p < 0.01$, ***$p < 0.001$).

4.2.2 SARS-CoV-2 replicates in adipose tissue of human patients.

Results of the Syrian golden hamster model showed that SARS-CoV-2 disseminated from the lung to the adipose tissue of the animals. There it caused infection and triggered a subsequent pro-inflammatory immune response.

In order to investigate if this is also the case in human patients, the dissemination to and infection of human adipose tissue was analyzed.

For this, a patient cohort from the University Medical Center Hamburg-Eppendorf, consisting of 30 patients, of which 18 were male and 12 female, was used. The patients in this cohort all succumbed to laboratory-confirmed COVID-19. Autopsies were performed at the Institute of Legal Medicine of the University Medical Center Hamburg-Eppendorf and tissue samples were collected at a median post-mortem interval of five days. Frozen subcutaneous and visceral adipose tissue (SAT and VAT) as well as lung and liver tissue was acquired. Total RNA was isolated from the tissues and subsequently samples were analyzed for SARS-CoV-2 RNA and ACE2 expression. Tissue samples that proved positive for viral RNA were subjected to plaque assay to determine the titers of viable SARS-CoV-2 particles. The patient cohort was divided by sex, age and BMI and grouped into underweight/normal weight, overweight and obese. The results of analyzed tissues are shown in table 1.

In males, 8 patients presented SARS-CoV-2 RNA in SAT and 5 male VAT samples were positive for viral RNA. Interestingly, 4 of the 5 positive VAT samples were from a donor also positive for SAT. In lung tissue of male patients we found 14 of 16 analyzed samples to be positive for SARS-CoV-2 RNA, while only 4 of 18 liver samples showed detectable viral RNA levels at the time of death.

In females, 2 of 12 SAT, but 5 out of 11 analyzed VAT samples were positive for SARS-CoV-2. Conversely to male patients, the 2 positive SAT samples were from donors also SARS-CoV-2 RNA-positive in VAT. Of the 8 analyzed lung tissue samples, 6 showed the presence of viral RNA and half of the female liver samples were positive for SARS-CoV-2 RNA.

In males as well as females, SARS-CoV-2 RNA in lung tissue was found in all BMI groups, underweight through obese. Curiously, in males, SARS-CoV-2 RNA in SAT and VAT was only found in patient material from donors who were classified as at least overweight (BMI ≥ 25). Furthermore, SARS-CoV-2 RNA-positive liver samples of male donors were only found in the group of obese patients (BMI ≥ 30). No such observation was made in patient material provided by female donors. In addition to the recovery of SARS-CoV-2 RNA from numerous human samples, it was possible to detect replication-competent viral particles in 4 of the analyzed

samples (not shown in table). This indicates that SARS-CoV-2 actively replicated in human adipose tissue.

Overall, the amount of virus RNA found in the adipose tissue of male and female patients does not seem to depend on the level of ACE2 in the respective tissue, although the necessary level of ACE2 for viral entry may differ between individuals. It is important to point out that the level of gene expression and viral RNA as well as the virus titers could be underestimated due to the relatively long post-mortem interval and the associated degradation of patient material. Although there seems to be the possibility of a correlation between the BMI and SARS-CoV-2 RNA-positive adipose and liver tissue in men, it is critical to note that the cohort is too small to draw any reliable conclusions in this regard.

However, these results showed that also in human patients, SARS-CoV-2 disseminated from the lungs to the adipose tissues and actively replicated there. It also showed that the virus was not successfully cleared at the time of death, allowing for detection and quantification of SARS-CoV-2 RNA and viable virus particles.

Sex	Age	BMI (kg/m²)	Adipose tissue (ACE2 expression, copy numbers)		Adipose tissue (SARS-CoV-2, copies / µl)		Lung (SARS-CoV-2, copies / µl)	Liver (SARS-CoV-2, copies / µl)
			subcutaneous	visceral	subcutaneous	visceral		
male	76	16.5	164	105	b.l.d.	b.l.d.	3,05E+03	b.l.d.
male	91	21.1	745	172	b.l.d.	b.l.d.	1,13E+07	b.l.d.
male	72	22.2	33	194	b.l.d.	b.l.d.	5,73E+03	b.l.d.
male	71	25.1	186	165	1,09E+02	1,19E+02	b.l.d.	b.l.d.
male	60	25.8	6382	3647	3,20E+02	7,76E+02	n.d.	b.l.d.
male	85	26.1	15	474	b.l.d.	b.l.d.	1,24E+03	b.l.d.
male	94	26.2	303	744	1,92E+03	b.l.d.	1,25E+07	b.l.d.
male	62	26.6	2101	2093	9,31E+01	b.l.d.	1,72E+05	b.l.d.
male	75	27.7	2694	285	b.l.d.	b.l.d.	3,72E+05	b.l.d.
male	78	28.6	193	140	b.l.d.	b.l.d.	n.d.	b.l.d.
male	76	31.5	1089	812	1,95E+03	b.l.d.	5,12E+00	1,03E+05
male	70	32.2	3250	774	2,76E+03	1,53E+04	9,74E+03	4,31E+03
male	45	32.6	915	1029	b.l.d.	b.l.d.	b.l.d.	b.l.d.
male	75	33.4	386	740	9,38E+02	2,44E+02	5,46E+06	5,84E+04
male	80	34.3	805	2222	b.l.d.	b.l.d.	4,20E+03	2,18E+02
male	79	36.2	b.l.d.	16	b.l.d.	7,98E+01	1,49E+07	b.l.d.
male	80	41.7	b.l.d.	49	2,77E+01	b.l.d.	9,67E+05	b.l.d.
male	26	46.8	1253	38	b.l.d.	b.l.d.	5,16E+01	b.l.d.
female	95	14.1	620	712	1,24E+02	4,78E+02	1,93E+03	4,41E+02
female	67	16.6	590	352	b.l.d.	3,70E+04	b.l.d.	1,81E+03
female	93	17.4	44	436	b.l.d.	b.l.d.	b.l.d.	b.l.d.
female	100	18.3	b.l.d.	418	b.l.d.	b.l.d.	4,93E+02	b.l.d.
female	77	22.2	776	177	b.l.d.	1,60E+03	-	3,79E+01
female	74	25.4	232	340	b.l.d.	-	n.d.	b.l.d.
female	84	27.0	18	271	b.l.d.	1,91E+04	3,58E+06	b.l.d.
female	35	27.4	426	1764	b.l.d.	b.l.d.	n.d.	b.l.d.
female	80	29.8	1855	808	b.l.d.	b.l.d.	2,30E+06	b.l.d.
female	56	36.2	726	3987	b.l.d.	b.l.d.	1,82E+03	1,80E+03
female	64	39.5	2587	1305	b.l.d.	b.l.d.	5,08E+06	2,31E+02
female	37	51.2	1212	1239	3,45E+02	1,23E+02	n.d.	6,97E+03

Below level of detection (b.l.d.), not determined (n.d.)

Table 16: Presence of SARS-CoV-2 in autopsy-derived tissue samples of deceased COVID-19 patients. 30 deceased COVID-19 patients, 18 male (highlighted in blue tones) and 12 female (highlighted in orange tones) were classified by sex, age and BMI (Body-Mass-Index) and further grouped into underweight/normal weight (BMI ≤ 24.9, light blue, light orange), overweight (25 ≤ BMI ≤ 29.9, blue, orange) and obese (BMI ≥ 30, dark blue, dark orange). Tissue samples from subcutaneous and visceral adipose tissue as well as lung and liver were analyzed for the presence of SARS-CoV-2 RNA and, when RNA-positive subjected to plaque assay. 4 tissue samples showed positive for viable virus particles (not shown in table). The median post-mortem interval for tissue sampling was 5 days.

4.3 SARS-CoV-2-mediated dysregulation of the lipid metabolism

4.3.1 SARS-CoV-2 downregulates genes critical for *de novo* lipogenesis in the adipose tissue of Syrian golden hamsters.

Previous results of this work showed that the pharmacological manipulation of the lipid metabolism in stem cell-derived as well as primary Syrian golden hamster and human adipocytes negatively affected SARS-CoV-2 replication (described in 4.1.3).

Based on this, the potential influence of adipose tissue infection with SARS-CoV-2 on the lipid metabolism in Syrian golden hamsters was investigated.

To this end, subcutaneous adipose tissue from SARS-CoV-2 infected male and female animals as well as from the uninfected controls was collected on day 1, 3 and 6 after infection. Following total RNA isolation from the tissue, the mRNA expression levels of a selection of genes, critical for energy homeostasis were analyzed. These included the Acetyl-CoA-carboxylase 1 (ACC1, encoded by Acaca), the ATP citrate lyase (Acly), the fatty acid synthase (Fasn), the phosphoenolpyruvate carboxykinase 1 (Pck1), the fatty acid binding protein 4 (Fabp4) and the lipoprotein lipase (Lpl).
ACC1, ACLY and FASN are critical for fatty acid synthesis (*de novo* lipogenesis, DNL), while PCK1 is a regulator of gluconeogenesis. FABP4 represents a fatty acid transport protein and LPL is involved in the hydrolysis of triglycerides (TGs) from lipoproteins (lipid breakdown).

The analysis in male hamsters revealed that the mRNA expression levels of Acaca did not change significantly between the treatment groups on day 1 and 3 post infection (Fig. 10 A, C, Acaca). After 6 days of infection, the Acaca mRNA level in infected animals were significantly downregulated compared to uninfected controls (Fig. 10 E, Acaca, blue bar). The Acly mRNA expression in infected animals decreased over the course of infection from a significantly increased level on day 1 to a significant downregulation on day 6 post infection compared to uninfected control-treated animals (Fig. 10 A, C, E, Acly, blue bars).
For Fasn, no differential mRNA expression was detected between the different treatment groups on day 1 after infection (Fig. 10 A, Fasn). In contrast, later during infection on day 3

and 6, the mRNA levels were downregulated in a highly significant manner in infected versus uninfected animals (Fig. 10 C, E, Fasn, blue bars). On day 1 after infection Pck1 mRNA was significantly increased in poly(I:C)-treated animals but downregulated significantly in infected animals compared to PBS-treated controls (Fig. 10 A, Pck1, red and blue bars respectively). The poly(I:C)-induced mRNA increase was lost on day 3 and remained comparable with the level of the PBS control on day 6 post infection (Fig. 10 C, E, Pck1 red bars). Conversely, infected animals showed a highly significant increase in Pck1 mRNA on day 3 and 6 post infection compared to uninfected controls (Fig. 10 C, E, Pck1, blue bars). In contrast to the other genes analyzed, no differences in mRNA expression levels were found for Fabp4 throughout the infection (Fig. 10, A, C, E, Fabp4). The mRNA expression of Lpl in infected animals versus uninfected controls decreased steadily over time and reached significant downregulation on day 6 after infection (Fig. 10, A, C, E, Lpl, blue bars).

In female hamsters, Acaca and Acly sowed a transient downregulation of mRNA expression in infected animals compared to uninfected controls on day 3 post infection (Fig. 10 D, Acaca, Acly, blue bars). The mRNA expression recovered to levels comparable to the uninfected control groups by day 6 after infection (Fig. 10 F, Acaca, Acly). The Fasn mRNA level did not significantly change between the treatment groups on day 1 post infection but showed a highly significant decrease in infected animals compared to uninfected controls on day 3 and 6 post infection (Fig. 10 B, D, F, Fasn blue bars).

For Pck1, a transient, but significant, increase of mRNA expression was detected in infected animals compared to uninfected controls on day 3 post infection (Fig. 10 D, Pck1, blue bar). The increase reverted to a level comparable with uninfected controls on day 6 after infection (Fig. 10, F, Pck1). The mRNA expression of Fabp4 remained unchanged between the groups on day 1 and 3 post infection, but was decreased significantly by day 6 post infection in infected animals compared to the uninfected controls (Fig. 10 B, D, F, Fabp4, blue bars). Lpl did not show a differential regulation of mRNA expression between the groups on day one (Fig. 10 B, Lpl). In contrast, on day 3 and 6 post infection, the mRNA level was significantly decreased in infected animals compared to the uninfected control groups (Fig. 10 D, F, Lpl, blue bars).

These results clearly showed that the infection of subcutaneous adipose tissue of male and female Syrian golden hamsters with SARS-CoV-2 affects the different pathways of the energy homeostasis. While the downregulation of genes critical for DNL indicated an interference with this process by SARS-CoV-2, downregulation of Lpl, important for the hydrolysis of TGs from lipoproteins, hinted towards a restriction of lipid breakdown. In contrast, the pronounced upregulation of Pck1, a regulator of gluconeogenesis, indicated a lack of glucose within the cells after infection. It is apparent that SARS-CoV-2 infection profoundly altered the energy metabolism in adipose tissue.
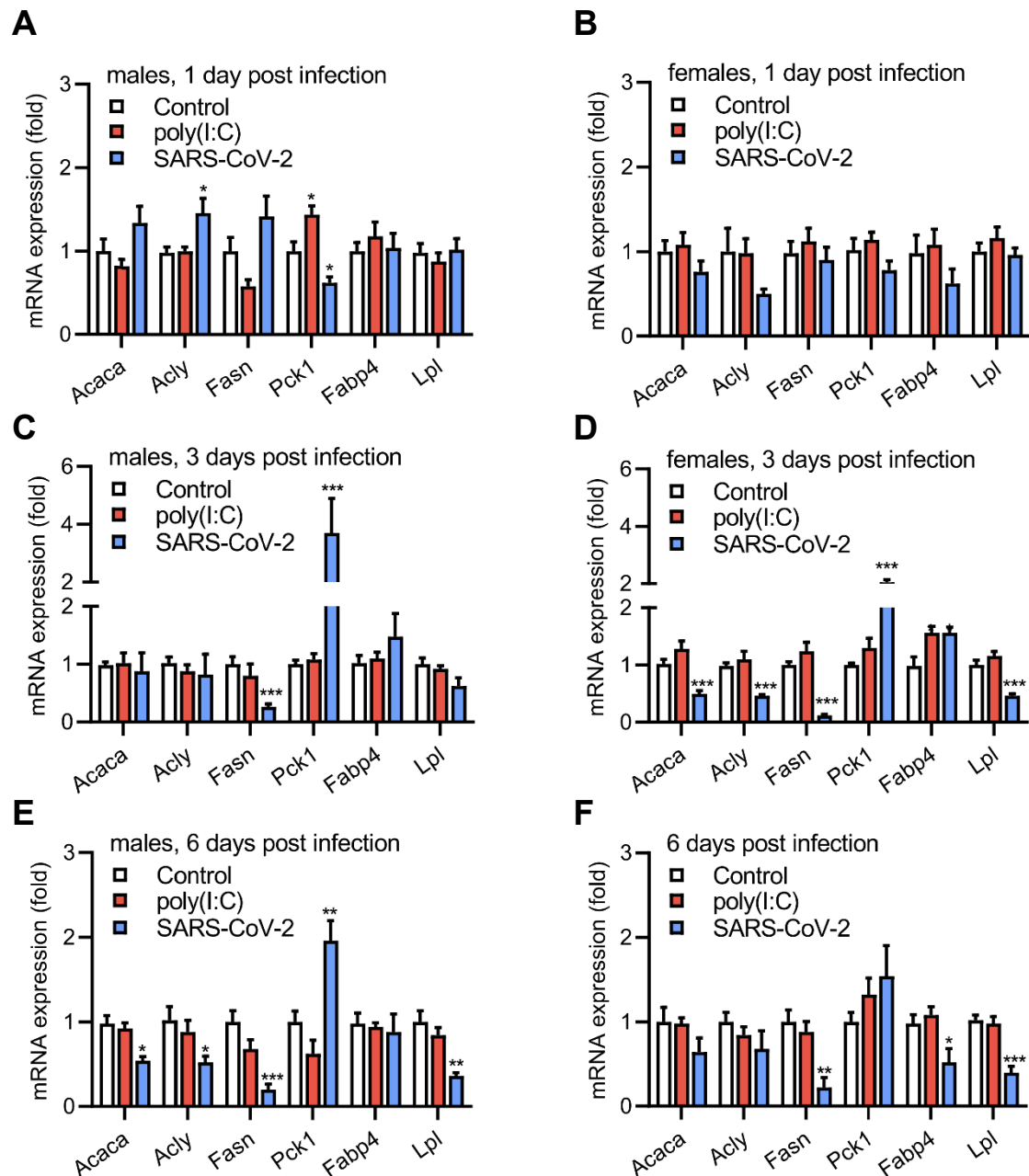
Figure 10: Expression analysis of genes critical for energy homeostasis in subcutaneous adipose tissue upon SARS-CoV-2 infection. Male and female animals were either treated with PBS (control, white bars), treated with poly(I:C) (red bars) or infected intranasally with SARS-CoV-2 (blue bars) and the gene expression of genes related to energy homeostasis was analyzed in subcutaneous adipose tissue. **A, C, E)** Expression analysis of genes related to energy homeostasis in male Syrian golden hamsters 1, 3 and 6 day post infection, respectively. **B, D, F)** Expression analysis of genes related to energy homeostasis in female Syrian golden hamsters 1, 3 and 6 day post infection, respectively. The gene expression levels of immune markers were determined by qPCR. Statistical significance of expression difference between the treatment groups was determined by two-way ANOVA and defined as $p < 0.05$ (*$p < 0.05$, **$p < 0.01$, ***$p < 0.001$).

4.3.2 SARS-CoV-2 infection alters the plasma lipidome of Syrian golden hamsters.

After results showed the organ-specific dysregulation of energy homeostasis, especially the lipid metabolism, in subcutaneous adipose tissue of hamsters following SARS-CoV-2 infection, the systemic consequences of infection were investigated.

For this, a targeted metabolomics approach was utilized. Plasma from uninfected and infected male and female Syrian golden hamsters was collected on day 1, 3, 6 and 14 post infection and subjected to metabolomic analysis. In order to identify the most significantly changed metabolites in male and female hamsters upon infection with SARS-CoV-2, first the relative changes of triglyceride species 1 day versus 3 days post infection were calculated (Fig. 11 A, B respectively). The volcano plots in Fig. 11 A (male) and B (female) show the relative change in targets between day 1 and day 3 after infection in dependence of the false discovery rate (FDR) (-$\log_{10}$ FDR). Only results with a negative $\log_{10}$ FDR $\geq$ 1.3 were considered for evaluation. Positive relative changes are depicted in red, while negative relative changes are shown in blue.

To evaluate the effect of SARS-CoV-2 infection on the systemic metabolite levels, the kinetic changes of the ten most significantly different targets identified by comparison of day 1 versus day 3 post infection were examined. The measurements of these targets from day 3, 6 and 14 post infection were compared to day 1 in order to assess the level of the metabolites over the course of infection. Interestingly, all the targets identified in the first screen were TG species. The results for male and female animals are shown in Fig. 11 C, D respectively.

In male hamsters, the analysis revealed that 6 out of 10 measured TG species were upregulated over the course of infection compared to day 1 post infection. Only one of the upregulated TG species dropped below the level of day 1 post infection before the last measurement on day 14 (Fig. 11 C, red data points). 4 out of 10 TG species were downregulated throughout the course of infection compared to the level on day 1 post infection (Fig. 11 C, blue data points).

The results for plasma from female hamsters differed from the results in male hamsters. Only 1 out of the 10 measured TG species was upregulated compared to day 1 post infection. This TG species also dropped below the level of day one after infection before the end of the 14-day period. Interestingly, this target is the same as the most upregulated TG species in infected male hamsters (Fig. 11 D, red data points). The other nine TG species were downregulated throughout the course of infection. All but one of the TG species recovered the level of 1 day post infection by the last measurement at 14 days after infection (Fig. 11 D, blue data points).

The largest difference in quantity of metabolites in either direction (up-or downregulation) was observed on day 3 post infection in both, male and female animals (Fig. 11 C, D, red and blue data points respectively).

Curiously, the strongest induction was found for TG species enriched in polyunsaturated fatty acids (PUFAs) in plasma from male as well as female hamsters. In contrast, the strongest decrease was observed for TG species containing mainly saturated or monounsaturated fatty acids (SFAs, MUFAs). These species are typical for DNL. This considerable decrease could be a result of the previously shown significant downregulation of DNL-related genes following SARS-CoV-infection (4.3.1).

These results showed that a SARS-CoV-2 infection not only affects the organ-specific lipid metabolism but changes the whole plasma lipidome in male and female Syrian golden hamsters.
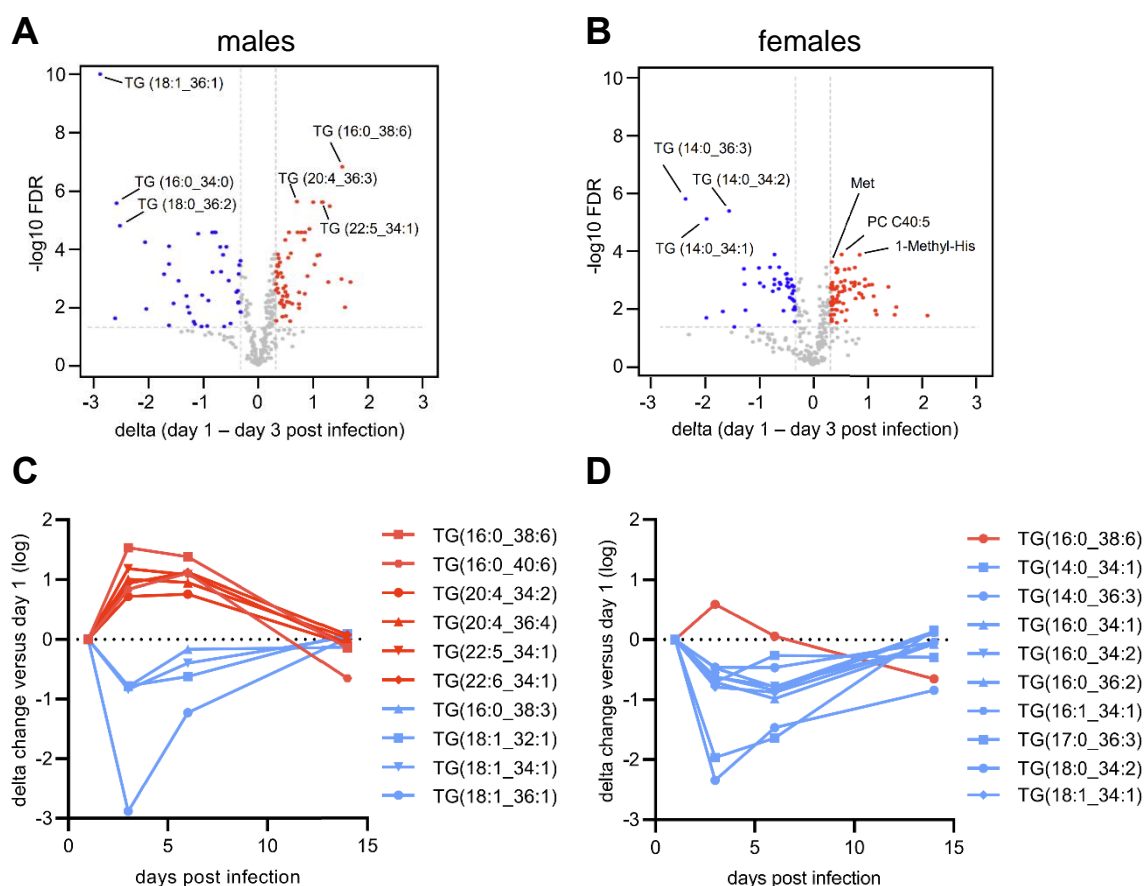
Figure 11: Metabolomic analysis of plasma from SARS-CoV-2 infected Syrian golden hamsters. Male and female Syrian golden hamsters were infected with SARS-CoV-2 and plasma was collected on day 1, 3, 6 and 14 post infection. The plasma was subjected to metabolomic analysis. **A, B)** Comparison of relative changes in metabolite quantity and identification of the 10 most severely dysregulated targets in males (**A**) and females (**B**) between day 1 and 3 post infection. Results with neg. false discovery rates (FDR) ≥ 1.3 are highlighted. **C, D)** Kinetic change of metabolite quantity of the 10 most significantly dysregulated targets throughout 14-day infection period in male (**C**) and female (**D**) animals.

4.3.3 SARS-CoV-2 causes a systemic dysregulation in the lipidome of human patients.

Since earlier data in this work showed that SARS-CoV-2 infection dysregulates the systemic plasma lipidome of Syrian golden hamsters, it was explored whether this could also be observed in human patients.

To this end, a cohort of severely ill SARS-CoV-2 patients at the University Medical Center Hamburg-Eppendorf, Hamburg, Germany was used. Plasma samples from 38 laboratory-confirmed male COVID-19 patients were collected at the day of admission to the intensive care unit (Schroeder *et al.*, 2021). As controls, plasma samples from 8 healthy males, were acquired from the Blood Donation Center at the University Medical Center Hamburg-Eppendorf, Hamburg, Germany. COVID-19 patients and healthy controls were of approximately the same age. Plasma samples were subjected to TG measurement and targeted metabolomic analysis to quantify changes in specific TG species.

The measurement of total plasma TG content revealed that the patients suffering from severe COVID-19 had a tendency towards higher plasma TG levels than their healthy counterparts (Fig. 12 A, blue bar).

The targeted metabolomic analysis of the plasma samples from severely ill male COVID-19 patients showed a very similar result, when compared to the results from male Syrian golden hamsters. The ten most significantly changed plasma TGs are displayed in Fig. 12 B. We found a highly significant decrease in all of these TG species in infected male patients compared to the uninfected controls (Fig. 12 B, blue bars).

Interestingly, all decreased TG species contain saturated and monounsaturated fatty acids, typical for DNL. This indicates a similar mechanism as seen in the male golden hamsters, where these TG species were also decreased in infected animals, possibly due to the downregulation of critical DNL genes by SARS-CoV-2. Unfortunately, the plasma of critically ill female COVID-19 patients was not analyzed, due to lack of availability of samples. Because of that no comparison to the results of female golden hamsters could be made.

However, these results showed that SARS-CoV-2 infection alters the plasma lipidome, not only in the Syrian golden hamster model, but also in human patients.
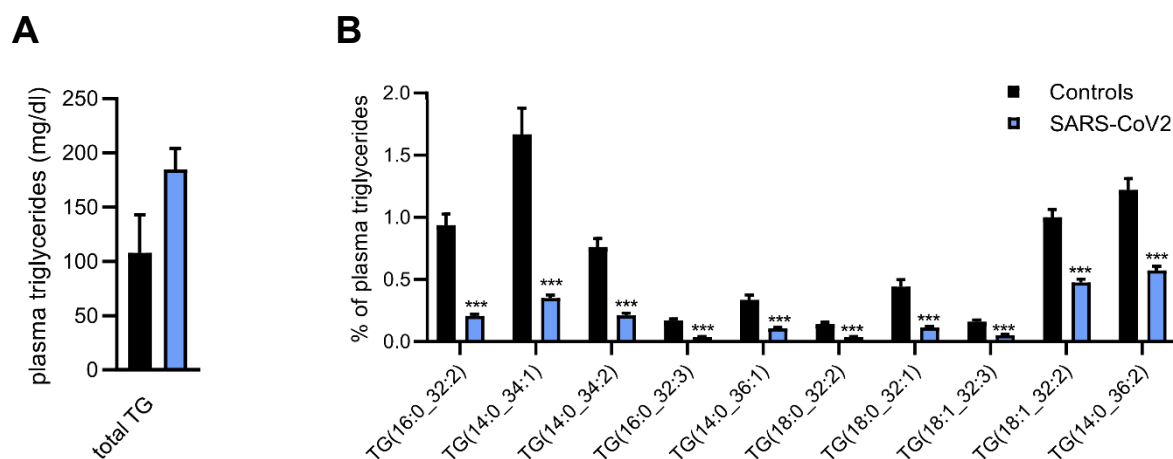
Figure 12: Human patient plasma triglyceride content systemic metabolite changes following SARS-CoV-2 infection. The plasma of 38 male, severely ill COVID-19 patients and 8 healthy controls were subjected to TG measurement and targeted metabolomic analysis. **A)** Comparison of absolute TG content in plasma from healthy individuals and severely ill, male, COVID-19 patients (black and blue bars respectively). **B)** Comparison of metabolite levels of the 10 most dysregulated targets in plasma from healthy individuals and severely ill, male COVID-19 patients (black and blue bars, respectively). Statistical significance of TG level difference between infected and uninfected samples was determined by multiple t-tests with Welsh correction and defined as $p < 0.05$ (*$p < 0.05$, **$p < 0.01$, ***$p < 0.001$).

In summary, the results in this thesis demonstrated the ability of SARS-CoV-2 to infect mature stem cell-derived as well as primary hamster and human adipocytes *in vitro*. Furthermore, we found that pharmacological disruption of the lipid metabolism in adipocytes negatively affects SARS-CoV-2 replication *in vitro*. This indicated that SARS-CoV-2 replication is dependent on a functioning lipid metabolism.

The *in vivo* studies conducted in the Syrian golden hamster model showed that SARS-CoV-2 disseminates from the lung to the adipose tissue of the animals where it causes infection and a subsequent pro-inflammatory response. This dissemination was also observed in human patients by detection of SARS-CoV-2 RNA in the adipose tissue of deceased patients. Higher BMI seemed to support replication in adipose tissue, at least in male patients. Due to the low number of patient samples, this observation remains speculative.

Gene expression analysis of infected subcutaneous adipose tissue in Syrian golden hamsters revealed a profound dysregulation of genes involved the energy metabolism. Genes critical for DNL as well as lipolysis were downregulated in both male and female hamsters upon infection, while a regulatory gene for the gluconeogenesis was upregulated following infection. This indicated a restriction of lipid synthesis and breakdown as well as a dysregulated glucose metabolism in infected adipose tissue.

The metabolomic analysis of plasma from infected hamsters showed a systemic decrease of TG species containing SFA and MUFA, that are typically derived from DNL as well as an

increase in PUFA-containing TGs. This showed that a SARS-CoV-2 infection led to organ-specific and systemic alterations in the lipid metabolism of infected hamsters.

The measurement of TG in severely ill male COVD-19 patients versus healthy individuals showed higher total TG levels in the plasma of infected patients. The targeted metabolomic analysis revealed a similar result to the male Syrian hamsters with a highly significant decrease in TGs containing SFAs and MUFAs derived from DNL. This demonstrated that not only in the animal model, but also in human patients SARS-CoV-2 can cause a systemic dysregulation of the lipid metabolism.

Overall, the results of this thesis clearly demonstrate that alongside the lung and other vital organs, adipose tissue plays a major role in SARS-CoV-2 infections. It presents a previously unknown reservoir for viral replication and is involved in the organ-specific and systemic lipid metabolism dysregulation upon infection.

5 Discussion

5.1 SARS-CoV-2 infection of adipocytes and adipose tissue

5.1.1 SARS-CoV-2 infects adipocytes *in vitro.*

Right from the onset of the SARS-CoV-2 pandemic, severe disease progression was frequently observed in patients with metabolic comorbidities. Since ACE2 was pinpointed as receptor for SARS-CoV-2, expression profiling was carried out in order to assess its distribution. It was found that ACE2 is expressed in adipose tissue (Hikmet *et al.*, 2020). There it functions as a key part of the Renin-angiotensin-aldosteron system (RAAS), where it converts the angiotensin II (Ang II) into angiotensin(1-7), thereby contributing to the balance between vasoconstriction and vasodilation as well as regulating inflammation.

Aside from its physiological role, ACE2 functions as the cellular entry receptor for SARS-CoV-2 in adipose tissue. This work demonstrated productive infection of adipocytes derived from an immortalized human mesenchymal stem cell line (hMSC-TERT20), depending on the adipogenic differentiation state. Thereby, only fully differentiated adipocytes showed high expression of the receptor and efficient infection with SARS-CoV-2. In line with this, it was recently reported that MSCs originating from different tissues do not express ACE2 (Generali *et al.*, 2022). This dependency on differentiation state is also documented in airway epithelial cells, where undifferentiated cells show very poor infection efficiencies for SARS-CoV compared to mature epithelium (Jia *et al.*, 2005). These results indicate that full adipogenic differentiation is a prerequisite for infection of adipose tissue.

Interestingly, transcriptomic analysis in humans revealed that the amount of ACE2 RNA is up to 5 times higher in adipose tissue than in the lung (Hikmet *et al.*, 2020). However, viral titers in permanent lung cell lines such as Calu-3 are significantly higher than in hMSC-TERT-20 differentiated adipocytes (Felgenhauer *et al.*, 2020). There are several possible reasons for this. The binding affinity of SARS-CoV-2 to ACE2 is significantly higher than it was for SARS-CoV, suggesting that lower receptor abundance is sufficient for successful infection (Shang *et al.*, 2020). Additionally, the starting viral load in the lung is presumably much higher than in adipose tissue, since the respiratory tract is the main viral entry point into the body. Consequently, higher virus titers might be achieved through an increased number of initial virus particles. Moreover, the transmembrane protease TMPRSS2, which is crucial for viral entry into the cell is expressed to higher amounts in the lung than in adipose tissue (*The Human Protein Atlas* accessed: 18 May 2023; Uhlén *et al.*, 2015), possibly increasing infection efficiency in the respiratory tract.

The finding that SARS-CoV-2 is able to infect and replicate in adipose tissue begged the question whether other respiratory viruses are capable of adipocyte infection. In this work, the pandemic H1N1 influenza A virus strain from 2009 was used as a control and showed no productive infection in adipocytes. Conversely, infection with the highly pathogenic avian influenza A subtype H7N9 yielded viral titers comparable with those of SARS-CoV-2 in stem cell-derived adipocytes (hMSC-TERT20). Since the pandemic H1N1 influenza A virus strain is the most human-adapted of all viruses tested in this thesis, one could speculate that this high level of host adaptation leads to a limited tissue tropism and decreased disease severity compared to non-adapted viruses. The fact that H7N9 is not as well adapted to the human host as the H1N1 subtype, may explain its ability to infect a greater range of tissues and their increased pathogenicity. This theory is corroborated by studies with the different SARS-CoV-2 variants of concern (VOC), which emerged in the later stages of the pandemic. The Omicron VOC is the currently circulating variant whose tissue tropism was demonstrated to have shifted from the lung towards bronchial cells (Hui *et al.*, 2022). In addition, Omicron shows higher ACE2 binding affinity and replicates faster in the bronchi than any previous variant. Still, it shows lower infection in lung cells itself, which may result in lower pathogenicity (Hui *et al.*, 2022; Suzuki *et al.*, 2022). Consequently, one could speculate that Omicrons' reduced tissue range would also entail lower replication in adipose tissue.

5.1.2 Replication of SARS-CoV-2 in adipocytes depends on lipid metabolism *in vitro.*

In light of the fact that obesity itself and obesity-related metabolic diseases are among the most frequent comorbidities in COVID-19 patients, it stands to reason that pharmacological interventions aimed at these comorbidities could improve the outcome of a SARS-CoV-2 infection. Among the drugs frequently used to treat these conditions are the cholesterol-lowering statins and the anti-obesity drug tetrahydrolipstatin (THL).

Different clinical studies analyzing the benefit of statin use in hospitalized COVID-19 patients with metabolic comorbidities present contradicting results. One study showed that patients that were taking statins prior to COVID-19-related hospitalization had substantially lower risk of death compared to those with untreated cardiovascular disease or hypertension (Daniels *et al.*, 2021). Conversely, a different study observed no influence of statins on the mortality of COVID-19 patients (Ayeh *et al.*, 2021). Reason for the contrasting results of the two studies could be the smaller cohort size of the second study or differences in the statistical analysis. In this thesis, it was shown that 4 h pre-treatment of hMSC-TERT20-derived adipocytes with Atorvastatin decreased viral replication significantly two days after infection *in vitro*. Here, the reason for lower replication of SARS-CoV-2 seems to be the statin-mediated downregulation

of ACE2. This drug-induced receptor downregulation was independent of SARS-CoV-2 infection.

Statins competitively inhibit the HMG-CoA reductase, the rate-limiting enzyme of the mevalonate pathway, thereby blocking the cholesterol synthesis. Cholesterol is a major component of the cellular membrane, especially of cholesterol-rich microdomains called lipid rafts. The SARS-CoV-2 receptor ACE2 was documented to reside in these lipid rafts, which played an important role in virus attachment and entry of SARS-CoV (Glende *et al.*, 2008). In line with this, Simvastatin treatment of Calu-3 cells led to the disruption of lipid rafts, displacement of ACE2 and subsequent inhibition of SARS-CoV-2 attachment and entry into the host cell (Teixeira *et al.*, 2022). These results are consistent with the findings in this dissertation, although the mechanism of inhibition might be different. While Simvastatin led to redistribution of ACE2 on the surface of Calu-3 cells, Atorvastatin treatment of hMSC-derived adipocytes inhibited viral replication by receptor downregulation. These differences might be explained by the different cell types used. Further, it was shown that Simvastatin mitigated the pro-inflammatory response to the infection *in vitro* as well as *in vivo*. Thereby, mice treated with Simvastatin showed lower lung inflammation than control animals and the pro-inflammatory responses of human neutrophils and monocytes were significantly diminished as well (Teixeira *et al.*, 2022). These results, taken together with the outstanding safety profile of statins, warrant further exploration of their use in SARS-CoV-2 patients.

Pharmacological treatment of obesity presents another approach to curb the severity of SARS-CoV-2 infection in vulnerable groups. THL is used to achieve body weight reduction in obese patients. It blocks the breakdown of triglycerides (TGs) by inhibition of lipases, thereby severely limiting the uptake of dietary fats. Additionally, THL inhibits the fatty acid synthase (FASN) and with that the *de novo* synthesis of fatty acids (Kridel *et al.*, 2004). Results of this dissertation have shown that treatment of primary Syrian golden hamster and hMSC-TERT20-derived adipocytes with THL decreases viral replication by approximately 10-fold and 100-fold, respectively. This finding is in line with a recent publication, where the authors found that the inhibition of FASN by THL effectively blocks SARS-CoV-2 replication *in vitro* as well as *in vivo* (Chu *et al.*, 2021). Furthermore, it was shown in a different study that the posttranslational palmitoylation of the viral S protein is essential for infection. Lipid synthesis inhibition decreases the amount of palmitoylated host as well as viral proteins in the cell (Wu *et al.*, 2021). Together, this data strongly suggests that lipid synthesis is crucial for SARS-CoV-2 infection. Interestingly, exogenous addition of BSA-conjugated palmitic acid only partially rescued the viral infection, indicating that THL also blocks lipases within the cells (Chu *et al.*, 2021). The inhibition of TG breakdown from lipid droplets possibly hinders SARS-CoV-2 replication in a way other than restricting palmitoylation of the S protein. It is known that SARS-

CoV-2 reorganizes cell compartment membranes to form replication organelles, especially those of the endoplasmic reticulum and Golgi apparatus (Hackstadt *et al.*, 2021). Since these membranes consist of lipids, the inhibition of lipid synthesis as well as breakdown disrupts the lipid homeostasis within the cell and possibly hampers the formation of replication organelles. Different publications showed that treatment with each of the drugs discussed above led to a significant decrease of SARS-CoV-2 replication *in vitro* and *in vivo* (Chu *et al.*, 2021; Teixeira *et al.*, 2022). Moreover, a synergistic effect of Atorvastatin and THL treatment has been shown in this thesis for both stem cell-derived as well as primary hamster adipocytes. This finding suggests that the concomitant disruption of cholesterol synthesis, receptor downregulation and interference with lipid homeostasis could have a profound antiviral effect. Taking into account that both drugs are safe, well tolerated and cheap to manufacture, clinical studies exploring the therapeutic value of a combined administration to patients suffering from obesity, cardiovascular or metabolic comorbidities would be of great interest.

5.1.3 SARS-CoV-2 actively disseminates to adipose tissue and triggers an antiviral response *in vivo.*

Early in the pandemic, reports already showed that SARS-CoV-2 not only infects the respiratory system, but can be found in a variety of tissues and organs including heart, liver, brain and kidneys (Puelles *et al.*, 2020). In this work, *in vivo* infection experiments in Syrian golden hamsters, demonstrated efficient virus replication in adipose tissue, providing proof of active dissemination from the lung as initial target organ. The detection of replicating virus in adipose tissue confirmed RNA-based results from an earlier study (Reiterer *et al.*, 2021). In line with the *in vitro* data, the viral titers in the lung of the animals were higher than those in the adipose tissue (Stanelle-Bertram *et al.*, 2020). Virus elimination from adipose tissue was achieved by day 6 after infection. A reason for this rapid clearance could be the hamsters' young age and healthy state, leading to a robust innate immune response characterized by cytokine expression. Intriguingly, viral clearance in the lung was delayed compared to the adipose tissue (Stanelle-Bertram *et al.*, 2020). The significantly higher initial viral load or more efficient spread within the lung could explain this result. The robust innate immune response to infection in adipose tissue was illustrated by the profound induction of the interferon-stimulated gene of 15 kDa (ISG15) in both male and female Syrian golden hamsters. This ubiquitin-like modifier serves a multitude of functions within the cell by conjugation to target proteins (ISGylation) or as free mediator ranging from antiviral actions to modulation of host damage and repair response. Direct antiviral action has been demonstrated for influenza virus, where ISG15 conjugates to viral NS1, thereby inhibiting its nuclear translocation (Zhao *et al.*, 2010).

However, even though data in this thesis report the induction of an effective innate immune response in adipose tissue upon infection, the immune evasive action of SARS-CoV-2 regarding ISG15 could be detrimental in patients. Studies have shown that the papain-like protease (PLpro) of SARS-CoV-2 is capable of removing ISG15 from target proteins (de-ISGylation) such as melanoma differentiation-associated protein 5 (MDA5). MDA5 is a RIG-I-like receptor (RLR) that recognizes newly synthesized viral RNA, thereby initiating a signaling cascade leading to antiviral interferon (IFN) induction. ISGylation of MDA5 is required for its oligomerization and translocation to the mitochondria, which is essential for proper function (Liu *et al.*, 2021). Furthermore, PLpro is known to de-ISGylate downstream signaling molecules such as IRF3, leading to impairment of RLR signaling (Shin *et al.*, 2020). Another consequence of the de-ISGylation of these proteins is a rise in free ISG15, which can bind and stabilize the ubiquitin specific peptidase 18 (USP18), a potent inhibitor of type I IFN signaling (Zhang *et al.*, 2015). Additionally, it has been shown that the ratio of free vs. conjugated ISG15 correlates with macrophage polarization towards the M1 phenotype, secretion of pro-inflammatory cytokines and attenuated antigen presentation (Munnur *et al.*, 2021). ISG15 is a part of robust immune response to viral infections, but viral immune evasion techniques can impede IFN-signaling and increase pro-inflammatory cytokine expression by macrophages, possibly contributing to excessive, uncontrolled inflammation.

In summary, the data displayed in this thesis show that adipose tissue is productively infected with SARS-CoV-2, presenting a previously unknown viral reservoir. This active replication contributes to increased viral load throughout the organism. Moreover, SARS-CoV-2 infection triggers an immune response in adipose tissue, which leads to viral clearance, but could also potentially exacerbate existing inflammation. The latter possibility is especially dangerous for patients with pre-existing inflammatory comorbidities such as obesity or obesity-related conditions, predisposing them to severe disease progression and possibly fatal outcome.

5.2 Influence of BMI on SARS-CoV-2 infection and COVID-19 severity

5.2.1 SARS-CoV-2 replicates in human adipose tissue *in vivo.*

Soon after the start of the pandemic, it became clear that obesity and obesity-related medical conditions are among the risk factors for hospital admission and severe COVID-19 disease (Lighter *et al.*, 2020; Petrilli *et al.*, 2020). It was suggested that obesity contributes to immune dysregulation and cardiorespiratory problems that appear in severely ill patients (Sattar, McInnes and McMurray, 2020). Later studies showed dissemination of SARS-CoV-2 to a

variety of human tissues (Puelles *et al.*, 2020) and to adipose tissue in the Syrian golden hamster model (Reiterer *et al.*, 2021), implicating a direct involvement of adipose tissue in the infection process.

Results of this work showed viral RNA in autopsy-derived tissue samples of 30 patients, 18 male and 12 female, who succumbed to SARS-CoV-2 infection. In 56 % of male patients SARS-CoV-2 RNA was found in either subcutaneous (SAT), visceral (VAT) or both adipose tissue depots. In females only 42 % of patients presented RNA in adipose tissues. Curiously, virus-positive adipose tissue samples in males were only found in patients with a BMI greater than 25 kg/m^2, whereas in females no such observation was made. Additionally, 50 % of male patients with a BMI above 30 kg/m^2 presented viral RNA in the liver, indicating that hepatic fat accumulation contributes to viral replication in these obese male individuals. In females, 50 % of patients showed viral RNA in liver samples, but again without clear association to BMI. It is important to point out that the patient cohort was too small for statistically significant assertions.

ACE2 is abundantly expressed in adipose tissue and diet-induced obesity was found to lead to elevated ACE2 levels in murine adipose tissue (Patel, Basu and Oudit, 2016; Hikmet *et al.*, 2020). Moreover, substantial weight loss in humans downregulated the ACE2 expression in SAT, indicating a correlation between the volume of adipose tissue and ACE2 expression (Al Heialy *et al.*, 2020). In the work presented in this thesis, the ACE2 levels in the two adipose tissue depots did not correlate with the BMI of the patients. A possible reason for this could be degradation of tissue samples due to the median post-mortem interval of 5 days and the small size of the cohort.

5.2.2 High BMI and obesity promote severe disease and lower vaccine-mediated protection.

Although not statistically significant, the connection between BMI and virus-positive fat samples is intriguing. Multiple clinical studies found a relationship between BMI and severe COVID-19 disease progression. One study showed a linear risk increase of hospital admission and death in patients with a BMI greater than 23 kg/m^2 and a positive correlation of ICU admission and BMI in general. Interestingly, this relationship of BMI and increased risk of severe disease was most notable in patients younger than 40 years of age (Gao *et al.*, 2021). Another study reported that the proportion of COVID-19 patients requiring invasive mechanical ventilation rose with BMI classes with the need being highest in individuals with a BMI greater than 35 kg/m^2 (Simonnet *et al.*, 2020). One reason for that could be that obese patients already suffer from respiratory problems such as a reduced total lung capacity, caused by increased intrathoracic fat accumulation (Watson *et al.*, 2010).

High BMI values are a key feature of overweight and obesity. These conditions are very often the root cause of metabolic diseases like hypertension, coronary heart disease or type 2 diabetes. All of these diseases, including obesity, are among the most frequent comorbidities in patients with severe or fatal COVID-19 disease progression (Y. Zhou *et al.*, 2020). A study from Italy reported that obese patients presented a worse pulmonary clinical picture and required oxygen supplementation for a longer period, consequently prolonging their hospitalization compared to non-obese patients. Additionally, these individuals showed virus-positive nasal or oropharyngeal swabs for a longer time than their non-obese controls, indicating prolonged virus shedding (Moriconi *et al.*, 2020).

The fact that obese individuals have a higher risk of adverse outcome of a respiratory virus infection has been observed before. During the 2009 H1N1 influenza pandemic, obese and morbidly obese patients had a substantially elevated risk of hospitalization and death compared to individuals with normal weight. As in SARS-CoV-2 infection, the increased risk was specific for obesity and independent from other comorbidities (Morgan *et al.*, 2010; Klang *et al.*, 2020). Results of this work showed no productive infection of adipocytes by H1N1 *in vitro,* indicating that the mechanism responsible for the increased risk of severe disease might differ between H1N1 influenza A virus and SARS-CoV-2. Furthermore, diet-induced obesity strongly reduced influenza vaccine efficacy in mice challenged with the 2009 pandemic H1N1 strain (Kim *et al.*, 2012). A study in humans demonstrated that, despite initial positive correlation of BMI and IgG antibodies stimulated by the trivalent influenza vaccine, 12 months after inoculation these antibodies were reduced in obese individuals compared to lean controls. Moreover, T cell activation and functional protein expression was decreased in obese study participants (Sheridan *et al.*, 2012). Although a different technology was used for the SARS-CoV-2 vaccines, similar results were reported regarding antibody waning in obese individuals upon inoculation with the Biontech/Pfizer vaccine BNT162b2 (Malavazos *et al.*, 2022). Another study showed that BMI is inversely correlated with humoral and cellular immune response upon vaccination in obese people. Interestingly, dietary restriction and substantial loss of body weight improved the adaptive response to the Biontech/Pfizer vaccine (Watanabe *et al.*, 2022). These findings suggest that obesity not only affects the course of disease progression, but also interferes with an adequate immune response towards vaccinations.

5.2.3 Obesity-mediated systemic inflammation contributes to high risk of severe disease.

Results of this work showed that SARS-CoV-2 productively infects adipose tissue *in vitro* and *in vivo*. This infection could contribute to the increased risk of adverse outcome of COVID-19 in obese individuals, by exacerbating the pro-inflammatory and uncontrolled immune response

already present due to the chronic low-grade inflammation. This adipose tissue inflammation has multiple causes. These include the process of expansion, changes in adipokine expression and secretion and subsequent alteration of stromal vascular fraction composition and activity.

In order to accommodate the excess energy intake during obesity, the adipose tissue expands through either hyperplasia or hypertrophy. It has been shown that the dominant process of fat mass expansion in adults is achieved by hypertrophy (Kim *et al.*, 2014). During hypertrophic growth, cells can rapidly reach the diffusional limit of oxygen, resulting in local hypoxia. This oxygen shortage leads to stress signaling in adipocytes and eventually to necrosis-like cell death (Cinti *et al.*, 2005). Moreover, stressed adipocytes have been shown to activate tissue resident NK cells, which in turn proliferate and increase their production of interferon-γ (IFN-γ). This contributes to the polarization of macrophages towards the pro-inflammatory M1 phenotype (Wensveen *et al.*, 2015). The necrosis-like cell death also recruits macrophages to the site of dead adipocytes, where they arrange in crown-like structures and form multinucleated giant cells to take up lipids and cell remnants. These syncytia are hallmarks of chronic inflammation and they actively produce and secrete pro-inflammatory cytokines including IL-6 and TNF-α (Cinti *et al.*, 2005). Additionally, oxygen shortage upregulates the hypoxia inducible factor-1α (HIF-1α). Studies showed that the expression of HIF-1α promotes the differentiation of Th17 cells and decreases Treg development (Dang *et al.*, 2011). Furthermore, it was shown that HIF-1α induces fibrosis in adipose tissue, thereby supporting inflammation (Halberg *et al.*, 2009).

Adipokines, such as leptin and adiponectin, also play an important role in adipose tissue inflammation. Serum leptin concentrations have been shown to positively correlate with fat mass in humans (Considine *et al.*, 1996). Multiple studies reported pro-inflammatory characteristics of leptin through the effect on nearly all immune cells. Leptin treatment was reported to decrease human Treg differentiation and production of the typical Th2 cytokine IL-4, and conversely enhance the production of Th1 cytokines like IFN-γ and IL-2 (Lord *et al.*, 1998; De Rosa *et al.*, 2007). In addition, leptin treatment of DCs led to an upregulation of IL-1β, IL-6, IL-12, TNF-α and the macrophage inflammatory protein (MIP)-1α as well as the downregulation of anti-inflammatory IL-10, thereby contributing to M1 polarization of macrophages. These DCs also promote the Th1 differentiation of naïve T cells (Mattioli *et al.*, 2005). Monocyte-enriched peripheral blood mononuclear cells (PBMC) exposed to leptin were reported to increase production and secretion of pro-inflammatory cytokines including IL-1β, IL-6, TNF-α and resistin (Tsiotra *et al.*, 2013). In contrast to leptin, the anti-inflammatory adipokine adiponectin decreases in concentration in obese individuals (Arita *et al.*, 1999). Adiponectin was shown to decrease FA levels in circulation by increased uptake and oxidation

in muscle cells and furthermore inhibit TLR-mediated pro-inflammatory signaling in macrophages (Yamauchi *et al.*, 2002; Yamaguchi *et al.*, 2005).

Taken together, the mechanism of fat mass expansion during the development of obesity, subsequent secretion of pro-inflammatory mediators and alteration of immune cell composition in adipose tissue contributes to a dysregulated immune response (Fig. 13). This, coupled with a SARS-CoV-2 infection of the adipose tissue and exacerbation of immune dysregulation could contribute to the higher rates of hospitalization and death.
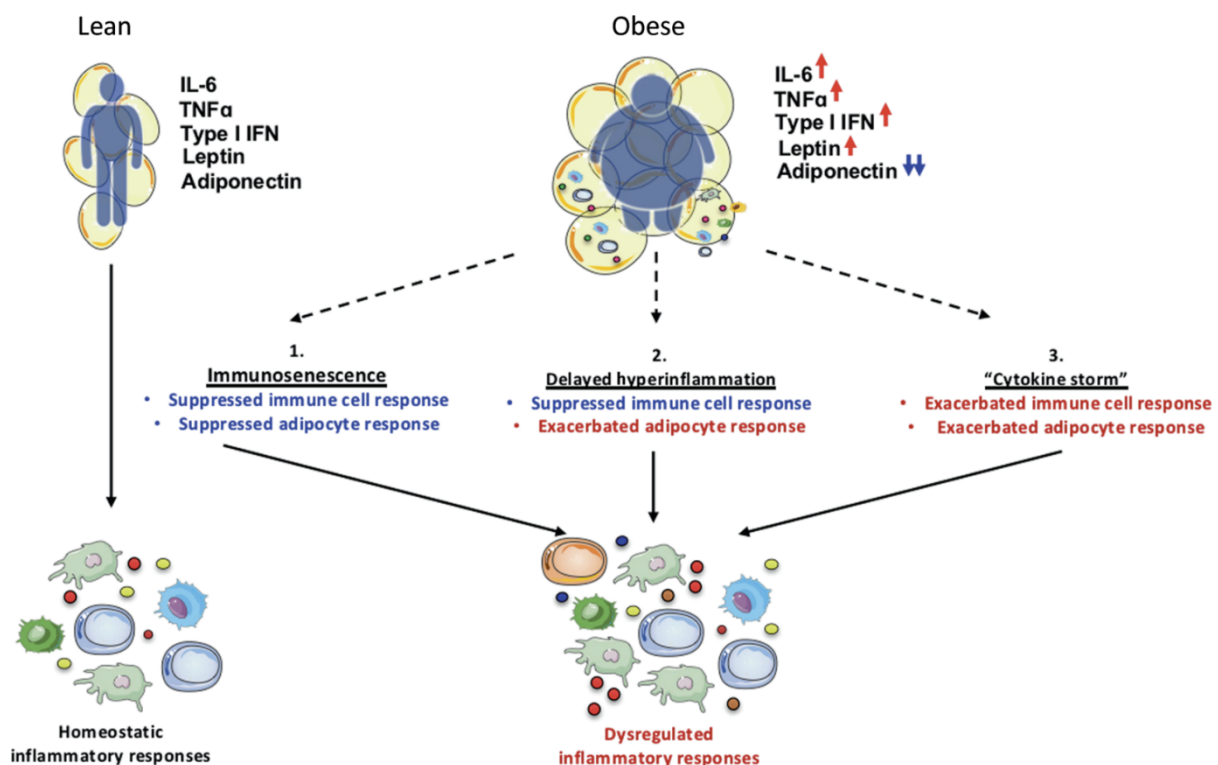

Figure 13: Dysregulation of the immune response in obese adipose tissue. Secretion of adipocyted-derived factors (*e.g.* IL-6, TNF-α, type I IFNs, leptin, adiponectin) is dysregulated in obese individuals. This can lead to immunosenescence (1), delayed hyperinflammation (2) and "cytokine storm" (3), culminating in a dysregulated immune response, to infection and contributes to the increased risk of adverse outcome of infection in obese patients (adapted from Alarcon *et al.*, 2021)

5.2.4 Sex-specific fat distribution impacts metabolic consequences and COVID-19 severity.

The connection between high BMI and SARS-CoV-2 RNA-positive adipose tissue samples in deceased male patients observed in this work may also be caused by the sex-specific body fat distribution and its consequences. Recent studies were able to report that not only total fat mass, but also its location plays an important role in the development of severe disease. One study showed that high visceral adiposity and high intramuscular fat deposition independently

predicted critical illness and significantly increased the risk of the need for mechanical ventilation upon SARS-CoV-2 infection (Y. Yang *et al.*, 2020). In line with this, another study reported that VAT area was associated with severe disease. Conversely, SAT area was shown not to differ between patients with mild and severe illness. Interestingly, the body fat distribution is dependent on sex hormone levels, thereby differing between men and women (Elbers *et al.*, 1999). Healthy males show higher amounts of VAT and lower amounts of SAT compared to women (Tchoukalova *et al.*, 2010). A gain in total fat mass is associated with a significantly greater VAT increase in men as compared to women (Lemieux *et al.*, 1993). Additionally, as was reported in mice, VAT expands hypertrophically, whereas SAT was found to increase mass in a hyperplastic manner upon feeding a high fat diet (Joe *et al.*, 2009). This might explain why abdominal adiposity is associated with pro-inflammatory processes and increased risk of cardiometabolic complications (Shah *et al.*, 2014).

Further, ACE2 mRNA positively correlated with BMI in VAT but not SAT, indicating that obese individuals express more SARS-CoV-2 receptor on their visceral than subcutaneous adipocytes (Favre *et al.*, 2021). This correlation was not observed in the results of this work. Reason for that could be possible degradation of samples due to the median post-mortem interval of five days.

Intriguingly, women showed higher fat mass percentage, but lower waist circumference than men, independent of BMI. This indicates a more pronounced abdominal adipose tissue depot in males. Consequently, obese males show higher prevalence of metabolic syndrome than obese females corroborating the observation of obese men's increased risk of metabolic consequences compared to women (Strack *et al.*, 2022).

Differential adipose tissue distribution, caused by sex-differences, coupled with the detrimental characteristics of severely elevated VAT mass could predispose obese males to an increased risk of SARS-CoV-2 infection of adipose tissue, an aberrant immune response and higher rates of severe disease and death. This presents a previously unrecognized link between COVID-19 severity and sex.

5.3 SARS-CoV-2-mediated dysregulation of lipid metabolism

Multiple viruses are known to alter cellular processes vital for homeostasis in order to facilitate their replication and spread. These actions include the takeover of mRNA transcription and protein translation, subversion of immune responses and alterations of energy metabolism. The latter process is of special interest in COVID-19 patients, since metabolic diseases have been shown to be a risk factor for severe disease (Y. Zhou *et al.*, 2020). Results in this thesis showed profound changes in the lipid metabolism of adipose tissue in male and female Syrian

golden hamsters upon infection. Three and six days after infection, mRNAs of three genes critical for *de novo* fatty acid biosynthesis were significantly downregulated. Those genes encode the acetyl-CoA carboxylase 1 (ACC1), the ATP citrate lyase (ACLY) and the fatty acid synthase (FASN). ACC1 is the first and rate-limiting enzyme in *de novo* fatty acid synthesis, ACLY links carbohydrate metabolism with lipogenesis and FASN catalyzes the reaction resulting in the simplest fatty acid, palmitate.

5.3.1 Downregulation and inhibition of *de novo* lipogenesis hampers SARS-CoV-2 replication.

It is known that inhibition of the fatty acid synthesis impedes SARS-CoV-2 replication and attenuates its spread by blocking the posttranslational modification of the S protein (Chu *et al.*, 2021; Mekhail *et al.*, 2022). Therefore, the observed downregulation of lipogenesis genes upon virus infection in this thesis seems to be detrimental for SARS-CoV-2. It has been shown that type I IFNs can suppress FASN and thereby contribute to decreased viral replication (Aliyari *et al.*, 2022). Consequently, the downregulation of lipogenesis genes upon SARS-CoV-2 infection could be attributed to a robust type I IFN response. This is underscored by the drastic increase of the IFN-stimulated gene *ISG15* on day three post infection. The *ISG15* upregulation was far more pronounced upon infection than upon treatment with the dsRNA analogue poly(I:C), an excellent inducer of IFN-stimulated genes. This high induction of IFN-stimulated genes by SARS-CoV-2 might contribute to the stronger downregulation of fatty acid biosynthesis-related genes upon infection compared to poly(I:C) treatment. The notion of a robust immune response in the Syrian golden hamsters following infection is corroborated by the fact that the virus is cleared from adipose tissue six days after infection. After virus clearance, the downregulation of fatty acid biosynthesis-related genes was less pronounced compared to day three post infection, and ISG15 mRNA expression reverted to almost normal levels, indicating an intact mechanism of immune control.

Importantly, the infection experiments presented in this thesis were carried out in young, healthy, immunocompetent male and female hamsters. In contrast, severely ill COVID-19 patients with metabolic comorbidities such as obesity likely have an impaired immune function. A study in rats showed that NK cells from obese animals were significantly less activated upon leptin stimulation than NK cells from lean controls, caused by leptin resistance upon the development of obesity (Nave *et al.*, 2008). Further, obese mice displayed only minimal induction of type I IFNs in the lung, delayed expression of pro-inflammatory cytokines and chemokines and reduced NK cell cytotoxicity upon influenza A virus infection (Smith *et al.*, 2007). Therefore, it stands to reason that patients with pre-existing metabolic conditions might also show an impaired immune response. This could cause a less appropriate response to

infection in obese patients and contribute to a higher risk of severe disease compared to lean individuals.

The pharmacological inhibition of *de novo* lipogenesis with FDA-approved drugs like Orlistat (THL) for FASN or Bempedoic acid for ACLY could be an attractive therapeutic intervention strategy. Inhibition of FASN led to decreased virus titers in the lung, reduced lung pathology and overall increased survival of infected mice expressing human ACE2. Similar results were reported for a study where ACLY was inhibited (Chu *et al.*, 2021; Yuen *et al.*, 2022). These medications could be especially beneficial for obese patients since adipose tissue is a reservoir for SARS-CoV-2 and fatty acid synthesis mainly occurs in adipocytes.

Interestingly, SARS-CoV-2 is not the only respiratory viral pathogen to rely on fatty acid synthesis. It has been shown that inhibition of FASN lead to a reduction of respiratory syncytial virus (RSV) replication and particle formation and impaired infectivity of released particles *in vitro*. RSV-infected mice, treated with a FASN inhibitor showed markedly reduced viral titers in the lung, upon administration in a prophylactic and even therapeutic fashion one day after infection (Ohol *et al.*, 2015). Additionally, the inhibition of the sterol regulatory element binding protein (SREBP)-mediated transactivation of genes critical for fatty acid synthesis impaired downstream processes that are crucial for MERS-CoV replication like the formation of DMVs. This inhibition contributes to decreased viral replication in a human hepatocellular carcinoma cell line (Yuan *et al.*, 2019).

Taken together, the data in this thesis demonstrate that the downregulation of *de novo* lipogenesis by a pronounced type I IFN response possibly contributes to decreased viral replication. This is in line with published studies showing a dependence of SARS-CoV-2 and other respiratory viruses on fatty acid synthesis, making the relevant enzymes prime targets for broad antiviral therapy.

5.3.2 SARS-CoV-2 infection causes systemic alterations in the lipid and glucose metabolism.

Besides the disruption of lipid metabolism in adipocytes and adipose tissue, SARS-CoV-2 has a systemic effect on energy homeostasis. Results of this work showed that total plasma triglyceride (TG) levels increased upon infection in COVID-19 patients. Interestingly, plasma triglyceride species typical for *de novo* lipogenesis containing saturated and mono-unsaturated fatty acids (SFAs and MUFAs respectively), were significantly decreased. Similar results were observed in plasma of SARS-CoV-2-infected Syrian golden hamsters. There, contrary to the decrease of SFA- and MUFA-containing fats, triglycerides comprised of poly-unsaturated fatty

acids (PUFAs) were enriched on day three post infection. These observations are in line with the downregulation of genes responsible for *de novo* fatty acid synthesis in infected animals.

The increased TG concentrations in plasma of humans and animals might result from the strong induction of pro-inflammatory cytokines following SARS-CoV-2 infection. A recent meta-analysis showed that levels of TNF-α and other pro-inflammatory cytokines were significantly higher in patients with severe compared to mild disease (Mulchandani, Lyngdoh and Kakkar, 2021). TNF-α decreases perilipin, the protein that shields lipids in intracellular droplets from endogenous lipases, and thereby increases lipolysis in adipose tissue (Brasaemle *et al.*, 2000; Rydén *et al.*, 2004). This leads to secretion of free fatty acids from the adipose tissue, which are taken up by the liver, re-esterified to TGs and loaded onto newly synthesized VLDL particles. Secreted VLDL particles are transported to target tissues where they are cleared by the enzyme lipoprotein lipase (LPL). It was shown that TNF-α decreases the expression of LPL in cultured adipocytes, possibly leading to lower clearance of VLDL and thereby increased TG content in the plasma (Khovidhunkit *et al.*, 2004).

This dysregulation of plasma TG levels was also shown for severe influenza A virus infections, where hypertriglyceridemia was associated with an enhanced pro-inflammatory cytokine profile (Zhai *et al.*, 2020). The increase in plasma TG levels is of particular interest in patients with metabolic diseases such as obesity. It has been reported that increased VAT in men correlates with hepatic hypersecretion and hypocatabolism of apolipoprotein B, the main component of VLDL particles (Watts *et al.*, 2003). This process might exacerbate the increase of lipid content in the plasma of obese COVID-19 patients.

This data suggests that the increased plasma TG level is at least in part a direct consequence of the pro-inflammatory cytokine induction mediated by SARS-CoV-2 infection.

In addition to the dysregulated lipid metabolism, patients with severe COVID-19 frequently suffer from hyperglycemia, which is shown to be a poor prognostic marker for disease outcome (Reiterer *et al.*, 2021). It has been reported that hyperglycemia is a common symptom in patients with acute respiratory distress syndrome (ARDS), independently of SARS-CoV-2 infection. Adipose tissue dysfunction in COVID-19 patients was associated with lowered adiponectin levels, increased insulin resistance and consequently hyperglycemia (Reiterer *et al.*, 2021). Adiponectin plays a distinctive role in energy homeostasis, immune function and satiety. In infection, the release of pro-inflammatory cytokines such as TNF-α, IL-1β and IFN-γ have been shown to reduce adiponectin secretion (Simons *et al.*, 2007). This reduction could explain the increased insulin resistance and hyperglycemic condition. Metabolic diseases like obesity and type 2 diabetes also seem to have an impact on adiponectin levels. Adiponectin concentration is decreased in obese individuals (Arita *et al.*, 1999). Further, it has been shown that adiponectin was inversely correlated with TNF-α, IL-1β, glucose, TGs, cholesterol and

LDL in overweight or type 2 diabetes patients. Positive correlations were found with HDL and anti-inflammatory cytokine IL-10 (Tong *et al.*, 2017). These results indicate that a suppression of adiponectin by increased weight and metabolic diseases, leads to decreased anti-inflammatory potential and an increased pro-inflammatory cytokine profile, possibly contributing to severe COVID-19 disease progression.

Taken together, the data in this work demonstrate a disruption of energy homeostasis caused by SARS-CoV-2 infection and subsequent cytokine expression in adipose tissue. Patients with pre-existing metabolic diseases are at higher risk for adverse outcome of infection, possibly because these comorbidities already disturb the glucose and lipid metabolism, thereby contributing to severe disease.

6 Conclusion

In this thesis, I have investigated the infection of adipocytes and adipose tissue with SARS-CoV-2 and resulting consequences for the lipid metabolism. Results showed efficient infection and replication of SARS-CoV-2 in human stem cell-derived adipocytes, depending on their differentiation state, as well as in primary human and Syrian golden hamster adipocytes. Drug-mediated interference in the cellular lipid homeostasis significantly decreased virus replication *in vitro.* Animal experiments in Syrian golden hamsters demonstrated successful dissemination of virus from the lungs to the fat and a subsequent immune response within the adipose tissue. These findings were confirmed in human autopsy samples. In human adipose tissues, SARS-CoV-2 RNA could be detected in males with excess weight. No such associations were found in female samples. However, it is important to point out that the cohort was very small and thus the interpretation of the results is limited. Nevertheless, these findings suggest a sex-specificity in SARS-CoV-2 infection and disease severity.

Moreover, results of this thesis showed that SARS-CoV-2 infection disturbs the organ-specific and systemic lipid metabolism in SARS-CoV-2 infected Syrian golden hamsters as well as COVID-19 patients. Interestingly, clinically approved cholesterol synthesis and lipogenesis inhibitors that specifically impair SARS-CoV-2 replication in human and golden hamster adipocytes were identified.

Taken together, this thesis suggests that adipose tissue likely serves as a reservoir for SARS-CoV-2 replication, contributing to the higher risk of severe disease in overweight and obese individuals. In addition, the sex-specific adipose tissue distribution possibly augments the male bias in adverse disease outcome. Further, the organ-specific and systemic alterations in energy metabolism are associated with increased COVID-19 severity. These results indicate an interdependence of metabolic disease, sex and disease severity.

References

Ahmed, S. and Ahmed, O. (2019) *Biochemistry, Lipids*, *StatPearls*. StatPearls Publishing. Available at: http://www.ncbi.nlm.nih.gov/pubmed/30247827 (Accessed: 21 July 2022).

Alarcon, P.C. *et al.* (2021) 'Adipocyte inflammation and pathogenesis of viral pneumonias: an overlooked contribution', *Mucosal Immunology*. Springer Nature, pp. 1224–1234. Available at: https://doi.org/10.1038/s41385-021-00404-8.

Aliyari, S.R. *et al.* (2022) 'Suppressing fatty acid synthase by type I interferon and chemical inhibitors as a broad spectrum anti-viral strategy against SARS-CoV-2', *Acta Pharmaceutica Sinica B*, 12(4), pp. 1624–1635. Available at: https://doi.org/10.1016/j.apsb.2022.02.019.

Ameer, F. *et al.* (2014) 'De novo lipogenesis in health and disease', *Metabolism: clinical and experimental*, 63(7), pp. 895–902. Available at: https://doi.org/10.1016/J.METABOL.2014.04.003.

Arita, Y. *et al.* (1999) 'Paradoxical decrease of an adipose-specific protein, adiponectin, in obesity', *Biochemical and Biophysical Research Communications*, 257(1), pp. 79–83. Available at: https://doi.org/10.1006/bbrc.1999.0255.

Ayeh, S.K. *et al.* (2021) 'Statins use and COVID-19 outcomes in hospitalized patients', *PLOS ONE*. Edited by A.R. Zivkovic, 16(9), p. e0256899. Available at: https://doi.org/10.1371/journal.pone.0256899.

Brasaemle, D.L. *et al.* (2000) 'Perilipin A increases triacylglycerol storage by decreasing the rate of triacylglycerol hydrolysis', *Journal of Biological Chemistry*, 275(49), pp. 38486–38493. Available at: https://doi.org/10.1074/jbc.M007322200.

Carlson, C.J. *et al.* (2022) 'Climate change increases cross-species viral transmission risk', *Nature*, pp. 1–1. Available at: https://doi.org/10.1038/s41586-022-04788-w.

Catalán, V. *et al.* (2013) 'Adipose tissue immunity and cancer', *Frontiers in Physiology*. Frontiers, p. 275. Available at: https://doi.org/10.3389/fphys.2013.00275.

Chen, Z. *et al.* (2021) 'Genomic and evolutionary comparison between SARS-CoV-2 and other human coronaviruses', *Journal of Virological Methods*, 289, p. 114032. Available at: https://doi.org/10.1016/j.jviromet.2020.114032.

Chu, J. *et al.* (2021) 'Pharmacological inhibition of fatty acid synthesis blocks SARS-CoV-2 replication', *Nature Metabolism*, 3(11), pp. 1466–1475. Available at: https://doi.org/10.1038/s42255-021-00479-4.

Cinti, S. *et al.* (2005) 'Adipocyte death defines macrophage localization and function in adipose tissue of obese mice and humans', *Journal of Lipid Research*, 46(11), pp. 2347–2355. Available at: https://doi.org/10.1194/jlr.M500294-JLR200.

Coelho, M., Oliveira, T. and Fernandes, R. (2013) 'Biochemistry of adipose tissue: An

endocrine organ', *Archives of Medical Science*. Termedia Publishing, pp. 191–200. Available at: https://doi.org/10.5114/aoms.2013.33181.

Colquitt, J.L. *et al.* (2014) 'Surgery for weight loss in adults', *The Cochrane Database of Systematic Reviews*, 2014(8). Available at: https://doi.org/10.1002/14651858.CD003641.PUB4.

Considine, R. V. *et al.* (1996) 'Serum Immunoreactive-Leptin Concentrations in Normal-Weight and Obese Humans', *New England Journal of Medicine*, 334(5), pp. 292–295. Available at: https://doi.org/10.1056/nejm199602013340503.

Coronavirus. Available at: https://www.who.int/health-topics/coronavirus#tab=tab_3 (Accessed: 18 May 2023).

Cortese, M. *et al.* (2020) 'Integrative Imaging Reveals SARS-CoV-2-Induced Reshaping of Subcellular Morphologies', *Cell Host and Microbe*, 28(6), pp. 853-866.e5. Available at: https://doi.org/10.1016/j.chom.2020.11.003.

COVID-19 vaccines: authorised | European Medicines Agency. Available at: https://www.ema.europa.eu/en/human-regulatory/overview/public-health-threats/coronavirus-disease-covid-19/treatments-vaccines/vaccines-covid-19/covid-19-vaccines-authorised#authorised-covid-19-vaccines-section (Accessed: 18 May 2023).

D'Aquila, T. *et al.* (2016) 'Recent discoveries on absorption of dietary fat: Presence, synthesis, and metabolism of cytoplasmic lipid droplets within enterocytes', *Biochimica et Biophysica Acta - Molecular and Cell Biology of Lipids*. Elsevier B.V., pp. 730–747. Available at: https://doi.org/10.1016/j.bbalip.2016.04.012.

Dallinga-Thie, G.M. *et al.* (2010) 'The metabolism of triglyceride-rich lipoproteins revisited: New players, new insight', *Atherosclerosis*. NIH Public Access, pp. 1–8. Available at: https://doi.org/10.1016/j.atherosclerosis.2009.12.027.

Dang, E. V. *et al.* (2011) 'Control of TH17/Treg balance by hypoxia-inducible factor 1', *Cell*, 146(5), pp. 772–784. Available at: https://doi.org/10.1016/j.cell.2011.07.033.

Daniels, L.B. *et al.* (2021) 'Relation of prior statin and anti-hypertensive use to severity of disease among patients hospitalized with COVID-19: Findings from the American Heart Association's COVID-19 Cardiovascular Disease Registry', *PLOS ONE*. Edited by A.R. Zivkovic, 16(7), p. e0254635. Available at: https://doi.org/10.1371/journal.pone.0254635.

Du, Z. *et al.* (2022) 'Shorter serial intervals and incubation periods in SARS-CoV-2 variants than the SARS-CoV-2 ancestral strain', *Journal of Travel Medicine*, 29(6). Available at: https://doi.org/10.1093/JTM/TAAC052.

Elbers, J.M.H. *et al.* (1999) 'Effects of sex steroid hormones on regional fat depots as assessed by magnetic resonance imaging in transsexuals', *American Journal of Physiology - Endocrinology and Metabolism*, 276(2 39-2). Available at: https://doi.org/10.1152/ajpendo.1999.276.2.e317.

Endo, A. (1992) 'The discovery and development of HMG-CoA reductase inhibitors', *Journal of Lipid Research*. Elsevier, pp. 1569–1582. Available at: https://doi.org/10.1016/s0022-2275(20)41379-3.

Favre, G. *et al.* (2021) 'Visceral fat is associated to the severity of COVID-19', *Metabolism: Clinical and Experimental*, 115, p. 154440. Available at: https://doi.org/10.1016/j.metabol.2020.154440.

Feikin, D.R. *et al.* (2022) 'Duration of effectiveness of vaccines against SARS-CoV-2 infection and COVID-19 disease: results of a systematic review and meta-regression', *The Lancet*, 399(10328), pp. 924–944. Available at: https://doi.org/10.1016/S0140-6736(22)00152-0.

Feingold, K.R. and Grunfeld, C. (2000) *Introduction to Lipids and Lipoproteins*, *Endotext*. MDText.com, Inc. Available at: http://www.ncbi.nlm.nih.gov/pubmed/26247089 (Accessed: 21 July 2022).

Felgenhauer, U. *et al.* (2020) 'Inhibition of SARS–CoV-2 by type I and type III interferons', *The Journal of Biological Chemistry*, 295(41), p. 13958. Available at: https://doi.org/10.1074/JBC.AC120.013788.

Fonseca-Alaniz, M.H. *et al.* (2007) 'Adipose tissue as an endocrine organ: from theory to practice', *Jornal de Pediatria*, 0(0). Available at: https://doi.org/10.2223/jped.1709.

Gao, M. *et al.* (2021) 'Associations between body-mass index and COVID-19 severity in 6·9 million people in England: a prospective, community-based, cohort study', *The Lancet Diabetes and Endocrinology*, 9(6), pp. 350–359. Available at: https://doi.org/10.1016/S2213-8587(21)00089-9.

Generali, M. *et al.* (2022) 'Heterogeneous expression of ACE2 and TMPRRS2 in mesenchymal stromal cells', *Journal of Cellular and Molecular Medicine*, 26(1), pp. 228–234. Available at: https://doi.org/10.1111/jcmm.17048.

Glende, J. *et al.* (2008) 'Importance of cholesterol-rich membrane microdomains in the interaction of the S protein of SARS-coronavirus with the cellular receptor angiotensin-converting enzyme 2', *Virology*, 381(2), pp. 215–221. Available at: https://doi.org/10.1016/j.virol.2008.08.026.

Go, A.S. *et al.* (2014) 'An effective approach to high blood pressure control: A science advisory from the american heart association, the american college of cardiology, and the centers for disease control and prevention', *Hypertension*, 63(4), pp. 878–885. Available at: https://doi.org/10.1161/HYP.0000000000000003/-/DC1.

Goldstein, J.L. and Brown, M.S. (2015) 'A century of cholesterol and coronaries: From plaques to genes to statins', *Cell*. Cell Press, pp. 161–172. Available at: https://doi.org/10.1016/j.cell.2015.01.036.

Gordon, C.J. *et al.* (2020) 'Remdesivir is a direct-acting antiviral that inhibits RNA-dependent

RNA polymerase from severe acute respiratory syndrome coronavirus 2 with high potency', *Journal of Biological Chemistry*. American Society for Biochemistry and Molecular Biology Inc., pp. 6785–6797. Available at: https://doi.org/10.1074/jbc.RA120.013679.

Gray, S.L. and Vidal-Puig, A.J. (2008) 'Adipose Tissue Expandability in the Maintenance of Metabolic Homeostasis', *Nutrition Reviews*, 65(SUPPL.1), pp. S7–S12. Available at: https://doi.org/10.1111/j.1753-4887.2007.tb00331.x.

Guerciolini, R. (1997) 'Mode of action of orlistat', in *International Journal of Obesity*, pp. S12-23.

Hackstadt, T. *et al.* (2021) 'Disruption of the Golgi Apparatus and Contribution of the Endoplasmic Reticulum to the SARS-CoV-2 Replication Complex', *Viruses*, 13(9), p. 1798. Available at: https://doi.org/10.3390/v13091798.

Halberg, N. *et al.* (2009) 'Hypoxia-Inducible Factor 1α Induces Fibrosis and Insulin Resistance in White Adipose Tissue', *Molecular and Cellular Biology*, 29(16), pp. 4467–4483. Available at: https://doi.org/10.1128/mcb.00192-09.

He, X. *et al.* (2020) 'Temporal dynamics in viral shedding and transmissibility of COVID-19', *Nature Medicine*, 26(5), pp. 672–675. Available at: https://doi.org/10.1038/s41591-020-0869-5.

Al Heialy, S. *et al.* (2020) 'Regulation of Angiotensin- Converting Enzyme 2 in Obesity: Implications for COVID-19', *Frontiers in Physiology*, 11, p. 1194. Available at: https://doi.org/10.3389/fphys.2020.555039.

Heymsfield, S.B. and Wadden, T.A. (2017) 'Mechanisms, Pathophysiology, and Management of Obesity', *New England Journal of Medicine*, 376(3), pp. 254–266. Available at: https://doi.org/10.1056/nejmra1514009.

Hikmet, F. *et al.* (2020) 'The protein expression profile of ACE2 in human tissues', *Molecular Systems Biology*, 16(7). Available at: https://doi.org/10.15252/msb.20209610.

Hui, K.P.Y. *et al.* (2022) 'SARS-CoV-2 Omicron variant replication in human bronchus and lung ex vivo', *Nature*, 603(7902), pp. 715–720. Available at: https://doi.org/10.1038/s41586-022-04479-6.

Jia, H.P. *et al.* (2005) 'ACE2 Receptor Expression and Severe Acute Respiratory Syndrome Coronavirus Infection Depend on Differentiation of Human Airway Epithelia', *Journal of Virology*, 79(23), pp. 14614–14621. Available at: https://doi.org/10.1128/jvi.79.23.14614-14621.2005.

Joe, A.W.B. *et al.* (2009) 'Depot-specific differences in adipogenic progenitor abundance and proliferative response to high-fat diet', *Stem Cells*, 27(10), pp. 2563–2570. Available at: https://doi.org/10.1002/stem.190.

Kabinger, F. *et al.* (2021) 'Mechanism of molnupiravir-induced SARS-CoV-2 mutagenesis',

Nature Structural and Molecular Biology, 28(9), pp. 740–746. Available at: https://doi.org/10.1038/s41594-021-00651-0.

Kershaw, E.E. and Flier, J.S. (2004) 'Adipose Tissue as an Endocrine Organ', *The Journal of Clinical Endocrinology & Metabolism*, 89(6), pp. 2548–2556. Available at: https://doi.org/10.1210/jc.2004-0395.

Khovidhunkit, W. *et al.* (2004) 'Effects of infection and inflammation on lipid and lipoprotein metabolism: Mechanisms and consequences to the host', *Journal of Lipid Research*. Lipid Research Inc., pp. 1169–1196. Available at: https://doi.org/10.1194/jlr.R300019-JLR200.

Kim, S.M. *et al.* (2014) 'Loss of white adipose hyperplastic potential is associated with enhanced susceptibility to insulin resistance', *Cell Metabolism*, 20(6), pp. 1049–1058. Available at: https://doi.org/10.1016/j.cmet.2014.10.010.

Kim, Y.H. *et al.* (2012) 'Diet-induced obesity dramatically reduces the efficacy of a 2009 pandemic H1N1 vaccine in a mouse model', *Journal of Infectious Diseases*, 205(2), pp. 244–251. Available at: https://doi.org/10.1093/infdis/jir731.

Kineret | European Medicines Agency (no date). Available at: https://www.ema.europa.eu/en/medicines/human/EPAR/kineret (Accessed: 18 May 2023).

Klang, E. *et al.* (2020) 'Severe Obesity as an Independent Risk Factor for COVID-19 Mortality in Hospitalized Patients Younger than 50', *Obesity*, 28(9), pp. 1595–1599. Available at: https://doi.org/10.1002/oby.22913.

Kridel, S.J. *et al.* (2004) 'Orlistat Is a Novel Inhibitor of Fatty Acid Synthase with Antitumor Activity', *Cancer Research*, 64(6), pp. 2070–2075. Available at: https://doi.org/10.1158/0008-5472.CAN-03-3645.

Lemieux, S. *et al.* (1993) 'Sex differences in the relation of visceral adipose tissue accumulation to total body fatness', *American Journal of Clinical Nutrition*, 58(4), pp. 463–467. Available at: https://doi.org/10.1093/ajcn/58.4.463.

Lighter, J. *et al.* (2020) 'Obesity in Patients Younger Than 60 Years Is a Risk Factor for COVID-19 Hospital Admission', *Clinical Infectious Diseases*, 71(15), pp. 896–897. Available at: https://doi.org/10.1093/cid/ciaa415.

Liu, G.Q. *et al.* (2021) 'ISG15-dependent activation of the sensor MDA5 is antagonized by the SARS-CoV-2 papain-like protease to evade host innate immunity', *Nature Microbiology*, 6(4), pp. 467–478. Available at: https://doi.org/10.1038/s41564-021-00884-1.

Long, B. *et al.* (2020) 'Cardiovascular complications in COVID-19', *American Journal of Emergency Medicine*. W.B. Saunders, pp. 1504–1507. Available at: https://doi.org/10.1016/j.ajem.2020.04.048.

Lord, G.M. *et al.* (1998) 'Leptin modulates the T-cell immune response and reverses starvation- induced immunosuppression', *Nature*, 394(6696), pp. 897–901. Available at:

https://doi.org/10.1038/29795.

Malavazos, A.E. *et al.* (2022) 'Antibody responses to BNT162b2 mRNA vaccine: Infection-naïve individuals with abdominal obesity warrant attention', *Obesity*, 30(3), pp. 606–613. Available at: https://doi.org/10.1002/oby.23353.

Malone, B. *et al.* (2022) 'Structures and functions of coronavirus replication–transcription complexes and their relevance for SARS-CoV-2 drug design', *Nature Reviews Molecular Cell Biology*. Nature Research, pp. 21–39. Available at: https://doi.org/10.1038/s41580-021-00432-z.

Manage High Blood Pressure | cdc.gov (no date). Available at: https://www.cdc.gov/bloodpressure/manage.htm (Accessed: 18 May 2023).

Mancuso, P. (2016) 'The role of adipokines in chronic inflammation', *ImmunoTargets and Therapy*. Dove Medical Press Ltd., pp. 47–56. Available at: https://doi.org/10.2147/ITT.S73223.

Mao, R. *et al.* (2020) 'Manifestations and prognosis of gastrointestinal and liver involvement in patients with COVID-19: a systematic review and meta-analysis', *The Lancet Gastroenterology and Hepatology*, 5(7), pp. 667–678. Available at: https://doi.org/10.1016/S2468-1253(20)30126-6.

Martin, A.E. and Montgomery, P.A. (1996) 'Acarbose: An α-glucosidase inhibitor', *American Journal of Health-System Pharmacy*, 53(19), pp. 2277–2290. Available at: https://doi.org/10.1093/AJHP/53.19.2277.

Matrosovich, M. *et al.* (2006) 'New low-viscosity overlay medium for viral plaque assays', *Virology Journal*, 3(1), p. 63. Available at: https://doi.org/10.1186/1743-422X-3-63.

Mattioli, B. *et al.* (2005) 'Leptin Promotes Differentiation and Survival of Human Dendritic Cells and Licenses Them for Th1 Priming', *The Journal of Immunology*, 174(11), pp. 6820–6828. Available at: https://doi.org/10.4049/jimmunol.174.11.6820.

Mayer, K.A. *et al.* (2019) 'Hijacking the supplies: Metabolism as a novel facet of virus-host interaction', *Frontiers in Immunology*, 10(JULY), p. 1533. Available at: https://doi.org/10.3389/FIMMU.2019.01533/BIBTEX.

McAloon, C. *et al.* (2020) 'Incubation period of COVID-19: A rapid systematic review and meta-analysis of observational research', *BMJ Open*, 10(8). Available at: https://doi.org/10.1136/bmjopen-2020-039652.

Mekhail, K. *et al.* (2022) 'FASN inhibitor TVB-3166 prevents S-acylation of the spike protein of human coronaviruses', *Journal of Lipid Research*, 63(9), p. 100256. Available at: https://doi.org/10.1016/j.jlr.2022.100256.

Morgan, O.W. *et al.* (2010) 'Morbid obesity as a risk factor for hospitalization and death due to 2009 pandemic influenza A(H1N1) disease', *PLoS ONE*, 5(3). Available at: https://doi.org/10.1371/journal.pone.0009694.

Moriconi, D. *et al.* (2020) 'Obesity prolongs the hospital stay in patients affected by COVID-19, and may impact on SARS-COV-2 shedding', *Obesity Research and Clinical Practice*, 14(3), pp. 205–209. Available at: https://doi.org/10.1016/j.orcp.2020.05.009.

Mulchandani, R., Lyngdoh, T. and Kakkar, A.K. (2021) 'Deciphering the COVID-19 cytokine storm: Systematic review and meta-analysis', *European Journal of Clinical Investigation*. Blackwell Publishing Ltd. Available at: https://doi.org/10.1111/eci.13429.

Munnur, D. *et al.* (2021) 'Altered ISGylation drives aberrant macrophage-dependent immune responses during SARS-CoV-2 infection', *Nature Immunology*, 22(11), pp. 1416–1427. Available at: https://doi.org/10.1038/s41590-021-01035-8.

Nalbandian, A. *et al.* (2021) 'Post-acute COVID-19 syndrome', *Nature Medicine*. Nature Research, pp. 601–615. Available at: https://doi.org/10.1038/s41591-021-01283-z.

Nave, H. *et al.* (2008) 'Resistance of Janus Kinase-2 Dependent Leptin Signaling in Natural Killer (NK) Cells: A Novel Mechanism of NK Cell Dysfunction in Diet-Induced Obesity', *Endocrinology*, 149(7), pp. 3370–3378. Available at: https://doi.org/10.1210/en.2007-1516.

Obesity - Our World in Data (no date). Available at: https://ourworldindata.org/obesity#obesity-is-one-of-the-leading-risk-factors-for-early-death (Accessed: 18 May 2023).

Obesity and overweight (no date). Available at: https://www.who.int/news-room/fact-sheets/detail/obesity-and-overweight (Accessed: 18 May 2023).

Obesity causes & treatments - Illnesses & conditions | NHS inform (no date). Available at: https://www.nhsinform.scot/illnesses-and-conditions/nutritional/obesity#treating-obesity (Accessed: 18 May 2023).

Ohol, Y.M. *et al.* (2015) 'Direct inhibition of cellular fatty acid synthase impairs replication of respiratory syncytial virus and other respiratory viruses', *PLoS ONE*, 10(12). Available at: https://doi.org/10.1371/journal.pone.0144648.

Overweight and Obesity - Causes and Risk Factors | NHLBI, NIH (no date). Available at: https://www.nhlbi.nih.gov/health/overweight-and-obesity/causes (Accessed: 18 May 2023).

Overweight and Obesity - Prevention | NHLBI, NIH (no date). Available at: https://www.nhlbi.nih.gov/health/overweight-and-obesity/prevention (Accessed: 18 May 2023).

Painter, S.D., Ovsyannikova, I.G. and Poland, G.A. (2015) 'The weight of obesity on the human immune response to vaccination', *Vaccine*. Elsevier Ltd, pp. 4422–4429. Available at: https://doi.org/10.1016/j.vaccine.2015.06.101.

Patel, V.B., Basu, R. and Oudit, G.Y. (2016) 'ACE2/Ang 1-7 axis: A critical regulator of epicardial adipose tissue inflammation and cardiac dysfunction in obesity', *Adipocyte*,

5(3), pp. 306–311. Available at: https://doi.org/10.1080/21623945.2015.1131881.

Peacock, T.P. *et al.* (2022) 'The altered entry pathway and antigenic distance of the SARS-CoV-2 Omicron variant map to separate domains of spike protein', *bioRxiv*, p. 2021.12.31.474653. Available at: https://doi.org/10.1101/2021.12.31.474653.

Petrilli, C.M. *et al.* (2020) 'Factors associated with hospital admission and critical illness among 5279 people with coronavirus disease 2019 in New York City: Prospective cohort study', *The BMJ*, 369. Available at: https://doi.org/10.1136/bmj.m1966.

Pneumonia of unknown cause – China (no date). Available at: https://www.who.int/emergencies/disease-outbreak-news/item/2020-DON229 (Accessed: 18 May 2023).

Puelles, V.G. *et al.* (2020) 'Multiorgan and Renal Tropism of SARS-CoV-2', *New England Journal of Medicine*, 383(6), pp. 590–592. Available at: https://doi.org/10.1056/nejmc2011400.

Pugliese, G. *et al.* (2022) 'Obesity and infectious diseases: pathophysiology and epidemiology of a double pandemic condition', *International Journal of Obesity*. Springer Nature, pp. 449–465. Available at: https://doi.org/10.1038/s41366-021-01035-6.

Reiterer, M. *et al.* (2021) 'Hyperglycemia in Acute COVID-19 is Characterized by Adipose Tissue Dysfunction and Insulin Resistance', *SSRN Electronic Journal* [Preprint]. Available at: https://doi.org/10.2139/ssrn.3837640.

Ritchie, S.A. and Connell, J.M.C. (2007) 'The link between abdominal obesity, metabolic syndrome and cardiovascular disease', *Nutrition, Metabolism and Cardiovascular Diseases*, 17(4), pp. 319–326. Available at: https://doi.org/10.1016/J.NUMECD.2006.07.005.

Ritonavir-Boosted Nirmatrelvir (Paxlovid) | COVID-19 Treatment Guidelines (no date). Available at: https://www.covid19treatmentguidelines.nih.gov/therapies/antiviral-therapy/ritonavir-boosted-nirmatrelvir--paxlovid-/ (Accessed: 18 May 2023).

RoActemra | European Medicines Agency (no date). Available at: https://www.ema.europa.eu/en/medicines/human/EPAR/roactemra (Accessed: 18 May 2023).

De Rosa, V. *et al.* (2007) 'A Key Role of Leptin in the Control of Regulatory T Cell Proliferation', *Immunity*, 26(2), pp. 241–255. Available at: https://doi.org/10.1016/j.immuni.2007.01.011.

Ruban, A. *et al.* (2019) 'Current treatments for obesity', *Clinical Medicine*, 19(3), p. 205. Available at: https://doi.org/10.7861/CLINMEDICINE.19-3-205.

Rydén, M. *et al.* (2004) 'Targets for TNF-α-induced lipolysis in human adipocytes', *Biochemical and Biophysical Research Communications*, 318(1), pp. 168–175. Available at: https://doi.org/10.1016/j.bbrc.2004.04.010.

Saely, C.H., Geiger, K. and Drexel, H. (2011) 'Brown versus white adipose tissue: A mini-review', *Gerontology*. Karger Publishers, pp. 15–23. Available at: https://doi.org/10.1159/000321319.

Safiabadi Tali, S.H. *et al.* (2021) 'Tools and techniques for severe acute respiratory syndrome coronavirus 2 (SARS-CoV-2)/COVID-19 detection', *Clinical Microbiology Reviews*, 34(3). Available at: https://doi.org/10.1128/CMR.00228-20.

Santaguida, P. *et al.* (2005) 'Diagnosis, Prognosis, and Treatment of Impaired Glucose Tolerance and Impaired Fasting Glucose: Summary'. Available at: https://www.ncbi.nlm.nih.gov/sites/books/NBK11923/ (Accessed: 10 March 2023).

Sattar, N., McInnes, I.B. and McMurray, J.J.V. (2020) 'Obesity Is a Risk Factor for Severe COVID-19 Infection: Multiple Potential Mechanisms', *Circulation*. Lippincott Williams and Wilkins, pp. 4–6. Available at: https://doi.org/10.1161/CIRCULATIONAHA.120.047659.

Sawadogo, W. *et al.* (2022) 'Overweight and obesity as risk factors for COVID-19-associated hospitalisations and death: systematic review and meta-analysis', *BMJ Nutrition, Prevention & Health*, p. e000375. Available at: https://doi.org/10.1136/bmjnph-2021-000375.

Schroeder, M. *et al.* (2021) 'High estradiol and low testosterone levels are associated with critical illness in male but not in female COVID-19 patients: a retrospective cohort study', *Emerging Microbes and Infections*, 10(1), pp. 1807–1818. Available at: https://doi.org/10.1080/22221751.2021.1969869.

Seckinger, P. *et al.* (1987) 'A urine inhibitor of interleukin 1 activity that blocks ligand binding.', *Journal of immunology (Baltimore, Md. : 1950)*, 139(5), pp. 1546–9. Available at: http://www.ncbi.nlm.nih.gov/pubmed/2957429 (Accessed: 19 May 2022).

Shah, R. V. *et al.* (2014) 'Visceral adiposity and the risk of metabolic syndrome across body mass index: The MESA study', *JACC: Cardiovascular Imaging*, 7(12), pp. 1221–1235. Available at: https://doi.org/10.1016/j.jcmg.2014.07.017.

Shang, J. *et al.* (2020) 'Structural basis of receptor recognition by SARS-CoV-2', *Nature*, 581(7807), pp. 221–224. Available at: https://doi.org/10.1038/s41586-020-2179-y.

Sheridan, P.A. *et al.* (2012) 'Obesity is associated with impaired immune response to influenza vaccination in humans', *International Journal of Obesity*, 36(8), pp. 1072–1077. Available at: https://doi.org/10.1038/ijo.2011.208.

Shimokawa, T., Kumar, M. V. and Lane, M.D. (2002) 'Effect of a fatty acid synthase inhibitor on food intake and expression of hypothalamic neuropeptides', *Proceedings of the National Academy of Sciences of the United States of America*, 99(1), p. 66. Available at: https://doi.org/10.1073/PNAS.012606199.

Shin, D. *et al.* (2020) 'Papain-like protease regulates SARS-CoV-2 viral spread and innate immunity', *Nature*, 587(7835), pp. 657–662. Available at: https://doi.org/10.1038/s41586-

020-2601-5.

Sia, S.F. *et al.* (2020) 'Pathogenesis and transmission of SARS-CoV-2 in golden hamsters', *Nature*, 583(7818). Available at: https://doi.org/10.1038/s41586-020-2342-5.

Simonnet, A. *et al.* (2020) 'High Prevalence of Obesity in Severe Acute Respiratory Syndrome Coronavirus-2 (SARS-CoV-2) Requiring Invasive Mechanical Ventilation', *Obesity*, 28(7), pp. 1195–1199. Available at: https://doi.org/10.1002/oby.22831.

Simons, P.J. *et al.* (2007) 'Pro-inflammatory delipidizing cytokines reduces adiponectin secretion from human adipocytes without affecting adiponectin oligomerization', *Journal of Endocrinology*, 192(2), pp. 289–299. Available at: https://doi.org/10.1677/JOE-06-0047.

Smith, A.G. *et al.* (2007) 'Diet-induced obese mice have increased mortality and altered immune responses when infected with influenza virus', *Journal of Nutrition*, 137(5), pp. 1236–1243. Available at: https://doi.org/10.1093/jn/137.5.1236.

Song, E. *et al.* (2021) 'Neuroinvasion of SARS-CoV-2 in human and mouse brain', *Journal of Experimental Medicine*, 218(3). Available at: https://doi.org/10.1084/JEM.20202135.

Stanelle-Bertram, S. *et al.* (2020) 'SARS-CoV-2 induced CYP19A1 expression in the lung correlates with increased aromatization of testosterone-to-estradiol in male golden hamsters'. Available at: https://doi.org/10.21203/RS.3.RS-107474/V1.

Stefan, N. (2022) 'Metabolic disorders, COVID-19 and vaccine-breakthrough infections', *Nature Reviews Endocrinology*. Nature Research, pp. 75–76. Available at: https://doi.org/10.1038/s41574-021-00608-9.

Strack, C. *et al.* (2022) 'Gender differences in cardiometabolic health and disease in a cross-sectional observational obesity study', *Biology of Sex Differences*, 13(1). Available at: https://doi.org/10.1186/s13293-022-00416-4.

Suzuki, R. *et al.* (2022) 'Attenuated fusogenicity and pathogenicity of SARS-CoV-2 Omicron variant', *Nature*, 603(7902), pp. 700–705. Available at: https://doi.org/10.1038/s41586-022-04462-1.

Takahashi, T. *et al.* (2020) 'Sex differences in immune responses that underlie COVID-19 disease outcomes', *Nature*, 588(7837), pp. 315–320. Available at: https://doi.org/10.1038/s41586-020-2700-3.

Taxon Details | ICTV (no date). Available at: https://ictv.global/taxonomy/taxondetails?taxnode_id=202101868 (Accessed: 18 May 2023).

Tchoukalova, Y.D. *et al.* (2010) 'Sex- and Depot-Dependent Differences in Adipogenesis in Normal-Weight Humans', *Obesity*, 18(10), pp. 1875–1880. Available at: https://doi.org/10.1038/oby.2010.56.

Teixeira, L. *et al.* (2022) 'Simvastatin Downregulates the SARS-CoV-2-Induced Inflammatory Response and Impairs Viral Infection Through Disruption of Lipid Rafts', *Frontiers in*

Immunology, 13. Available at: https://doi.org/10.3389/fimmu.2022.820131.

The Human Protein Atlas (no date). Available at: https://www.proteinatlas.org/ (Accessed: 18 May 2023).

Thupari, J.N. *et al.* (2002) 'C75 increases peripheral energy utilization and fatty acid oxidation in diet-induced obesity', *Proceedings of the National Academy of Sciences of the United States of America*, 99(14), pp. 9498–9502. Available at: https://doi.org/10.1073/PNAS.132128899.

Tiwari, S. and Siddiqi, S.A. (2012) 'Intracellular trafficking and secretion of VLDL', *Arteriosclerosis, Thrombosis, and Vascular Biology*. NIH Public Access, pp. 1079–1086. Available at: https://doi.org/10.1161/ATVBAHA.111.241471.

Tong, H. Van *et al.* (2017) 'Adiponectin and pro-inflammatory cytokines are modulated in Vietnamese patients with type 2 diabetes mellitus', *Journal of Diabetes Investigation*, 8(3), pp. 295–305. Available at: https://doi.org/10.1111/jdi.12579.

Tonkin, A. and Byrnes, A. (2014) 'Treatment of dyslipidemia', *F1000Prime Reports*, 6. Available at: https://doi.org/10.12703/P6-17.

Treskova-Schwarzbach, M. *et al.* (2021) 'Pre-existing health conditions and severe COVID-19 outcomes: an umbrella review approach and meta-analysis of global evidence', *BMC Medicine*, 19(1), pp. 1–26. Available at: https://doi.org/10.1186/s12916-021-02058-6.

Tsiotra, P.C. *et al.* (2013) 'High insulin and leptin increase resistin and inflammatory cytokine production from human mononuclear cells', *BioMed Research International*, 2013. Available at: https://doi.org/10.1155/2013/487081.

Uhlén, M. *et al.* (2015) 'Tissue-based map of the human proteome', *Science*, 347(6220). Available at: https://doi.org/10.1126/science.1260419.

V'kovski, P. *et al.* (2021) 'Coronavirus biology and replication: implications for SARS-CoV-2', *Nature Reviews Microbiology*. Nature Research, pp. 155–170. Available at: https://doi.org/10.1038/s41579-020-00468-6.

Wang, C.C. *et al.* (2021) 'Airborne transmission of respiratory viruses', *Science*. American Association for the Advancement of Science. Available at: https://doi.org/10.1126/science.abd9149.

Watanabe, M. *et al.* (2022) 'Rapid Weight Loss, Central Obesity Improvement and Blood Glucose Reduction Are Associated with a Stronger Adaptive Immune Response Following COVID-19 mRNA Vaccine', *Vaccines*, 10(1), p. 79. Available at: https://doi.org/10.3390/vaccines10010079.

Watson, R.A. *et al.* (2010) 'Reduction of total lung capacity in obese men: Comparison of total intrathoracic and gas volumes', *Journal of Applied Physiology*, 108(6), pp. 1605–1612. Available at: https://doi.org/10.1152/japplphysiol.01267.2009.

Watts, G.F. *et al.* (2003) 'Fat Compartments and Apolipoprotein B-100 Kinetics in

Overweight-Obese Men', *Obesity Research*, 11(1), pp. 152–159. Available at: https://doi.org/10.1038/oby.2003.24.

Wensveen, F.M. *et al.* (2015) 'NK cells link obesity-induced adipose stress to inflammation and insulin resistance', *Nature Immunology*, 16(4), pp. 376–385. Available at: https://doi.org/10.1038/ni.3120.

WHO Coronavirus (COVID-19) Dashboard | WHO Coronavirus (COVID-19) Dashboard With Vaccination Data (no date). Available at: https://covid19.who.int/ (Accessed: 18 May 2023).

WHO Director-General's opening remarks at the media briefing on COVID-19 - 11 March 2020 (no date). Available at: https://www.who.int/director-general/speeches/detail/who-director-general-s-opening-remarks-at-the-media-briefing-on-covid-19---11-march-2020 (Accessed: 18 May 2023).

Wilson, P.W.F. *et al.* (2005) 'Metabolic Syndrome as a Precursor of Cardiovascular Disease and Type 2 Diabetes Mellitus', *Circulation*, 112(20), pp. 3066–3072. Available at: https://doi.org/10.1161/CIRCULATIONAHA.105.539528.

Woolhouse, M. *et al.* (2012) 'Human viruses: Discovery and emeraence', *Philosophical Transactions of the Royal Society B: Biological Sciences*, 367(1604), pp. 2864–2871. Available at: https://doi.org/10.1098/rstb.2011.0354.

Worobey, M. *et al.* (2022) 'The Huanan Seafood Wholesale Market in Wuhan was the early epicenter of the COVID-19 pandemic', *Science*, 377(6609), pp. 951–959. Available at: https://doi.org/10.1126/science.abp8715.

Wright, J.M., Musini, V.M. and Gill, R. (2018) 'First-line drugs for hypertension', *The Cochrane Database of Systematic Reviews*, 2018(4). Available at: https://doi.org/10.1002/14651858.CD001841.PUB3.

Wu, Z. *et al.* (2021) 'Palmitoylation of SARS-CoV-2 S protein is essential for viral infectivity', *Signal Transduction and Targeted Therapy*. Springer Nature, pp. 1–4. Available at: https://doi.org/10.1038/s41392-021-00651-y.

Yadav, R. *et al.* (2021) 'Role of structural and non-structural proteins and therapeutic targets of SARS-CoV-2 for COVID-19', *Cells*. MDPI, p. 821. Available at: https://doi.org/10.3390/cells10040821.

Yamaguchi, N. *et al.* (2005) 'Adiponectin inhibits Toll-like receptor family-induced signaling', *FEBS Letters*, 579(30), pp. 6821–6826. Available at: https://doi.org/10.1016/j.febslet.2005.11.019.

Yamauchi, T. *et al.* (2002) 'Adiponectin stimulates glucose utilization and fatty-acid oxidation by activating AMP-activated protein kinase', *Nature Medicine*, 8(11), pp. 1288–1295. Available at: https://doi.org/10.1038/nm788.

Yang, X. *et al.* (2020) 'Clinical course and outcomes of critically ill patients with SARS-CoV-2

pneumonia in Wuhan, China: a single-centered, retrospective, observational study', *The Lancet Respiratory Medicine*, 8(5), pp. 475–481. Available at: https://doi.org/10.1016/S2213-2600(20)30079-5.

Yang, Y. *et al.* (2020) 'Visceral Adiposity and High Intramuscular Fat Deposition Independently Predict Critical Illness in Patients with SARS-CoV-2', *Obesity*, 28(11), pp. 2040–2048. Available at: https://doi.org/10.1002/oby.22971.

Yuan, S. *et al.* (2019) 'SREBP-dependent lipidomic reprogramming as a broad-spectrum antiviral target', *Nature Communications*, 10(1), pp. 1–15. Available at: https://doi.org/10.1038/s41467-018-08015-x.

Yuen, T.T.T. *et al.* (2022) 'Targeting ACLY efficiently inhibits SARS-CoV-2 replication', *International Journal of Biological Sciences*, 18(12), pp. 4714–4730. Available at: https://doi.org/10.7150/ijbs.72709.

Zhai, T. *et al.* (2020) 'Inflammatory risk factors for hypertriglyceridemia in patients with severe influenza', *Journal of International Medical Research*, 48(8). Available at: https://doi.org/10.1177/0300060520918058.

Zhang, Q. *et al.* (2021) 'Molecular mechanism of interaction between SARS-CoV-2 and host cells and interventional therapy', *Signal Transduction and Targeted Therapy*. Springer Nature, pp. 1–19. Available at: https://doi.org/10.1038/s41392-021-00653-w.

Zhang, X. *et al.* (2015) 'Human intracellular ISG15 prevents interferon-α/β over-amplification and auto-inflammation', *Nature*, 517(7532), pp. 89–93. Available at: https://doi.org/10.1038/nature13801.

Zhao, C. *et al.* (2010) 'ISG15 conjugation system targets the viral NS1 protein in influenza A virus-infected cells', *Proceedings of the National Academy of Sciences of the United States of America*, 107(5), pp. 2253–2258. Available at: https://doi.org/10.1073/pnas.0909144107.

Zhou, F. *et al.* (2020) 'Clinical course and risk factors for mortality of adult inpatients with COVID-19 in Wuhan, China: a retrospective cohort study', *The Lancet*, 395(10229). Available at: https://doi.org/10.1016/S0140-6736(20)30566-3.

Zhou, Y. *et al.* (2020) 'Comorbidities and the risk of severe or fatal outcomes associated with coronavirus disease 2019: A systematic review and meta-analysis', *International Journal of Infectious Diseases*. Elsevier B.V., pp. 47–56. Available at: https://doi.org/10.1016/j.ijid.2020.07.029.

Zickler, M. *et al.* (2022) 'Replication of SARS-CoV-2 in adipose tissue determines organ and systemic lipid metabolism in hamsters and humans', *Cell Metabolism*, 34(1), pp. 1–2. Available at: https://doi.org/10.1016/j.cmet.2021.12.002.

Acknowledgements

This work would not have been possible without a great team and a productive environment. I am extremely grateful for the help, guidance and jokes from everyone in the lab throughout the last 4 years with its ups and downs. I will use these lines to especially thank the following people:

Prof. Dr. Gülşah Gabriel for giving me the opportunity to do my PhD in your group and to contribute to the scientific field in this time. Thank you for the interesting project, the supervision, guidance and motivational meetings during my PhD. I have learned so much in these past years, giving me the confidence to tackle whatever comes next.

Prof. Dr. Thomas Dobner for being a reviewer of this thesis the feedback you have given in project meetings.

Dr. Stephanie Stanelle-Bertram for always having an open door for questions and helping out wherever you could, even if you did not always have the time. Thank you for your corrections of the thesis, they helped a lot.

Dr. Sebastian Beck for your guidance, especially at the beginning of my time in the lab, during my first few visits to the S3 lab and of course thank you for the creative smoking breaks in between.

Dr. Nancy Mounogou Kouassi for your optimism, the good mood, laughs and German-French mixed sentences. Thanks to your Gummibärchen addiction, I don't feel so bad about my Nougat Bit problem.

Tian Bai for the great work atmosphere, the lessons in Chinese music in the S3 and the fun the office.

Fabian Stoll, for the high quality S3 sessions with background music ranging from good to questionable and the help with everything statistics or image related. Thank you for always trying to find solutions and discussing all problems, whether they are important or not.

Dr. Zoé Schmal for your scientific support and your ability to always find something funny in any given situation, even 9 hrs at the Amsterdam airport. For being part of fat face and together with Fabian, taking any discussion that one bit too far.

Hanna Jania for all your help in the lab, for always being calm and collected, regardless of the stress level and for bringing delicious beer to my attention.

Annette Gries for all the conversations when I came over to only get a new pen, for always having an open ear for problems and your words of encouragement.

Anna Lüttjohann for the excellent help in the lab, your "can do" attitude and cheery mood.

Jenny Ruschinski and **Britta Weseloh** for the scientific support and good conversations in the office.

Ursula Müller for the excellent help with all hamster-related projects and general guidance in all questions regarding animals.

Ute Neumann for support in all office-related questions and organizational matters.

Martin Müller for being a good friend, for the real time translations of songs on the radio, the discussions in flawless French and the occasional after work drinks at the Alster. Too bad we could not finish this thing together.

Dr. Ulrike Felgenhauer for being one of my best friends since our University days, for your constant support and readiness to help with anything that comes up. Thank you for pre-correcting my thesis, it was a tremendous help.

All the people that I did not mention by name, who were part of this journey and contributed to the different projects in one way or another.

And last but not least I want to thank my family and friends for all the mental support over the past years. My **parents** for always being supportive and believing in me, my **sister and her family** for the words of encouragement and great times when we're together. I am especially deeply grateful to my girlfriend **Maria** for going through everything together with me and always being on my side and our little daughter **Elin** for making every day special, I love you both.

Declaration under oath
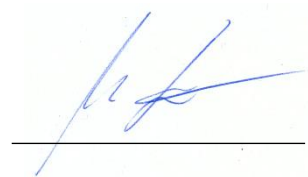
Eidesstattliche Versicherung

I hereby declare, under oath, that I have written the present dissertation independently and on my own. Any content taken from other sources are clearly marked as such and listed in the reference section.

Hiermit erkläre ich an Eides statt, dass ich die vorliegende Dissertation unabhängig und eigenständig verfasst habe. Jeglicher Inhalt fremder Quellen ist als deutlich als solcher markiert und in der Referenzliste angegeben.

Cambridge, 17.06.2023

City and Date

Ort und Datum

Signature

Unterschrift